学位論文

Theoretical study on a renormalization-group limit cycle in Efimov physics

(エフィモフ物理における繰り込み群のリミットサイクルの理論的研究)

2016年12月 博士(理学)申請

理学系研究科物理学専攻

東京大学

堀之内裕理

Ph. D Thesis

Theoretical study on a renormalization-group limit cycle in Efimov physics

Submitted: December 2016

Department of Physics, Graduate School of Science

University of Tokyo

Yusuke Horinouchi

Abstract

Physics is often said to be universal when microscopically distinct systems show the same low-energy behavior. In critical phenomena, the universality of the second-order phase transition is elucidated by the renormalization-group (RG) method, which provides a powerful computational tool for the critical exponents of the power-law behavior of observables. In particular, the attraction of different RG-flow trajectories to a small-dimensional sub-theory space accounts for the universal nature. The attraction structure motivates us to extract universal physical observables by investigating the sub-theory space called the renormalized trajectory, onto which RG flows are attracted. To put the motivation forward, we consider the universality in quantum few-body physics, in which the RG exhibits another characteristic flow than the fixed points. The Efimov physics, which is renowned for self-similar trimer states, shows an RG limit-cycle behavior that refers to a periodic RG-flow trajectory. In this thesis, we investigate the relation between the RG limit cycle and the universality in Efimov physics.

Firstly, to verify that the RG limit cycle is the renormalized trajectory in Efimov physics, we demonstrate that the RG-flow trajectories of microscopically distinct systems universally exhibit the RG limit-cycle behavior at sufficiently low energy, thereby giving a numerical evidence of the attraction structure of the RG-flow trajectories to the RG limit cycle; in other words, we show that the RG limit cycle behaves as an attractor of various RG flows. To address this point unbiasedly, we perform an exact RG calculation for various effective models of identical bosons that features Efimov physics at low energy. We apply an exact functional renormalization-group (FRG) method to effective separable models for various systems of identical bosons with short-range resonant interactions. For a given microscopic three-body model, we numerically demonstrate for the first time that the RG-flow trajectory converges at the RG limit cycle in the low-energy regime. Physical observables such as Efimov's scaling factor and the three-body parameter can be extracted from the RG limit cycle.

Secondly, we investigate the role of RG limit cycle in a four-body extension of Efimov physics, which has attracted considerable attention in recent years. Although the universality in four-body physics has been established both theoretically and experimentally, the relationship between the RG limit cycle and the four-body physics remains an open question. By performing an FRG calculation for a simple effective field theory, we obtain for the first time the RG limit cycle in the four-body sector that reproduces the universality of the four-body physics. As the first attempt, we develop a simple separable pole approximation of the four-body FRG equation and successfully reproduce qualitative features of the four-body physics. A systematic improvement of the approximation quantitatively reproduces the numbers and the binding energies of tetramer states that emerge universally at low energy.

Acknowledgment

I would like to thank greatly my Phd supervisor, Professor Masahito Ueda, for his advice, many fruitful discussions and encouragement. I would like also to thank Professor Shunsuke Furukawa, Dr. Pascal Naidon, Dr. Shimpei Endo, Dr. Tatsuhiko Ikeda and Dr. Yuya Tanizaki who gave me a lot of advice throughout my Phd course. I am also grateful for Ms. Asako Takeuchi and Ms. Aya Tamai for their help on research bugets.

Contents

Chapter 1

Introduction

1.1 General motivation

Universality in physics often refers to a situation in which microscopically distinct systems show the same low energy behavior. A prominent example is the critical phenomena in which apparently distinct physical systems are grouped into universality classes sharing the same power-law singularities of observables [1]. For instance, the same critical exponents are shared by the ferromagnetic transition and the liquid/gas transition, that belong to the Ising universality class [2]. The modern foundation for understanding the universality is given by Wilson's renormalization group (RG) [3, 4], which follows the change of a system viewed at different energy scales by continuously performing a coarse-graining transformation on Hamiltonians. In the RG, the continuously coarse-grained Hamiltonians form a set of RG flows in theory space (the space of Hamiltonians), where the RG flows are typically attracted to a sub-theory space of very small dimensions at sufficiently low energy [1, 5, 6], as small rivers departing from different valleys flow into the same large river.[1] This convergent behavior represents the universality of observables at low energy, since the convergence signifies that microscopically distinct Hamiltonians will arrive at the same low-energy effective Hamiltonian by the RG transformation, which does not alter the dynamics of low-energy degrees of freedom. In other words, all the universal low-energy features of a given microscopic model can be obtained by the RG flow on the "large river". In particular, the universality of critical phenomena is accounted for by the attraction of different RG flows towards the same RG fixed point, which represents the scale invariance of the second-order phase transition, and therefore, the universality classes of critical phenomena are determined by attraction domains of several fixed points in theory space [6].

The small sub-theory space, onto which RG flows are attracted, is called by Wilson and Kogut [1] the renormalized trajectory, which represents all the universal low-energy properties of any microscopic model flowing into the renormalized trajectory. The general motivation underlying this thesis is to elucidate relations between the renormalized trajectory and universal low-energy observables. To elucidate the relations, we deal with quantum-mechanical few-body systems with a strong short-range interaction, where all the low-energy physical observables are described univer-

[1] The metaphor of rivers is due to Bagnuls and Bervillier [6] They study this convergent behavior in detail for the $\mathbb{Z}_2$-invariant theories.

sally by a few parameters irrespective of details of each individual Hamiltonian. In particular, we focus on the Efimov physics that is renowned for the discrete scale-invariant bound-state spectrum. Compared with the critical phenomena, that is represented by an RG fixed point, the Efimov physics is represented by an RG limit cycle which refers to a periodic RG-flow trajectory. In line with the general motivation mentioned above, we will show that the RG limit cycle has the essential pieces of information about universal observables in the Efimov physics. We also make a conjecture that a topological property of how the renormalized trajectory is embedded in theory space may account for the universal numbers of bound states in the Efimov physics.

1.2 Efimov physics

To place the idea of the last section in a proper historical context, we here briefly overview the history of the Efimov physics. In the early days of quantum mechanics, Thomas [7] presented the theorem stating that the three distinguishable nucleons with a resonant zero-range interaction have no well-defined ground state. He considered the interaction with depth V_0 and range r_0 that supports a single two-body bound state, and studied the zero-range limit $r_0 \to 0$ and the infinite potential-depth limit $V_0 \to \infty$ with fixed two-body binding energy E_2, i.e., he dealt with the parameter region of large and positive scattering length $a \gg r_0$. By a variational approach, he showed that the three-nucleon energy is unbounded from below, which means that the stable ground state is absent. Based on the rigorous three-body scattering equation given by Skornyakov and Ter-Martirosian [8], Danilov [9] pointed out that the "Thomas collapse" originates from the short-range property of the interaction, and that the short-range information can be encapsulated in a single three-body parameter Λ_* which determines the ground state. In the early 1970s, Efimov generalized [10, 11] the Thomas theorem to an arbitrary but large scattering length $|a| \gg r_0$, and predicted an infinite series of shallow three-body bound states that obey a peculiar scaling law: In the limit of the diverging scattering length $a = \pm\infty$, the three-body bound states exhibit a geometric energy spectrum $E_{n+1}/E_n = e^{-\pi/s_0}$ and the bound-state wave functions obey the scaling law of $\psi_n(x_i) = \psi_{n+1}(e^{-\pi/s_0}x_i)$, where $e^{\pi/s_0} \simeq 22.694$ ($s_0 \simeq 1.00624$). Efimov attributed this scaling behavior to the effective three-body interaction that features inverse-square attraction $-1/R^2$, where the hyperradius $R \sim \sqrt{x_{12}^2 + x_{23}^2 + x_{31}^2}$ represents the size of three particles. He also discussed that the inverse-square-attraction profile emerges universally in the length scale of $r_0 \lesssim R \lesssim a$, since the profile does not depend on the details of a particular two-body interaction.[2] Soon after, an exact proof and an unequal-mass-extension of the Efimov effect were made by Amado and Noble [12, 13], who pointed out that the scaling factor e^{π/s_0} depends on the mass ratio among the three particles. The universality of the Efimov effect and an emergence of a renormalization-group (RG) limit cycle were manifested by Bedaque *et al.* [14, 15] within a zero-range effective field theory framework: Compared with the critical phenomena that are represented by scale-invariant RG fixed points, the Efimov effect was shown to exhibit a periodic RG flow, reflecting its discrete scale invariance.[3]

[2] The restriction $r_0 \lesssim R \lesssim a$ on the length scale limits the binding energy E_t of the Efimov trimers as $\frac{\hbar}{ma^2} \lesssim E_t \lesssim \frac{\hbar}{mr_0^2}$.

[3] A similar discrete scale-invariant phenomenon is known for the doubly excited H^- ion, in which two valence electrons are excited from their ground states [16]. In the doubly excited H^- ion, an interaction between an electron-

Because of the universal emergence of the inverse square attraction in resonantly interacting systems, the realization of the Efimov trimers is expected in various three-body systems. As possible candidates in nuclear physics, Efimov suggested ^{12}C and ^{3}H nuclei which can be regarded as a trimer of α particles and that of nucleons, respectively. For the ^{3}H nucleus, a zero-range model with an effective-range correction was applied by Efimov *et al.* [17, 18, 19, 20] and later by Bedaque *et al.* [21]. The obtained trimer binding energy[4] $E_t \simeq 8.8$MeV [19, 20] ($E_t \simeq 8.3$MeV [21]) agrees with that of the triton $E_t \simeq 8.4820$MeV within a few percent, in favor of Efimov's scenario in the ^{3}H nucleus. In addition, the linear dependence of the triton energy on the neutron-deutron doublet scattering length (the Phillips line [22]) could be qualitatively understood from Efimov's scenario, since any physical observable is represented by a single three-body parameter Λ_* in the limit of the divergent nucleon-nucleon singlet / triplet scattering length [19, 20]. For the ^{12}C nucleus, the so-called Hoyle state [23] was conjectured by Higa and Hammer [24] to be a remnant of an Efimov trimer modified by the Coulomb repulsion; however, calculations by Suno *et al.* [25] suggest that the potential that stabilizes the Hoyle state is the short-range nuclear forces rather than Efimov's inverse square attraction which turned out to be unable to overcome the Coulomb repulsion, as opposed to the Efimov's scenario [26]. Concerning the atomic physics, Lim *et al.* conjectured [27] a possible Efimov trimer in three ^{4}He atoms. Cornelius *et al.* [28] and later Esry *et al.* [29] provided convincing numerical evidences for the existence of an excited trimer state and its Efimov character by observing an increasing number of trimers if the depth of the He-He interaction potential is artificially deepened. In particular, the obtained scattering-length dependence of the excited-trimer energy agrees with the prediction of the zero-range theory [26].[5]

As other candidates for the Efimov trimers, Efimov [33] and later Fedorov *et al.* [34] suggested two-neutron halo nuclei[6] in which two neutrons and a nucleus are loosely bounded. However, there is no conclusive evidence of the Efimov effect in halo nuclei. Among halo nuclei, ^{6}He nucleus, which consists of an α particle and two valence neutrons, was shown [36] to be bound by a resonant p-wave α-neutron interaction [37], which does not support Efimov trimers [38, 39]. Mazumdar *et al.* investigated ^{14}Be, ^{19}B, ^{18}C, ^{20}C, ^{22}C nuclei [40, 41] by applying separable neutron-neutron and neutron-core potentials, and confirmed an increasing number of trimer states as the neutron-core scattering length is increased. In particular, when input parameters are fixed by the neutron-neutron scattering length, the neutron-neutron effective range and the neutron-core binding energy, ^{20}C nucleus turned out to be the only nucleus which can support an excited shallow Efimov trimer. Within an effective field theory framework, Amorim *et al.* [42] and later Canham *et al.* [43]

---

proton dipole and an electron produces an inverse square attraction that leads to a log-periodic dependence of Fano resonances on the photon energy, which is experimentally observed. We note that the doubly excited H^- ion is not an Efimov state since the origin of the inverse square attraction is not a resonant interaction between two particles.

[4]The values of the binding energy can be read from the figures plotting the trimer binding energy as a function of the neutron-deutron scattering length in Refs. [19, 20, 21]. An input neutron-deutron doublet scattering length a_3 is set to be $a_3 \simeq 0.65$fm.

[5]There are arguments that the lowest-lying He trimer is also an Efimov trimer in the sense that the energies of the ground and the first excited trimers obey an universal scaling law derived from a zero-range effective field theory. (see Ref. [30, 31, 32] for details)

[6]In Ref. [33], Efimov did not use the term 'halo nuclei' which was firstly discovered thirteen years later by Tanihata *et al* [35].

investigated the halo nuclei of ^{11}Li, ^{12}Be, ^{18}C, ^{20}C. They reached the conclusion that an excited Efimov trimer emerges only in ^{20}C nucleus.

In the candidates discussed above, a major difficulty in realizing the Efimov trimers originates in the condition of the resonant interaction $a \gg r_0$ which is rarely met in reality: Efimov estimated the number of the Efimov trimers as $N \sim \log \frac{|a|}{r_0}$. Therefore, $N \geq 2$ requires $|a|/r_0 \gtrsim 500$ and $N \geq 3$ requires $|a|/r_0 \gtrsim 10000$. Due partly to this difficulty, an experimental realization of the Efimov trimers had remained elusive until the creation of ultracold atomic gases which are systems of optically or magnetically trapped atomic gases cooled down to 1-100nK. In ultracold atoms, the s-wave scattering length a between atoms can be tuned from 0 to $\pm\infty$ via a magnetic Feshbach resonance [44, 45] and, in particular, the geometric scaling of the Efimov trimers gives rise to as the log-periodic dependence on the scattering length of the atomic loss resonances from the trap [46]. Relying on the high tunability of the s-wave scattering length of the ultracold atomic gases, Nägerl and Grimm's group at Innsbruck firstly observed [47, 48] a signature of the Efimov trimers in ultracold ^{133}Cs atoms by measuring the atomic loss resonances from an optical trap. Subsequently, the signature of the Efimov effect is experimentally observed in various atomic species including ^{39}K [49], ^{7}Li [50, 51] and ^{85}Rb [52]. More recently, through the measurements of several atomic loss resonances, Efimov's scaling factor was directly observed to be 21.0(1.3) [53] which agrees with the theoretical value of $e^{\pi/s_0} \simeq 22.694$.

Since the experimental realizations of the Efimov trimers, a number of theoretical efforts have been devoted to the reveal an emergence of the Efimov effect in a rich variety of physical systems including dipoles [54], magnets [55] and particles in mixed dimensions [56]. Experimentally, the signatures of the Efimov effect for unequal-mass particles were observed in the K-Rb mixture [57, 58] and the Li-Cs mixture [59, 60] and the observed mass-ratio dependent scaling factor agrees perfectly with the theoretical value. In investigating the universality of the Efimov physics, the four-body extension of the Efimov effect and its universality have been one of major fundamental problems in recent years. Theoretically, studies by Platter *et al.* [61], Hammer *et al.* [62], Yamashita *et al.* [63], Hadizadeh [64], von Stecher *et al.* [65] and Deltuva [66, 67, 68, 69, 70, 71, 72, 73, 74] revealed the universality of the four-boson systems with a resonant interaction. In particular, two-tetramer resonances were found [65] to accompany every Efimov trimer in the four-boson energy spectrum near the unitarity limit $a = \pm\infty$, as firstly conjectured by Hammer *et al.* [62]. The energies and the widths of the two tetramers were precisely calculated by Deltuva in his series of papers [66, 67, 68, 69, 70, 71, 72, 73, 74] and were found to take on a universal value determined only by the scattering length a and the three-body parameter Λ_*. Experimentally, atomic loss resonances due to the two accompanying tetramers were recently observed [75] in ultracold ^{133}Cs atoms and the obtained locations of the resonances are in good agreement with the theoretical prediction [65].

In this context, we address the RG counterpart of the Efimov physics in this thesis. First, we address the question of what is the renormalized trajectory which represents the low-energy universality of the three-body Efimov physics. Since Bedaque *et al.* [14, 15] have shown that a local effective field theory of identical bosons exhibits an RG limit cycle, the RG limit cycle is a natural candidate of the renormalized trajectory. Based on numerical calculations of non-perturbative RG flows for identical bosons with various interparticle interactions, we demonstrate that RG flows starting from microscopically distinct systems will arrive at the RG limit cycle at sufficiently low

energy; in other words, we provide for the first time a numerical evidence that the RG limit cycle is an attractor of various RG flows reflecting the low-energy universality of the three-body Efimov effect. The results are based on our publication of Ref. [76]. In line with the general motivation mentioned in the last section, we then investigate the RG counterpart of the four-body universality, which remains a major missing link in this subject. In particular, the connection between the RG limit cycle and the four-body universality is not clear. By developing an effective field theory that reproduces the three-body Efimov effect and by performing a functional renormalization-group calculations for the effective field theory, we demonstrate for the first time that the RG limit cycle indeed contains essential pieces of information about the four-body universality, i.e., the RG limit cycle reproduces the numbers and the energies of the universal tetramer states. The essential parts of the results are based on our publication of Ref. [77].

1.3 Organization of this thesis

This thesis is organized as follows. In Chap. 2, we review the Efimov physics in ultracold atoms. Following Efimov's original discussions, we first review the Efimov effect in identical bosons. Emergence of a renormalization group (RG) limit cycle is also discussed briefly by using an effective field theory. After reviewing some experimental aspects of the Efimov effect in ultracold atoms, extensions of the Efimov effect to higher angular-momentum sectors, unequal-mass particles and particles in mixed dimensions are also reviewed briefly to demonstrate the universal emergence of the Efimov effect in a variety of systems. We finally review N-particle extensions of the Efimov effect, among which the four-body extension is of our central interest in this thesis. Chapter 3 is devoted for the review of the functional renormalization group (FRG), in which we first briefly review the concept of the FRG and its applications to a rich variety of physical systems. We then formulate the FRG so that the formulation is suitable for our purpose of dealing with the low-energy universality in quantum few-body physics. In line with the general motivation discussed in Sec. 1.1, we address the question of "What is the renormalized trajectory in Efimov physics." in Chap. 4. To address the question, we devise a method that combines the FRG formalism developed by Tanizaki [78] with a separable model approximation [79, 80] for various realistic interparticle interactions. By applying the method to various microscopic models, we numerically show that the RG limit cycle plays the role of an attractor of various RG flows: We demonstrate that the RG flows of a three-body coupling constant universally exhibit limit-cycle behavior at sufficiently low energy, whereas they behave non-universally at high energy depending on each individual microscopic model. The results provide a numerical evidence that the renormalized trajectory that represents the low-energy universality of the Efimov effect is the RG limit cycle. The methods and the results discussed in Sec. 4.3.2 is based on our original research article of Ref. [76]. The RG counterpart of the two-body universality, which is not investigated in Ref. [76], is also discussed in some detail in Sec. 4.3.1. Based on the results obtained in Chap. 4, we investigate the relation between the RG limit cycle and the universality in the four-body physics in identical bosons in Chap. 5. To deal with a non-perturbative RG flows of a four-body coupling constant, we first develop an effective field theory that reproduces the three-body Efimov effect. We then develop a numerically tractable method by combining the FRG and a separable pole approximation. By using the

method, we numerically obtain the RG limit cycle in the four-body sector, which has been elusive before our work. We will see that the universal number of tetramers and their binding energies are extracted from the RG limit cycle in the four-body sector, thereby demonstrating for the first time that the RG limit cycle contains the essential pieces of universal low-energy observables of the four-body physics. We also make a conjecture that a topological property of how the RG limit cycle is embedded in theory space accounts for the number of universal four-body bound states. The methods and the results discussed in Sec. 5.1, 5.2 and 5.3 are based on our original research article of Ref. [77]. A systematic improvement, which is not discussed in Ref. [77], of the evaluation of the binding energies is investigated in Sec. 5.4. The methodological difference between the Faddeev-Yakubovski equation and our FRG approach in dealing with the four-body problem is the following: While the Faddeev-Yakubovski equation deals with the correlation functions which includes the entire quantum fluctuations, our FRG method investigate the variation of an effective Hamiltonian in which quantum fluctuations parametrized by the RG cutoff are partially integrated out. Namely, we investigate the four-body system via the RG cutoff parameter, which is the extent of the coarse-graining of the system, instead of the momentum variables of the correlation functions. Our results presented in Sec. 5.3 and 5.4 demonstrate the applicability of our FRG method in predicting the universal low-energy observables in Efimov physics.

Chapter 2

Efimov physics in ultracold atoms

In this chapter, we review the Efimov physics in ultracold atoms. In Sec. 2.2, we review the three-body physics of identical bosons with short-range resonant interactions and discuss experimental realizations of the Efimov effect in ultracold atoms. The renormalization-group (RG) limit cycle in the Efimov effect is also discussed. Then in Sec. 2.3, the Efimov effect in various systems is discussed to see its universality. Finally, theoretical and experimental study on the N-body extension of the Efimov effect is discussed in the last section.

2.1 Scattering theory and Feshbach resonance

Two-body elastic scattering

As a preliminary for the following sections, we start from an elastic scattering theory for short-range interactions. Let us consider the Schrödinger equation for relative motion of two particles:

$$\left[-\frac{\hbar^2}{2\mu_{12}}\Delta + V(r)\right]\psi_k(\mathbf{r}) = \frac{\hbar^2 k^2}{2\mu_{12}}\psi_k(\mathbf{r}), \tag{2.1}$$

where $\mu_{12} = \frac{m_1 m_2}{m_1+m_2}$ is the reduced mass of the two particles, $V(r)$ is a centrally symmetric interaction potential and $\frac{\hbar^2 k^2}{2\mu_{12}}$ is the energy eigenvalue. Because of the centrally symmetric nature of $V(r)$, a solution of the Schrödinger equation should be axially symmetric with respect to the direction of the incident particles. Also, a physical consideration suggests that the solution satisfies a boundary condition in the long-distance limit, where the solution should be a superposition of incident and scattering wave functions. Indeed, by assigning θ for the scattering angle and assuming that the direction of the incident particles is the z-axis, we obtain

$$\psi_k(\mathbf{r}) = e^{ikz} + f_k(\theta)\frac{e^{ikr}}{r}, \tag{2.2}$$

$$f_k(\theta) = \sum_{l=0}^{\infty}(2l+1)f_k^l P_l(\cos\theta), \tag{2.3}$$

where $f_k(\theta)$ is the scattering amplitude, P_l is the Legendre polynomial and f_k^l is the scattering amplitude for the l-th partial-wave channel. Here we note that the scattering amplitude $f_k(\theta)$ is

related to physical observables such as the differential cross section $\frac{d\sigma}{d\Omega}$ and the total cross section $\sigma(k)$ via

$$\frac{d\sigma}{d\Omega} = |f_k(\theta)|^2 , \tag{2.4}$$

$$\sigma(k) = 2\pi \int_0^\pi d\theta \, |f_k(\theta)|^2 \sin\theta = \frac{4\pi}{k^2} \sum_{l=0}^{\infty} (2l+1) \sin^2 \delta_l(k). \tag{2.5}$$

Under the partial-wave decomposition in Eq. (2.3), the l-th partial wave scattering amplitude f_k^l can be represented as

$$f_k^l = \frac{1}{k \cot \delta_l(k) - ik}, \tag{2.6}$$

where $\delta_l(k)$ is the phase shift of the wave function induced by the scattering.

Now let us consider the low-energy scattering at $k \simeq 0$. If the interaction potential $V(r)$ decreases more rapidly than $1/r^3$ in the long-distance limit[1], the phase shift $\delta_l(k)$ and the l-th wave scattering amplitude behave asymptotically as

$$\delta_l(k) \sim k^{2l+1}, \tag{2.7}$$

$$f_k^l \sim k^{2l}, \tag{2.8}$$

for sufficiently small k, showing that the s-wave (i.e. $l = 0$) scattering amplitude f_k^0 dominates the low-energy scattering amplitude. Due to the s-wave dominance, we can perform a low-energy expansion for the total scattering amplitude as

$$f_k(\theta) \simeq f_k^0 = \frac{1}{-\frac{1}{a} - ik + \frac{1}{2} r_{\text{eff}} k^2 + O(k^3)}, \tag{2.9}$$

where a is the s-wave scattering length, and r_{eff} is the effective range. Since we are interested in a strongly correlated regime, where exotic three-body phenomena occur, we here consider the unitarity limit, where the total cross section $\sigma(k)$ takes on its maximum value. Due to Eq. (2.5), $\sigma(k)$ becomes maximal when

$$\cot \delta_0(k) = 0. \tag{2.10}$$

The condition Eq. (2.10) is often called the unitarity limit since the total cross section saturates the upper bound imposed by the unitarity of the S-matrix.[2] If the scattering length a is much larger than the effective range r_{eff}, the phase shift becomes

$$\cot \delta_0(k) \simeq -\frac{1}{ak} \ll 1. \tag{2.11}$$

[1] If $V(r)$ does not decrease more rapidly than $1/r^3$, the effect of $V(r)$ becomes comparable to that of the centrifugal barrier, and a naive asymptotic analysis of the Schrödinger equation at $r \to \infty$ is no longer valid. In particular, the factor $(2l+1) f_k^l$ for any l contributes equally in Eq. (2.3) if $V(r) \gtrsim 1/r^3$.

[2] The S-matrix for the s-wave two-body scattering is given by $S(\mathbf{n}, \mathbf{n}') = e^{2i\delta_0(k)} = 1 + 2ikf_k(\mathbf{n}, \mathbf{n}')$, where $\mathbf{n}$ and $\mathbf{n}'$ are unit vectors whose relative angle is θ. On the other hand, the total cross section $\sigma(k)$ can be represented as $\frac{\pi}{k^2}(2 - S^\dagger(\mathbf{n}, \mathbf{n}) - S(\mathbf{n}, \mathbf{n}))$, which takes on the maximum value when $S(\mathbf{n}, \mathbf{n}') = e^{2i\delta_l(k)} = -1$. Thus we obtain $\sigma(k) \leq \frac{4\pi}{k^2}$ for the s-wave sector. We note that the bound is due to the unitarity of the S-matrix whose eigenvalues x satisfies $|x| = 1$.

for sufficiently small energy $k \ll \frac{1}{r_{\rm eff}}$, and, in particular, the s-wave scattering amplitude becomes

$$f_k(\theta) = \frac{1}{-\frac{1}{a} - ik}, \tag{2.12}$$

which reproduces the scattering amplitude of two-body scattering by a contact interaction. Since the two-body correlation can be calculated by the contact interaction in the low-energy limit irrespective of a given microscopic system, the parameter region of $a \gg r_{\rm eff}$ is often called the universal regime. Also, the region is often called the unitarity regime since the cross section $\sigma(k)$ almost saturates.

Feshbach resonance in ultracold atoms

In ultracold atoms, a technique using a Feshbach resonance is available to tune the s-wave scattering length a much larger than the effective range $r_{\rm eff}$, so that the low-energy two-body correlation is dominated by a. Here we briefly review the mechanism of the Feshbach resonance. Since atoms are prepared in their hyperfine states in ultracold atoms, let us first consider the situation where two atoms possess total-spin angular-momentum quantum numbers $(J_1, J_2) = (\alpha, \beta)$ or $(J_1, J_2) = (\alpha', \beta')$. We refer to the channels of $(J_1, J_2) = (\alpha, \beta)$ or $(J_1, J_2) = (\alpha', \beta')$ as the open channel and the closed channel, respectively. If the two atoms are located at a long distance, where the interaction between the two atoms are absent, the two states $|\alpha, \beta\rangle$ and $|\alpha', \beta'\rangle$ have different energies of $\epsilon_\alpha + \epsilon_\beta$ and $\epsilon_{\alpha'} + \epsilon_{\beta'}$, respectively, due to the hyperfine splitting. On the other hand, when the two atoms come close to each other, they begin to interact each other, where the interaction depends on the spins of their valence electrons:

$$V = V_s P_0 + V_t P_1, \tag{2.13}$$

where P_0 and P_1 are projection operators to the singlet and the triplet states, respectively. Therefore, two atoms prepared in the open channel can couple to a different state in the closed channel via the multi-channel interaction $V_{\rm mc} = P_{\alpha'\beta'} V P_{\alpha\beta}$, where $P_{\alpha\beta}$ and $P_{\alpha'\beta'}$ are projection operators onto the open channel and the closed channel, respectively. The situation is summarized in Fig. 2.1, where the second order (in $V_{\rm mc}$) process in the Lippmann-Schwinger equation produces the multi-channel-coupling contribution to the T-matrix element of the open-channel-atom scattering:

$$\langle \alpha\beta|T(E)|\alpha\beta\rangle \simeq \langle \alpha\beta|T_0(E)|\alpha\beta\rangle + \sum_n \frac{|\langle n; \alpha'\beta'|V_{\rm mc}|\alpha\beta\rangle|^2}{E - E_n + i\delta}, \tag{2.14}$$

where E is the energy of the two atoms, E_n is the energy of a molecular state $|n; \alpha'\beta'\rangle$[3] in the closed channel, and $T_0(E)$ is the T-matrix without multi-channel coupling. Due to the Zeeman effect, the hyperfine splitting $(\epsilon_\alpha + \epsilon_\beta) - (\epsilon_{\alpha'} + \epsilon_{\beta'})$ of the open channel and the closed channel can be tuned by an external magnetic field. As a consequence, the energy E_n of a closed-channel molecule can take on a value very close to $\epsilon_\alpha + \epsilon_\beta$, an therefore the scattering length a becomes resonantly large:

$$a \propto \langle \alpha\beta|T(E = \epsilon_\alpha + \epsilon_\beta)|\alpha\beta\rangle \propto \frac{1}{\epsilon_\alpha + \epsilon_\beta - E_n}. \tag{2.15}$$

[3] More precisely, $|n; \alpha'\beta'\rangle$ is an energy eigenstate of $P_{\alpha'\beta'} H P_{\alpha'\beta'}$, where H is the total Hamiltonian of the two atoms.

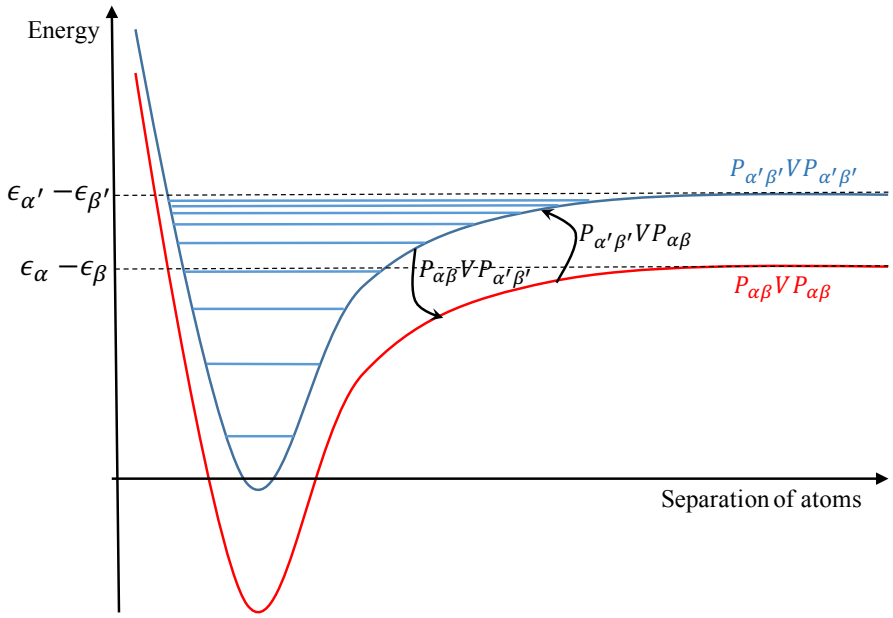

Figure 2.1: Schematic illustration of the Feshbach resonance. Red-colored and blue-colored curves show the interaction potentials between two atoms in the open channel ($(J_1, J_2) = (\alpha, \beta)$) and the closed channel ($(J_1, J_2) = (\alpha', \beta')$), respectively. Energy levels of the closed-channel molecules are schematically illustrated by the blue horizontal lines in the potential curve of $P_{\alpha'\beta'}VP_{\alpha'\beta'}$. At long distance, the energy of two atoms in the open channel and that in the closed channel are $\epsilon_\alpha + \epsilon_\beta$ and $\epsilon_{\alpha'} + \epsilon_{\beta'}$, respectively, due to the hyperfine splitting; on the other hand, at short distance, the two channels are coupled via the multi-channel interactions $V_{\rm mc} = P_{\alpha'\beta'}VP_{\alpha\beta}$ and $V_{\rm mc}^\dagger = P_{\alpha\beta}VP_{\alpha'\beta'}$, which produce a resonance in the T-matrix as in Eq. (2.14).

In particular, if $\epsilon_\alpha + \epsilon_\beta - E_n$ is linearized around the resonant magnetic field B_0, the scattering length a becomes $a \propto \frac{\Delta B}{B - B_0}$, where ΔB determines the width of the resonance. This is the mechanism of the Feshbach resonance. Experimentally, a Feshbach resonance in ultracold atoms was realized in ^{23}Na atoms by Inouye *et al.* [44] in 1998. They prepared a Bose-Einstein condensate of ^{23}Na atoms in an optical dipole trap[4] and located the resonant magnetic field B_0 by measuring a resonant loss of atoms from the trap with the phase-contrast imaging. They also measured the released energy $E_I \propto a$ from ^{23}Na-condensate by the time-of-flight absorption imaging to determine the scattering length a. A more detailed review of the experimental aspects of the Feshbach resonance can be found in Ref. [45].

[4] An optical dipole trap is often preferred to a magnetic trap in the collision studies since the Feshbach resonance may affect the trapping potential if we use a magnetic trap.

2.2 Efimov physics for identical bosons

2.2.1 Hyperspherical formalism and Faddeev equation

Attractive inverse square potential

As a starting point of our discussion, we follow Efimov's original discussion [10, 11] and consider three identical bosons with a short-range resonant interaction. For comprehensive reviews, we refer to Refs. [32, 26]. Since we are interested in the unitaity regime, where any two-body correlation is calculated by a contact interaction, we approximate interparicle interaction by the Lee-Huang-Yang pseudopotential [81]:

$$V(r) = \frac{4\pi\hbar^2 a}{m}\delta(\mathbf{r})\frac{\partial}{\partial r}(r\cdot), \tag{2.16}$$

where a is an s-wave scattering length. The pseudopotential can equivalently be implemented as a boundary condition for a many-body wave function when any two particles with distance r come close to each other:

$$\frac{\partial r\Psi}{\partial r} = -\frac{1}{a}r\Psi \text{ at } r = 0, \tag{2.17}$$

which is often referred to as the Bethe-Peierls boundary condition [82]. Based on this model, we solve the Schrödinger equation of three identical bosons in the center-of-mass frame:

$$\left(-\sum_{i=1}^{3}\frac{\hbar^2}{2m}\nabla_i^2 + \sum_{(i,j)=(1,2)(2,3)(3,1)} V(\mathbf{r}_i - \mathbf{r}_j)\right)\Psi(\mathbf{r}_1,\mathbf{r}_2,\mathbf{r}_3) = E\Psi(\mathbf{r}_1,\mathbf{r}_2,\mathbf{r}_3). \tag{2.18}$$

Firstly, in consideration of the Bose-Einstein statistics, we perform the Faddeev decomposition [83] for the three-particle wave function which is rewritten by the decomposition as

$$\Psi(\mathbf{r}_1,\mathbf{r}_2,\mathbf{r}_3) = \chi(\mathbf{r}_{12},\mathbf{r}_{12,3}) + \chi(\mathbf{r}_{23},\mathbf{r}_{23,1}) + \chi(\mathbf{r}_{31},\mathbf{r}_{31,2}), \tag{2.19}$$

where the function χ is the Faddeev component, r_{ij} and $r_{ij,k}$ are the Jacobi coordinates defined as

$$\mathbf{r}_{ij} := \mathbf{r}_i - \mathbf{r}_j, \tag{2.20}$$

$$\mathbf{r}_{ij,k} := \frac{2}{\sqrt{3}}\left(\mathbf{r}_k - \frac{\mathbf{r}_i + \mathbf{r}_j}{2}\right). \tag{2.21}$$

Here, (i, j, k) is a permutation of $(1, 2, 3)$. In solving the three-body Schrödinger equation (2.18), we have to deal with the Faddeev component χ which contains six independent variables $\mathbf{r}_{ij}$ and $\mathbf{r}_{ij,k}$, which can be mapped to more convenient hyperspherical coordinates given by

$$R := \sqrt{r_{ij}^2 + r_{ij,k}^2} = \sqrt{\frac{2}{3}\left(r_{12}^2 + r_{23}^2 + r_{31}^2\right)}, \tag{2.22}$$

$$\alpha_k := \arctan\left(\frac{r_{ij}}{r_{ij,k}}\right), \tag{2.23}$$

$$\hat{\mathbf{r}}_{ij} := \frac{\mathbf{r}_{ij}}{r_{ij}}, \quad \hat{\mathbf{r}}_{ij,k} := \frac{\mathbf{r}_{ij,k}}{r_{ij,k}}, \tag{2.24}$$

where (i, j, k) is a permutation of $(1, 2, 3)$, R is the hyperradius and α_k is the Delves hyperangle [84] that satisfies $0 \leq \alpha_k \leq \frac{\pi}{2}$. With the hypershperical coordinate, the Schrödinger equation for the Faddeev component $\chi(\mathbf{r}_{12}, \mathbf{r}_{12,3})$ becomes

$$-\frac{\hbar^2}{m}\left(\frac{\partial^2}{\partial R^2} + \frac{1}{R}\frac{\partial}{\partial R} + \frac{1}{R^2}\frac{\partial^2}{\partial \alpha_3^2} - \frac{\mathbf{L}_{12}^2}{R^2 \sin^2\alpha_3} - \frac{\mathbf{L}_{12,3}^2}{R^2\cos^2\alpha_3}\right)\chi_0(\mathbf{r}_{12}, \mathbf{r}_{12,3}) = E\chi_0(\mathbf{r}_{12}, \mathbf{r}_{12,3}), \quad (2.25)$$

where $\mathbf{L}_{12}$ and $\mathbf{L}_{12,3}$ are the angular momentum operator for $\hat{\mathbf{r}}_{12}$ and $\hat{\mathbf{r}}_{12,3}$, respectively, and the function χ_0 is defined by $\chi_0(\mathbf{r}_{12}, \mathbf{r}_{12,3}) := r_{12}r_{12,3}\chi(\mathbf{r}_{12}, \mathbf{r}_{12,3})$. Due to the general suppression of higher angular momentum at low energies, we concentrate on the s-wave sector of $\mathbf{L}_{12}$ and $\mathbf{L}_{12,3}$, and thus, the wave function χ_0 depends only on r_{12} and $r_{12,3}$ (or equivalently on R and α_3). At the unitarity limit where the scattering length diverges ($a = \pm\infty$), we can solve Eq. (2.25) by a separation of variables:

$$\chi_0(r_{12}, r_{12,3}) = F_s(R)\phi_s(\alpha_3). \quad (2.26)$$

By substituting Eq. (2.26) into Eq. (2.25), we arrive at the one-dimensional differential equations for F_s and ϕ_s:

$$\left[-\left(\frac{\partial^2}{\partial R^2} + \frac{1}{R}\frac{\partial}{\partial R}\right) - \frac{s_0^2}{R^2}\right]F_s(R) = -k^2F_s(R), \quad (2.27)$$

$$\frac{\partial^2}{\partial \alpha^2}\phi_s(\alpha) = s_0^2\phi_s(\alpha), \quad (2.28)$$

where $-k^2 = \frac{mE}{\hbar^2}$. We note that Eq. (2.27) is identical with the one-dimensional Schrödinder equation given by

$$\left(-\frac{\partial^2}{\partial R^2} - \frac{s_0^2 + \frac{1}{4}}{R^2}\right)\sqrt{R}F_s(R) = -k^2\sqrt{R}F_s(R), \quad (2.29)$$

which describes a particle, whose wave function is $\sqrt{R}F_s(R)$, moving in $R \in [0, \infty)$ under an inverse square attraction of $-\frac{s_0^2+\frac{1}{4}}{R^2}$. We can see a clear scale invariance in Eq. (2.27) or Eq. (2.29), in which a scale transformations of $R \to \lambda R$ and $k \to k/\lambda$ do not alter the form of the equation.

Discrete scale invariant energy spectrum at $a = \pm\infty$

We now solve Eqs. (2.27) and (2.28) at the unitarity limit $a = \pm\infty$. In solving Eqs. (2.27) and (2.28), we should note that the function ϕ_s satisfies the following two boundary conditions:

$$\phi_s\left(\frac{\pi}{2}\right) = 0, \quad (2.30)$$

$$\frac{\partial\phi_s}{\partial\alpha}(0) + \frac{8}{\sqrt{3}}\phi_s\left(\frac{\pi}{3}\right) = -\frac{R}{a}\phi_s(0), \quad (2.31)$$

where the first condition is obtained from $\chi_0(r_{12}, r_{12,3} = 0) = 0$ and the second condition is obtained by substituting Eqs. (2.26) and (2.19) into the Bethe-Peierls boundary condition in Eq. (2.17). If the scattering length does not diverge ($a \neq \pm\infty$), the second condition introduces the R dependence

to ϕ_s and the separation of variables in Eq. (2.26) is not justified. In the case of finite scattering length, we have to rely, in general, on the adiabatic hyperspherical approximation [85] in which $\phi_s(\alpha)$ and s_0 are replaced by $\phi_s(R,\alpha)$ and $s(R)$, respectively. Here we focus on the unitarity limit $a = \pm\infty$, where the solution of Eq. (2.28) under the boundary conditions in Eqs. (2.30) and (2.31) can be analytically obtained as

$$\phi_s(\alpha) \propto \sinh\left[s_0\left(\frac{\pi}{2}-\alpha\right)\right], \tag{2.32}$$

$$s_0 = \frac{8}{\sqrt{3}}\frac{\sinh\frac{s_0\pi}{6}}{\cosh\frac{s_0\pi}{2}}, \tag{2.33}$$

where the second equation has a unique real positive solution of $s_0 \simeq 1.00624$ ($e^{\pi/s_0} \simeq 22.694$), which is Efimov's scaling factor. Other imaginary solutions of Eq. (2.33) give rise to as repulsive inverse square potentials which support no bound state. The remaining radial Schrödinger equation (2.27) is the modified Bessel equation and its square-integrable solution becomes

$$F_s(k,R) \propto K_{is_0}(kR), \tag{2.34}$$

where K_ν is the modified Bessel functions of the second kind. Here the solution seems to allow an arbitrary value for k, reflecting the scale invariance of Eq. (2.27); however, a quantum anomaly explicitly breaks the continuous scale invariance of Eq. (2.27), leading to the discrete scale invariance. In deriving the quantum anomaly, or Efimov's discrete scale invariant energy spectrum, the hermiticity of the Hamiltonian, or equivalently the orthogonality of wave functions plays a crucial role. The orthogonality condition for the radial wave function is given by

$$\int_0^\infty dR\,\sqrt{R}F_s^*(k,R)\,\sqrt{R}F_s(k',R) = 0 \text{ if } k \neq k', \tag{2.35}$$

which leads to an additional short-range boundary condition as follows [86, 87]:

$$\left(\sqrt{R}F_s^*(k,R)\frac{d\,\sqrt{R}F_s^*(k',R)}{dR} - \sqrt{R}F_s^*(k',R)\frac{d\,\sqrt{R}F_s^*(k,R)}{dR}\right)_{R=0} = 0 \text{ if } k \neq k'. \tag{2.36}$$

By substituting the solution (2.34) into Eq. (2.36), we obtain the discrete energy eigenvalues:

$$k/k' = e^{n\pi/s_0}, \tag{2.37}$$

where n is an integer. Since the hermiticity of the Hamiltonian, or Eq. (2.35), is incompatible with the continuous scale invariance, the discretization of the energy spectrum is often referred to as a quantum scale anomaly. We note that the short-range boundary condition Eq. (2.36) fixes the value of the logarithmic derivative $\frac{d}{dR}\ln\left(\sqrt{R}F_s(R)\right)$, which, arises from the matching condition of wave functions in two regions $R \leq R_0$ and $R \geq R_0$ [11]:

$$\frac{d}{dR}\ln\left(\sqrt{R}F_s(k,R)\right)\Big|_{R=R_0} = \Lambda_0. \tag{2.38}$$

where R_0 determines a cutoff above which the inverse square profile of the three-body effective potential is justified. The parameter Λ_0 has the dimension of wave number and introduces a new

energy scale, thereby violating the scale invariance of Eq. (2.27). We note that the wave function $\sqrt{R}F_s(k,R)$ is real valued when R is sufficiently small, and thus $\sqrt{R}F_s^*(k,R) = \sqrt{R}F_s(k,R)$. With Eq. (2.38), we arrive at the energy spectrum as follows:

$$E_n = \frac{\hbar^2\Lambda_0^2}{m} e^{-2\theta/s_0} e^{2n\pi/s_0}, \tag{2.39}$$

$$\theta = -\frac{1}{2}s_0 \ln 2 - \frac{1}{2}\arg\frac{\Gamma(1+is_0)}{\Gamma(1-is_0)}. \tag{2.40}$$

Energy spectrum for $a \neq \pm\infty$

Aside from the unitarity limit, the separation of variables in Eq. (2.26) is not justified, and thus, $\phi_s(\alpha)$ and s_0 in Eqs. (2.27), (2.28), (2.30) and (2.31) should be replaced by $\phi_s(R,\alpha)$ and $s(R)$, respectively. In this case, $\phi_s(R,\alpha)$ satisfies

$$\phi_s(R,\alpha) \propto \sinh\left[s(R)\left(\frac{\pi}{2}-\alpha\right)\right], \tag{2.41}$$

$$-s(R) + \frac{8}{\sqrt{3}}\frac{\sinh\frac{s(R)\pi}{6}}{\cosh\frac{s(R)\pi}{2}} = -\frac{R}{a}\tanh\frac{s(R)\pi}{2}, \tag{2.42}$$

which reduce to Eqs. (2.32) and (2.33) if $R \ll a$. The radial Schrödinger equation is also modified from Eq. (2.27) as

$$\frac{\hbar^2}{m}\left[-\left(\frac{\partial^2}{\partial R^2}+\frac{1}{R}\frac{\partial}{\partial R}\right)-\frac{s(R)^2}{R^2}\right]F_s(R) = -\frac{\hbar^2k^2}{m}F_s(R), \tag{2.43}$$

in which the effective potential $-\frac{\hbar^2}{m}\frac{s(R)^2}{R^2}$ is determined from $s(R)$. In the long-distance limit $R \gg |a|$, Eq. (2.42) can be solved analytically and the functional form of $s(R)$ which gives the lowest lying potential $-\frac{s(R)^2}{R^2}$ in the radial Schrödinger equation can be obtained as

$$s(R) \sim \begin{cases} \frac{R}{a} + \frac{8}{\sqrt{3}}\exp\left(-\frac{\pi R}{3a}\right) & \text{when } a > 0, \\ 2i - \frac{12i}{\pi}\frac{|a|}{R} & \text{when } a < 0. \end{cases} \tag{2.44}$$

For these asymptotic solutions, the effective potential in the radial Schrödinger equation becomes

$$-\frac{\hbar^2}{m}\frac{s(R)^2}{R^2} \sim \begin{cases} \frac{\hbar^2}{m}\left[-\frac{1}{a^2} - \frac{16}{\sqrt{3}aR}\exp\left(-\frac{\pi R}{3a}\right)\right] & \text{when } a > 0, \\ \frac{\hbar^2}{m}\left[\frac{4}{R^2} - \frac{48|a|}{\pi R^3}\right] & \text{when } a < 0. \end{cases} \tag{2.45}$$

For positive scattering length $a > 0$, the energy threshold is shifted by the dimer energy $-\frac{\hbar^2}{ma^2}$, and this potential profile leads to a dissociation of a trimer if the trimer energy exceeds the dimer one. If the scattering length is negative, the repulsive barrier $\frac{4}{R^2}$ overwhelms the attractive one in the long-distance limit $R \gg |a|$, and the infinitely many shallow trimers, which appear at the unitarity limit, disappear. These observations suggest that the Efimov trimer is absent if the three-body energy satisfies $|E| \gtrsim \frac{\hbar^2}{ma^2}$. We thus obtain the lower bound of the trimer spectrum.

The above discussions are based on the Lee-Huang-Yang pseudopotential defined in Eq. (2.16), which assumes that the parameters other than the scattering length is negligible in two-body correlations. As we discussed in Sec. 2.1, the assumption is justified in the unitarity regime where the

effective range $r_{\rm eff}$ is much smaller than the scattering length a. In the unitarity regime, two-body correlations are universally determined by a at sufficiently low energy $|E| \ll \frac{\hbar^2}{mr_{\rm eff}^2}$. The observation gives an upper bound for the Efimov spectrum. We expect that an Efimov trimer becomes unbound if the trimer binding energy exceeds $\frac{\hbar^2}{mr_{\rm eff}^2}$, since the effective range $r_{\rm eff}$, in general, determines a distance inside which particles cannot come close to one another. We thus obtain the bound for energy spectrum:

$$\frac{\hbar^2}{mr_{\rm eff}^2} \gtrsim |E| \gtrsim \frac{\hbar^2}{ma^2}, \tag{2.46}$$

which leads to an estimation of the number N of Efimov trimers, originally given by Efimov [10]:

$$N \sim \frac{s_0}{\pi} \ln\left(\frac{a}{r_{\rm eff}}\right). \tag{2.47}$$

2.2.2 Renormalization group limit cycle

The discrete scale invariance of the Efimov trimer is closely related to the renormalization-group (RG) limit cycle. The connection between the Efimov effect and the RG limit cycle was firstly suggested in Ref. [88], where the authors prove that a self-adjoint extension, which is determined by the Bethe-Peierls boundary condition, of the three-particle-kinetic (Laplace) operator is scale periodic. Later, Bedaque *et al.* manifested the connection by performing a renormalization of the three-body physics [14, 15]. They develop a local effective field theory of a boson ψ and an auxiliary dimer d [5]:

$$\mathcal{L} = \psi^\dagger\left(i\partial_t + \frac{\nabla^2}{2}\right)\psi + \frac{g_2}{4}d^\dagger d - \frac{g_2}{4}\left(d^\dagger\psi^2 + {\psi^\dagger}^2 d\right) - \frac{g_3}{36}d^\dagger d\psi^\dagger\psi, \tag{2.48}$$

which, by eliminating the d field, reduces to

$$\mathcal{L} = \psi^\dagger\left(i\partial_t + \frac{\nabla^2}{2}\right)\psi - \frac{g_2}{4}\left(\psi^\dagger\psi\right)^2 - \frac{g_3}{36}\left(\psi^\dagger\psi\right)^3, \tag{2.49}$$

up to the three-body sector. Here we employ the units $\hbar = m = 1$, where m is the mass of a boson. By summing up ladder-type Feynman diagrams of the effective field theory, we can reproduce the Skornyakov-Ter-Martirosian equation [8], which is an exact three-body scattering equation, for the particle-dimer s-wave scattering amplitude $T(E; p, q)$:

$$\begin{aligned} T(E;p,q) &= \frac{16\pi}{a}\left(\frac{1}{2pq}\ln\frac{p^2+q^2+pq-E}{p^2+q^2-pq-E} - \frac{g_3}{9g_2^2}\right) \\ &\quad + \frac{4}{\pi}\int_0^\Lambda dl\, l^2\left(\frac{1}{2pl}\ln\frac{p^2+l^2+pl-E}{p^2+l^2-pl-E} - \frac{g_3}{9g_2^2}\right)\frac{T(E;l,q)}{-1/a + \sqrt{3l^2/4-E}}, \end{aligned} \tag{2.50}$$

where a is the s-wave scattering length and Λ is the ultraviolet (UV) cutoff. The renormalization is performed so that the physical quantity $T(E; p, q)$ approaches a limit as an inverse power of the UV

[5] We here follow the discussion by Braaten and Hammer [32] with a modification.

cutoff Λ in the limit $\Lambda \to \infty$. To understand the UV behavior of the scattering amplitude, the authors of Refs. [14, 15] perform an asymptotic analysis in the parameter region of $\Lambda \gg p \gg q$, $\sqrt{E}, 1/|a|$ and $g_3 = 0$. In this parameter region, $T(E; p, q) = T(p)$ satisfies

$$T(p) = \frac{4}{\sqrt{3}\pi p} \int_0^\infty dl \ \ln \frac{p^2 + l^2 + pl}{p^2 + l^2 - pl} T(l), \tag{2.51}$$

where $T(p)$ can be identified with the Bethe-Salpeter wave function of the zero-energy particle-dimer scattering at the unitarity limit. Here $T(p)$ has an asymptotic solution of

$$T(p) = Ap^{-1+is_0} + Bp^{-1-is_0}, \tag{2.52}$$

where $s_0 \simeq 1.00624$ is Efimov's scaling parameter, A and B are constants. Now we consider Eq. (2.50) with nonzero g_3, and impose the condition that the constants A and B in Eq. (2.52) are independent of the UV cutoff Λ. By substituting Eq. (2.52) into Eq. (2.50), and by neglecting $E, q, 1/a$, we obtain

$$0 = \frac{8}{\sqrt{3}\pi} \int_\Lambda^\infty dl \left(Al^{-2+is_0} + Bl^{-2-is_0} \right) + \frac{8}{\sqrt{3}\pi} \frac{g_3}{9g_2^2} \int_0^\Lambda dl \left(Al^{is_0} + Bl^{-is_0} \right), \tag{2.53}$$

where we make use of the facts that Eq. (2.52) satisfies Eq. (2.51), and that $p/\Lambda \ll 1$. Since the constants A and B are Λ independent, g_3 must satisfy

$$\frac{g_3}{9g_2^2} = \frac{1}{\Lambda^2} \frac{\frac{A}{-1+is_0}\Lambda^{is_0} + \frac{B}{-1-is_0}\Lambda^{-is_0}}{\frac{A}{1+is_0}\Lambda^{is_0} + \frac{B}{1-is_0}\Lambda^{-is_0}}. \tag{2.54}$$

If we define a dimensionless three-body coupling constant $H(\Lambda)$ by $H(\Lambda) = -\Lambda^2 \frac{g_3}{9g_2^2}$, $H(\Lambda)$ becomes a log-periodic function of Λ with Efimov'sscaling factor, i.e.

$$H(\Lambda e^{\pi/s_0}) = H(\Lambda), \tag{2.55}$$

which represents the RG limit cycle of the three-body system parameter. In particular, one period of the limit cycle e^{π/s_0} represents the discrete scale invariance of the Efimov effect. In Refs. [14, 15], Bedaque *et al.* also numerically demonstrate that physical observables such as the trimer-binding energy and the s-wave phase shift become independent of the cutoff under the renormalization in Eq. (2.54); they show the (non-perturbative) renormalizability of the effective field theory Eq. (2.48).

2.2.3 Experimental realization in ultracold atoms

The Efimov effect was first observed in ultracold atoms that are trapped in a vacuum chamber by an optical dipole trap. Here atoms are lost from the optical dipole trap due to a three-body recombination process in which three atoms collide to form a diatomic molecule and an atom. Through the recombination process, the diatomic molecule and the atom can go out of the trap due to the released binding energy of the diatomic molecule which turns into the kinetic energy of the three particles. In particular, the particle-number density n in the trapping potential obeys

$$\frac{dn(t)}{dt} = -L_3 n(t)^3, \tag{2.56}$$

where L_3 is the three-body loss rate coefficient. On the right-hand side of Eq. (2.56), the number of the three-body recombination process is set to be proportional to $n(t)^3$ which parametrizes the collision probability of three atoms. If the scattering length a is negative, three atoms collapse into an atom and a deep dimer through the recombination process. In particular, when an Efimov trimer merges to the three-atom continuum, the overlap between the wave function of an Efimov trimer and that of scattering states becomes large. A large overlap of the wave functions enhances three-body inelastic scattering due to the Fermi's golden rule. As a result, the loss rate L_3 at zero temperature becomes [89, 32]

$$L_3 \simeq n_l \frac{4590 \sinh(2\eta)}{\sin^2\left(s_0 \ln \frac{a}{a_-}\right) + \sinh^2 \eta} \frac{\hbar a^4}{m}, \tag{2.57}$$

where $a_- < 0$ is the value of the scattering length a at which an Efimov trimer merges into the three-atom continuum and η is the inelasticity parameter which parametrizes the transition probability from three atoms to a deep dimer and an atom. The constant n_l is the number of atoms lost per recombination event and $n_l = 3$ for cold gases.[6] In addition to the recombination process at $a < 0$, three atoms can also collapse into an atom and a shallow dimer with energy $\sim 1/a^2$, if the scattering length a is positive. In this case the loss rate L_3 becomes [89, 32]

$$L_3 \simeq n_l \left\{ 67.12 e^{-2\eta} \left[\sin^2\left(s_0 \ln \frac{a}{a_*} + 1.67 \right) + \sinh^2 \eta \right] + 16.84(1 - e^{-4\eta}) \right\} \frac{\hbar a^4}{m}, \tag{2.58}$$

where $a_* > 0$ is the value of the scattering length at which an Efimov trimer merges into the atom-dimer continuum. a_* and a_- in Eq. (2.57) are related via $a_-/a_* \simeq 22.0 e^{n\pi/s_0}$, where n is an integer [32]. We can see that Eqs. (2.57) and (2.57) both exhibit the log-periodic dependence on the scattering length a, reflecting the discrete scale invariance of the Efimov effect as firstly suggested by Esry *et al.* [46]. In particular, L_3 has peaks at $a = a_-$ and a_* due to an enhanced inelastic three-body scattering.

After 40 years from Efimov's first prediction, Nägerl and Grimm's group at Innsbruck firstly observed a peak of L_3 and determined $a_- < 0$ [47] in ultracold ^{133}Cs atoms, and subsequently they located $a_* > 0$ by studying an atom-dimer inelastic scattering [48]. Later, L_3 for both negative and positive scattering lengths was studied [49] in ^{39}K atoms by the group of Modugno and Inguscio at LENS (see, however, Ref. [92], where the value of a_- is corrected). They found two peaks (dips) of L_3 in the positive a region and obtained the scaling factor of 26.7(0.9) that is larger than the theoretical prediction of 22.694. They also determined the value $a_-/a_* \simeq -22(2)$ which agrees with the theoretical value of $a_-/a_* \simeq 22.0 e^{n\pi/s_0}$ [32]. Moreover, L_3 was measured in ^{7}Li atoms to determine a_- and a_* by the group of Khaykovich at Bar-Ilan university [51] and by the group of Hulet at Rice university [50] (see, however, Ref. [93] where the values of a_- and a_* are corrected.). More recently, the group at Innsbruck found the second loss peak in the negative a region and obtained a scaling factor of 21.0(1.3).

[6] For Bose-Einstein condensates, $n_l = 1/2$ [90, 91], due to the symmetrization factor $1/3!$ of the condensate wave function.

2.3 Universality of Efimov physics

Since a resonant two-body interaction always produces an attractive inverse square profile of the three-body effective potential, the Efimov effect is expected to appear in various three-body systems. Therefore, researchers have tried to extend the universality of the Efimov effect to a variety of physical systems. So far, a number of theoretical efforts have been devoted to extend the universality in higher partial-wave sectors, fermionic systems, mass-imbalanced systems, particles in mixed dimensions, and four or more particles. In this section, we briefly summarize the results without derivation.

2.3.1 Bosons in 3d

AAB systems

One of the simplest extensions of the Efimov effect is to consider two identical bosons AA that interact with a distinguishable particle B, which can be a boson or a fermion. Such a system is often referred to as the AAB system, and is a natural extension that can be realized in ultracold atoms, where the interaction between two species of atoms can be tuned by a Feshbach resonance. For AAB systems, the mass ratio $\alpha = m_A/m_B$ between the two species are varied and the Efimov effect is found to occur. In particular, Efimov's scaling factor s_0 is found to depend on the mass ratio α [11] by the following transcendental equation:

$$1 = \frac{1}{\sin\theta\cos\theta}\frac{1}{is_0}\frac{\sin is_0\theta}{\cos\frac{is_0\pi}{2}}, \tag{2.59}$$

where $\theta = \arcsin\frac{\alpha}{\alpha+1}$. Equation (2.59) can be obtained by the same procedure as the identical bosons, for which the Bethe-Peierls boundary condition gives rise to as the transcendental equation. We should note that Eq. (2.59) has a unique real positive solution of s_0, which produces the Efimov's inverse square attraction of $-\frac{s_0^2}{R^2}$. Therefore, the Efimov effect can occur for an arbitrary mass ratio α in the AAB systems with bosonic A particles. In particular, for an extremely large mass ratio, $\alpha \to \infty$, scaling factor s_0 approaches ∞, leading to a very dense trimer energy spectrum. In other words, we can expect larger number of Efimov trimers in AAB systems than in identical bosons, if the mass ratio is large. Such a behavior can be understood in the following manner. For an extremely large mass ratio, the motion of the heavier particles is much slower than the lighter one, and thus, we can use the Born-Oppenheimer approximation [94]. In the approximation, three-body wave function is decomposed into $\phi_{AA}(\mathbf{R})\phi_B(\mathbf{R},\mathbf{r})$, where $\phi_{AA}(\mathbf{R})$ describes the relative motion of the two heavier particles AA, and $\phi_B(\mathbf{R},\mathbf{r})$ describes the motion of the lighter particle B with a fixed configuration for the heavier particles. The Schrödinger equation is considered in the center-of-mass frame of the two heavier particles:

$$-\frac{\hbar^2\nabla_{\mathbf{r}}^2}{2m_B}\phi_B(\mathbf{R},\mathbf{r}) = -\frac{\hbar^2\kappa(\mathbf{R})^2}{2m_B}\phi_B(\mathbf{R},\mathbf{r}), \tag{2.60}$$

$$\left(-\frac{\hbar^2\nabla_{\mathbf{R}}^2}{m_A} - \frac{\hbar^2\kappa(\mathbf{R})^2}{2m_B}\right)\phi_{AA}(\mathbf{R}) = E\phi_{AA}(\mathbf{R}), \tag{2.61}$$

where $\mathbf{R}$ is the relative coordinate between the two heavier particles A and $\mathbf{r}$ is the relative coordinate of the lighter particle B. The first equation for ϕ_B leads to

$$\phi_B(\mathbf{R},\mathbf{r}) = \frac{\exp\left(-\kappa(\mathbf{R})\,|\mathbf{r}-\mathbf{R}/2|^2\right)}{|\mathbf{r}-\mathbf{R}/2|} + \frac{\exp\left(-\kappa(\mathbf{R})\,|\mathbf{r}+\mathbf{R}/2|^2\right)}{|\mathbf{r}+\mathbf{R}/2|}. \tag{2.62}$$

By substituting Eq. (2.62) into the Bethe-Peierls boundary condition Eq. (2.17), we obtain

$$\kappa(\mathbf{R}) - \frac{\exp[-\kappa(\mathbf{R})R]}{R} = \frac{1}{a}, \tag{2.63}$$

which, at the unitarity limit, leads to

$$\kappa(\mathbf{R}) \simeq \frac{0.567143}{R}. \tag{2.64}$$

Thus, the Schrödinger equation (2.61) becomes

$$\left(-\frac{\hbar^2\nabla^2_{\mathbf{R}}}{m_A} - 0.321651\frac{\hbar^2}{2m_BR^2}\right)\phi_{AA}(\mathbf{R}) = E\phi_{AA}(\mathbf{R}), \tag{2.65}$$

where the motion of a lighter particle gives rise to as an effective interaction $-\frac{\hbar^2}{m_BR^2}$ between heavier particles, while the motion of heavier particles amounts to the energy of $-\frac{\hbar^2\nabla^2_{\mathbf{R}}}{m_A}$. Since the interaction term scales as $m_A/m_B \gg 1$ compared with the kinetic term, the interaction becomes effectively deep for the large mass ratio. The three particles are urged to become bound because of the enhanced interaction.

Experimentally, a mixture of ^{40}K and ^{87}Rb was investigated by the group of Jin at JILA [57]. They identified a peak of atomic loss originating in the atom-dimer recombination, and determined $a_* > 0$, while they found no peak for negative Rb-K scattering length. The group of Inouye at Tokyo found an atom-dimer resonance $a_* > 0$ in a mixture of ^{41}K and ^{87}Rb [58].[7] Later, the group of Chin at Chicago [59] and the group of Weidemüller at Heidelberg [60] investigated an ultracold ^{133}Cs-^{6}Li mixture by measuring the three-body loss rate L_3. Both groups observed several loss peaks for negative scattering lengths and obtained the scaling factor e^{π/s_0} of 5.07(6)(13)(2) [60] and 4.9(4) [59][8], the latter being close to the theoretical value of 4.88.

Higher partial waves

For AAB systems with large mass ratio $\alpha = m_A/m_B$, higher partial wave sectors are known to support Efimov's discrete scale invariant trimers. To understand the essence, we employ the Born-Oppenheimer picture, in which Eq. (2.65) can be rewritten as

$$\left[-\frac{\partial^2}{\partial R^2} - \frac{2}{R}\frac{\partial}{\partial R} - \left(\frac{0.321651}{2}\frac{m_A}{m_B} - l(l+1)\right)\frac{1}{R^2}\right]\phi_{AA}(\mathbf{R}) = \frac{m_AE}{\hbar^2}\phi_{AA}(\mathbf{R}), \tag{2.66}$$

[7] The LENS group reported a signature of the Efimov effect in ultracold ^{87}Rb-^{41}K mixture [95]. They observed two peaks of atomic loss at negative Rb-K scattering lengths, and identified them with the emergence of RbRbK and KKRb Efimov trimers by studying the ratio of lost K and Rb. However, the results have not yet been reproduced by other groups [96].

[8] The Chicago group obtained three loss peaks, where the measured ratio of scattering lengths between the first and second peaks was 5.1(2), and that for the second and third peaks was 4.8(7).

where l is the relative angular-momentum quantum number for two heavier particles. As we can see, for a large mass ratio $\alpha = \frac{m_A}{m_B}$, the attractive inverse square potential $-\frac{0.321651}{2}\frac{m_A}{m_B}\frac{1}{R^2}$ overwhelms the centrifugal potential barrier $\frac{l(l+1)}{R^2}$ and the total potential supports Efimov trimers. In particular, we obtain a critical mass ratio $\alpha^* = \frac{2l(l+1)}{0.321651}$ above which Efimov trimers in the l-th wave sector emerge. We should note that the wave function $\phi_{AA}(\mathbf{R})$ should have even parity due to the bosonic nature of the heavier particles A. Therefore, the angular momentum of l=(even) can support Efimov trimers in bosonic AAB systems.

We can sophisticate the above discussion by the adiabatic hyperspherical approximation introduced in Sec. 2.2.1. In particular, the Bethe-Peierls boundary condition Eq. (2.17) gives rise to a transcendental equation of Efimov's scaling factor s_l for the higher partial-wave sector in the bosonic AAB systems:

$$\begin{aligned} 1 \;=\; & \frac{(-1)^l}{\sin 2\theta}\sum_{k=0}^{k_{\max}}\frac{(2l-2k)!}{(l-k)!k!}\frac{(-1)^k}{2^{2l-2k}\sin^{l-2k}\theta} \\ & \times\sum_{m=0}^{l-2k}\frac{1}{m!(l-2k-m)!}\frac{2}{is_l+2m-l+2k}\frac{\sin\left[(is_l+2m-l+2k)\theta\right]}{\cos\left[(is_l+2m-l+2k)\frac{\pi}{2}\right]}, \end{aligned} \tag{2.67}$$

where $\theta = \arcsin\frac{\alpha}{\alpha+1}$, l is the angular-momentum quantum number[9] and

$$k_{\max} = \begin{cases} l/2 & \text{for even } l, \\ (l-1)/2 & \text{for odd } l. \end{cases} \tag{2.68}$$

Equation (2.67) admits no real positive s_l for odd l, prohibiting attractive inverse square interaction. Also, the scaling factor s_l tends to increase as the mass ratio $\alpha = m_A/m_B$ becomes large. The results are in favor of the above-mentioned intuitive discussions based on the Born-Oppenheimer approximation. For the even partial-wave sectors, the critical mass ratios α^* are obtained as

$$\alpha^* \simeq 38.630 \text{ (l=2)}, \alpha^* \simeq 125.765 \text{ (l=4)}, \cdots, \tag{2.69}$$

above which the Efimov trimers emerge.

2.3.2 Fermions in 3d

AAB systems

For identical fermions, the Pauli principle prohibits the s-wave interaction between particles. The simplest fermionic extension of the Efimov effect is, thus, considered in two component fermions, where two identical fermions AA interact resonantly with an additional distinguishable particle B, which can be a boson or a fermion. Efimov's scaling factor s_l for the fermionic AAB system can

[9]For general AAB systems, the angular momentum is defined by $\mathbf{L}_{12,3}$ in Eq. (2.25). In Eq. (2.25), $\mathbf{L}_{12}$ should vanish because of the Bethe-Peierls boundary condition, which guarantees the s-wave configuration of scattering two particles.

be obtained by

$$1 = -\frac{(-1)^l}{\sin 2\theta}\sum_{k=0}^{k_{\max}}\frac{(2l-2k)!}{(l-k)!k!}\frac{(-1)^k}{2^{2l-2k}\sin^{l-2k}\theta} \times\sum_{m=0}^{l-2k}\frac{1}{m!(l-2k-m)!}\frac{2}{is_l+2m-l+2k}\frac{\sin\left[(is_l+2m-l+2k)\theta\right]}{\cos\left[(is_l+2m-l+2k)\frac{\pi}{2}\right]}, \tag{2.70}$$

which differs from Eq. (2.67) by an additional minus factor on the right-hand side. Recalling the discussions based on the Born-Oppenheimer approximation for bosonic AAB systems, we expect that fermionic AAB systems can support Efimov trimers only for odd angular momentum quantum numbers l. Indeed, the transcendental equation (2.70) allows a unique real positive solution for s_l only for odd l. For the odd partial wave sectors, the critical mass ratios α^* are obtained as

$$\alpha^* \simeq 13.607 \text{ (l=1)}, \alpha^* \simeq 75.994 \text{ (l=3)}, \cdots, \tag{2.71}$$

above which the Efimov trimers emerge.

Kartavtsev-Malykh trimer and crossover trimer

We see in Eq. (2.71) that fermionic AAB systems with mass ratio $\alpha = m_A/m_B$ larger than 13.607 support p-wave Efimov trimers. Kartavtsev and Malykh noticed that the system can support trimer states even below the critical mass ratio. To see this, we rely on the Born-Oppernheimer approximation. For a positive scattering length a, Eq. (2.63) leads to the effective potential in Eq. (2.66) as

$$\begin{cases} -\frac{\alpha}{a^2}-\frac{2\alpha}{a}\frac{\exp(-R/a)}{R}+\frac{2}{R^2} & (R\gtrsim a), \\ \frac{2-0.160826\alpha}{R^2} & (R\lesssim a), \end{cases} \tag{2.72}$$

which becomes attractive in the long-range regime $R \gtrsim a$ while it becomes repulsive in the short-range regime $R \lesssim a$. Since the depth of the attraction potential is of order $\frac{1}{a^2}$, one can expect that the attraction support trimer states with the binding energy of $\sim \frac{1}{a^2}$. Kartavtsev and Malykh have sophisticated this idea by the hyperspherical formalism introduced in Sec. 2.2.1, and have shown that there appears one trimer for $8.173 \lesssim \alpha \lesssim 12.917$ and two trimers for $12.917 \lesssim \alpha \lesssim 13.607$. They also show that the energies of those trimers are proportional to $\frac{1}{a^2}$. The trimer states are often called the Kartavtsev-Malykh trimers or the universal trimers, since the energies are determined only by the scattering length a irrespective of a given microscopic three-body system. Later, Endo *et al.* investigated the connection between the Kartavtsev-Malykh trimers and the Efimov trimers and proposed a crossover trimer scenario: As we decrease the scattering length a, a Kartavtsev-Malykh trimer continuously turn into a crossover trimer, which depends not only on the scattering length a but also on the one-parameter three-body boundary condition in Eq. (2.38). For increasing mass ratio $\alpha \lesssim 13.607$, two Kartavtsev-Malykh trimers become crossover trimers even for a large scattering length, and finally turn into the ground and the first excited Efimov trimers.

Three distinguishable fermions

A simple but important extension is the Efimov effect in three distinguishable fermions with equal mass. In this case, the Efimov effect can occur only in the s-wave sector. In particular, if the three particles interact resonantly, the scaling factor s_0 is determined from

$$0 = \left[\cos\left(\frac{is_0\pi}{2} + \frac{4}{\sqrt{3}}\frac{\sin\left(\frac{is_0\pi}{6}\right)}{is_0}\right)\right]^2 \left[\cos\left(\frac{is_0\pi}{2} - \frac{8}{\sqrt{3}}\frac{\sin\left(\frac{is_0\pi}{6}\right)}{is_0}\right)\right], \tag{2.73}$$

which gives the same scaling factor $s_0 \simeq 1.00624$ as the identical bosons (see Eq. (2.33)). The result is important for an application to the three-component ultracold ^{6}Li atoms, for which the scattering lengths between three particles are approximately tuned to their resonances. Indeed, an atomic loss resonance due to the Efimov trimers was observed in the three-component ^{6}Li atoms by the group of O'Hara at Pennsylvania [97, 98], the group of Jochim at Heidelberg [99, 100] and the group of Mukaiyama at Tokyo [101]. Later, the group at Heidelberg [102] and the group at Tokyo [103] directly measured the bound-state energy of an Efimov trimer.

2.3.3 Dimensional extension

Mixed dimensions

For identical bosons, it has been shown that the Efimov effect can occur only in the dimension d over $2.30 < d < 3.76$ [104]. In one dimension, there appears one trimer state whose energy E depends on the one-dimensional scattering length $a_{1\mathrm{d}}$ as $E = -\frac{4\hbar^2}{ma_{1\mathrm{d}}^2}$ [105, 106]. In two dimensions, two trimers emerge and the trimer energies E_1 and E_2 are given [107] by $E_1 = -66.08e^{-\gamma}\frac{\hbar^2}{ma_{2\mathrm{d}}^2}$ and $E_2 = -5.068e^{-\gamma}\frac{\hbar^2}{ma_{2\mathrm{d}}^2}$, respectively, where $a_{2\mathrm{d}}$ is the two-dimensional scattering length and γ is the Euler's constant.[10]

The situation motivates Nishida and Tan to address the question of "how can we liberate the Efimov physics from $3d$?" [56]. To answer the question, they introduced the concept of the mixed dimensions where different species of particles live in different dimensional space. As we see in Sec. 2.2.1, the Efimov effect originates in the attractive inverse-square interaction that is a consequence of the scale invariant nature of the short-range Bethre-Peierls boundary condition in Eq. (2.17) at the unitarity limit $a = \pm\infty$. In addition, to support an infinitely shallow trimer state, the Bethre-Peierls boundary condition should ensure an increasing probability that the two particles come close to each other. Based on these considerations, Nishida and Tan point out the uniqueness of $3d$. Here we briefly follow their discussions.

The D-dimensional radial Schrödinger equation for two particles interacting via a contact interaction is given by

$$\left(-\frac{\partial^2}{\partial r^2} - \frac{D-1}{r^2}\frac{\partial}{\partial r} + \frac{L(L+D-2)}{r^2}\right)\psi_L(r) = k^2\psi_L(r), \tag{2.74}$$

[10] By using a harmonic confinement potential with a variable trap frequency, Levinsen *et al.* investigated how the two trimers in $2d$ evolve into the Efimov trimers in $3d$. They found that the two Kartavtsev-Malykh-like trimers in $2d$ evolve into the ground and the first excited Efimov trimers; however, due to the harmonic confinement potential, the two states never merge into the three-particle continuum unlike in free space without confinement.

B \ A	3D		2D		1D	
	Bosons	Fermions	Bosons	Fermions	Bosons	Fermions
3D	✓	13.6	✓	6.35	✓	2.06
2D	✓	28.5	✓	11	✓	×
1D	✓	155	✓	×		

Figure 2.2: AAB systems in mixed dimensions. Presence ✓ and absence × of Efimov trimers are presented for the $l = 0$ sector of bosonic AAB system and for the $l = 1$ sector of the fermionic AAB system. If there is a critical mass ratio, above which Efimov trimers appear, the mass ratio is explicitly presented. The figure is adapted from Ref. [56]

where $r \neq 0$, L is the D-dimensional angular-momentum quantum number and $L(L+D-2)$ gives an eigenvalue of the Laplace-Beltrami operator on the $(D-1)$-sphere. The radial Schrödinger equation has the asymptotic solution of $\psi_L(r) = r^b (r \to 0)$ with $b = L, -(D+L-2)$. For the solution, we find the following condition:

$$0 < D + L - 2 < D/2, \tag{2.75}$$

where the first inequality ensures an increasing probability that the two particles come close to each other and the second inequality ensures the square integrability of the solution. We immediately notice that the condition can be satisfied only when $D = 3$ and $L = 0$.

An important point here is that what matters is not the spatial dimension $D = 3$ but the dimension of the relative motion of two particles. Therefore, Nishida and Tan consider two particles A and B that live in D_A- and D_B-dimensional spaces, respectively. The two spaces are assumed to share a $D_\parallel$-dimensional intersection. In the system, the relative motion of the two particles are described by a $D = (D_A + D_B - D_\parallel)$-dimensional vector, since the total momentum in the direction of the common intersection is conserved. The condition of $D = 3$ restricts the possible sets to $(D_A, D_B, D_\parallel)$ as $(D_A, D_B, D_\parallel) = (3,3,3), (3,2,2), (3,1,1), (2,3,2), (2,2,1), (2,1,0), (1,3,1), (1,2,0)$. For these eight sets of dimensions, bosonic AAB systems with even parity ($l = 0$) and fermionic AAB systems with odd parity ($l = 1$) are investigated and the result is summarized in Fig. 2.2. Remarkably, for a fixed mass ratio $\alpha = m_A/m_B$, Efimov's scaling factor tends to decrease as we strengthen the confinement of A particles. Nishida and Tan call this phenomena the confinement-induced Efimov effect.

Super Efimov effect in 2d

An interesting extension can be found in two dimensions where three identical fermions interact via a resonant p-wave interaction. Nishida *et al.* [108] demonstrate that the system supports an infinite series of trimer states that exhibit a double exponential scaling. That is, the energy E_n of the n-th trimer is found to satisfy

$$E_n = E_* \exp\left[-2\exp\left(\frac{3\pi n}{4} + \theta\right)\right], \tag{2.76}$$

where E_* and θ are determined from short-range details of the system. Because of the double exponential scaling, the effect is called the super Efimov effect, that is yet to be observed because of the large ratio of $\ln E_{n+1}/\ln E_n \simeq 10.6$. The second excited super Efimov trimer exceeds the size of the universe even if the size of the lowest-lying trimer is of the order of atomic size $\sim$ 10nm. Moroz et al. [109] generalize the super Efimov effect to AAB systems, which are found to decrease the ratio $\ln E_{n+1}/\ln E_n$ as we increase the mass ratio m_A/m_B.

2.4 N-body extension

In this section, we review extensions of the Efimov effect to N-particle systems. Firstly, the four-body physics for identical bosons, which are of our particular interest, is reviewed. Efforts to extend the Efimov physics to five or more particles are also briefly summarized. Finally, we give a brief summary for the N-body extension for systems other than identical bosons.

2.4.1 Identical bosons

Tetramers tied to Efimov trimers

In 1973, Amado and Greenwood investigated an extension of the Efimov effect to four identical bosons, and showed that the existence of a zero-energy Efimov state does not support an infinite series of four-body bound states, by showing that the trace of the kernel of the four-body Bethe-Salpeter (Faddeev) equation does not diverge [110]. Adhikari *et al.* [111] showed perturbative non-renormalizability of the non-relativistic N-boson problem: Within a perturbation theory, an increasing number of fitting parameters are necessary as we increase N so that we can obtain a finite N-body correlation functions. The results by Adhikari *et al.* suggests that low-energy observables in $N \geq 4$-body physics depend on the short-range parameters of a given Hamiltonian, even the low-energy three-body observables are parametrized universally by the scattering length and the three-body parameter.

The energy spectrum and the low-energy universality of resonantly interacting four bosons are first investigated by Platter, Hammer and Meißner [61, 62], based on the Faddeev-Yakubovski equation [112], which is a generalization of the Faddeev equation (see Sec. 2.2.1). They applied the Faddeev-Yakubovski equation to an effective field theory of four bosons interacting via effective contact two- and three-body interactions whose coupling constants are renormalized by the two- and three-body binding energies, and showed that there appear two tetramer states tied to the ground Efimov trimer. In particular, they showed that the binding energies of the tetramers are independent of the UV cutoff once the renormalization of the two- and three-body sectors are completed, in favor of the existence of universality in four-body physics: Low-energy four-body observables are also determined by the scattering length and the three-body parameter irrespective of the short-range details of a given microscopic system.[11] In other words, the results by Platter, Hammer and

[11] Later, Yamashita *et al.* [63, 64] introduced an additional four-body interaction to the effective field theory and showed a four-body coupling dependence of the tetramer energies; however, the non-universality was discussed for tightly bound tetramers in the high-energy regime where observables depend on the short-range details of a given

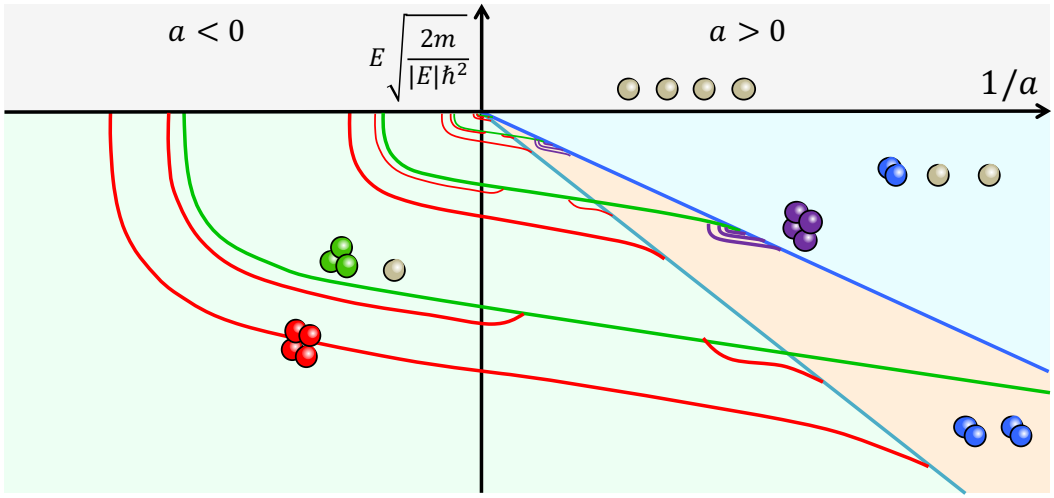

Figure 2.3: Schematic illustration of the energy spectrum as a function of the inverse scattering length $1/a$. The atom-atom-dimer (blue-colored curve), dimer-dimer (sky-blue-colored curve) , and atom-trimer (green-colored curves) thresholds are presented. In particular, tied to a atom-trimer threshold, we find two tetramer states (red-colored curves) one of which merges into the atom-trimer threshold in some positive scattering-length region. Also, we find atom-atom-dimer Efimov trimers (purple curves) below the atom-atom-dimer threshold. The figure is reproduced from [74]

Meißner [61, 62] provide a numerical evidence of the non-perturbative renormalizability of their effective field theory, while the effective field theory is perturbatively non-renormalizable [111]. Hammer and Platter also conjectured [62] that the two tetramer resonances are tied to every Efimov trimer. The conjecture and the universality were manifested by von Stecher *et al.* [65] by adiabatic hyperspherical approximation (see Sec. 2.2.1) of the four-body Schrödinger equation. In particular, at the unitarity limit of $a = \pm\infty$, they obtain a ratio between three- and four-body binding energies as

$$E^{(n)}_{4b,1} = 4.58E^{(n)}_{3b}, E^{(n)}_{4b,2} = 1.01E^{(n)}_{3b}, \tag{2.77}$$

where $E^{(n)}_{3b}$ is the energy of the n-th Efimov trimer and $E^{(n)}_{4b,m}$ $(m = 1, 2)$ are the energies of accompanying tetramers. Origin of the universal nature of the tetramer was also discussed by von Stecher *et al.* who point out that the two tetramers are supported by an effective four-body hyperradial potential that appears below each trimer-atom threshold. The effective potential has a potential barrier and prevents four atoms to come close to each other, thereby preventing the four atoms to be affected from short-range details of interaction potentials. Aside from the unitarity limit, it has been pointed out that there appears another set of tetramers of atom-atom-dimer Efimov states near the atom-atom-dimer threshold, when the atom-dimer scattering length diverges [32]. The atom-atom-dimer Efimov states are numerically vindicated in Ref. [65].

microscopic system in general [65].

The entire energy spectrum of four-identical bosons with resonant interaction was precisely obtained by Deltuva in his series of papers [66, 67, 68, 69, 70, 71, 72, 73, 74]. He employs the Alt-Grassberger-Sandhas equation, which is an equivalent equation to the Faddeev-Yakubovski equation, to the four-boson system and obtains the entire energy spectrum which is schematically illustrated in Fig. 2.3. The two tetramers tied to an Efimov trimer are shown not to be stable bound states but resonances (in agreement with the Amado-Greenwood theorem [110]), and the energies ($E^{(n)}_{4b,1}$, $E^{(n)}_{4b,2}$) and the widths ($\Gamma^{(n)}_{4b,1}$, $\Gamma^{(n)}_{4b,2}$) of the resonances at the unitarity limit are determined to be

$$E^{(n)}_{4b,1} + i\Gamma^{(n)}_{4b,1} = (4.610(1) + i0.01483(1))E^{(n)}_{3b}, \tag{2.78}$$

$$E^{(n)}_{4b,2} + i\Gamma^{(n)}_{4b,2} = (1.00227(1) + i0.000238(1))E^{(n)}_{3b}. \tag{2.79}$$

in agreement with the calculations by von Stecher *et al.* [65]. Also, Deltuva found that an excited tetramer of the two companions turns into an inelastic virtual state in some positive scattering-length region. Another set of tetramers, which are understood as the atom-atom-dimer Efimov trimers, are also vindicated below the atom-atom-dimer threshold.

A crucial suggestion for observing the tetramers was made by von Stecher *et al.* [65]: An experimental signature of the tetramer states tied to an Efimov trimer can be captured by measuring an enhanced four-body recombination rate in ultracold atoms, similarly to the Efimov trimers. Base on the suggestion, the Innsbruck group measured the atomic loss from an optical dipole trap and obtained two four-body loss peaks at which the scattering length takes on the values of $a^{(4,1)}_- = 0.47a_-$ and $a^{(4,2)}_- = 0.84a_-$ [75], where $a_- < 0$ is introduced in Eq. (2.57). The obtained values are in good agreement with the theoretical prediction of $a^{(4,1)}_- \simeq 0.44a_-$ and $a^{(4,2)}_- \simeq 0.9a_-$.[12]

Five or more particles

Presence or absence of universality in N-body physics is one of fundamental questions which has not yet been answered conclusively. We here briefly summarize the theoretical and experimental results obtained so far. von Stecher firstly investigated ground N-body bound states below the lowest-lying Efimov trimer up to $N \leq 13$ [113]. Based on a model Hamiltonian that reproduces the low-energy universal three- and four-body observables, he identified ground N-body clusters that accompany the lowest-lying Efimov trimer. Later, he identified three pentamers and two hexamers tied to the lowest-lying Efimov trimer [114]. Gattobigio *et al.* also investigated the N-body clusters up to $N \leq 16$ and revealed two N-body clusters tied to the lowest-lying $(N-1)$-body cluster [115, 116, 117]. The results by von Stecher and those by Gattobigio *et al.* disagree quantitatively, due to a non-universal nature of two-body finite-range interaction that affects the tightly bound ground N-body clusters. To resolve the situation and to deal with the universal nature of the N-body clusters, Yan and Blume [118] devised a model Hamiltonian with the contact two-body interaction regulated by a three-body repulsive interaction that is proportional to R^{-p}, which was confirmed to reproduce the low-energy universal three-body observables when p becomes large. They obtained

[12] The groups at Rice [50] and at LENS [49] also reported observation of two loss peaks due to the tetramer states at $a = a^{(4,1)}_-, a^{(4,2)}_-$; however, after a recalibration of the scattering length and reassiginment of loss peaks, the two peaks vanished [93, 92], although one of the peaks at $a = a^{(4,1)}_-$ remained in the Rice experiment.

energies of the lowest-lying N-body clusters extrapolated to $p \to \infty$ up to $N \leq 13$. The obtained energies agree with those obtained in Ref. [113] for small $N \leq 6$ but disagree for a larger N. Another interesting approach was developed by Nicholson [119], who deduced a linear dependence of energy per particle $E_N/N = (N/2-1)E_4/4$ for the ground N-body cluster by assuming a log-normal distribution of the two-particle correlator in the presence of a Hubbard-Stratonovich auxiliary field. However, the results disagree with other results discussed above. Experimentally, the Innsbruck group reported an enhanced five-body recombination rate at $a = a_-^{(5)} = 0.64 a_-^{(4,1)}$ [120], which agrees with the theoretical prediction of $a_-^{(5)} = 0.65 a_-^{(4,1)}$ [113] for the ground pentamer.

The N-body clusters tied to the first excited Efimov trimer was investigated by von Stecher [114], who revealed that there emerge at least one pentamer and one hexamer resonances that accompany the first excited Efimov trimer. In particular, the energies of the resonances have a character different from those of the ground pentamers and hexamers. The low-energy properties of the N-body physics are, thus, not completely understood and remain open questions.

Systems other than identical bosons

We here briefly summarize the theoretical results obtained so far, concerning the N-body extension of the Efimov effect in systems other than identical bosons.

- Castin *et al.* [121] investigated three-heavy fermions A interacting with a light particle B with the total angular momentum of $l = 1$ and the parity of $+1$ and found a pure four-body Efimov effect for the mass ratio $\alpha = m_A/m_B$ of $13.384 < \alpha < 13.606$. Although no three-body Efimov effect exists for the mass ratio $\alpha < 13.606$ as we reviewed in Sec. 2.3.2, the four particles form an infinite series of self-similar "Efimov tetramers", with a mass-ratio dependent scaling factor. So far, the result is the only example of purely four-body Efimov effect. Later on, Blume [122] showed that in the parameter region of $9.5 < \alpha < 13.384$, there appears a tetramer state whose energy depends only on the (positive) scattering-length, similarly to the Kartavtsev-Malykh trimers reviewed in Sec. 2.3.2.

- For two heavy and two light fermions, with mass ratio $\alpha < 13.606$, there appear neither Efimov tetramers nor tetramers of the Kartavtsev-Malykh character [123, 124, 125].

- Three heavy bosons interacting with a light particle were investigated by Wang *et al.* [126] and later by Blume and Yan [127]. Based on the Born-Oppenheimer approximation, Wang *et al.* show that a tetramer accompanies each Efimov trimer if $\alpha \lesssim 50$; on the other hand, Blume and Yan show that the number of tied tetramer (to the ground Efimov trimer) is one if $\alpha \lesssim 13$ and two if $\alpha \gtrsim 13$ based on a variational method with the correlated Gaussian basis set. The two results disagree also quantitatively. The disagreement may due to the non-conserving relative angular momentum of the four particles, which is neglected in Ref. [126] and included in Ref. [127]. Blume and Yan also reveal the existence of a pentamer and a hexamer tied to the lowest-lying Efimov trimer.

Chapter 3

Functional renormalization group

In this chapter, we review the functional renormalization group (FRG), which is the central technique employed in this thesis. Based on the idea of Wilson's continuous renormalization group (RG), we first discuss in Sec. 3.1 the philosophy and some applications of the FRG. In Sec. 3.2, we then formulate the FRG for a general field theory so that the formulation becomes suitable for the application to the quantum few-body physics, which is the subject of our thesis.

3.1 Philosophy and applications

In quantum field theory, we deal with the partition function to compute various observables such as scattering amplitudes, susceptibilities, currents, Wilson loops, thermodynamic functions, and so on. The partition function Z is often represented in path-integral form as

$$Z = \int d\phi \exp\left(-S\left[\phi\right]\right) = \int d\phi \exp\left(-\int d^4x\, \mathcal{L}[\phi(x)]\right), \tag{3.1}$$

where $\phi(x)$ represents a field, $S\left[\phi\right]$ and $\mathcal{L}[\phi(x)]$ are the action and the Lagrangian density, respectively. Equation (3.1) shows that that the partition function Z is composed of all quantum fluctuations around the classical path $\frac{\delta S}{\delta\phi(x)} = 0$ which gives the stationary point contribution in the integral. In general, the non-linearity (interactions) of $\mathcal{L}[\phi(x)]$ with respect to $\phi(x)$ makes it very difficult to perform integration of the quantum fluctuations exactly, and therefore, we almost always rely on approximate methods such as perturbative expansions, the large-N expansions, ϵ expansions, semi-classical approximations, the Baym-Kadanoff approximation and so on. Among these methods is Wilson's renormalization group (RG), in which we perform integration of the quantum fluctuations stepwise, rather than do it all at once.

Wilson's idea

Here let us briefly sketch the idea of Wilson [1] in a scaler field theory with the action $S\left[\phi\right]$, where we assume that $S\left[\phi\right]$ is properly non-dimensionalized. The degrees of freedom in the theory arise from those $\phi(q)$ with momentum q. In the RG, we divide the degrees of freedom into two parts as

$\phi(q) = \phi_>(q) + \phi_<(q)$, where we introduce rapid modes $\phi_>(q)$ ($q \in [k, \Lambda]$) and slow modes $\phi_<(q)$ ($q \in [0, k]$) with Λ being the cutoff momentum. Then the partition function Z is rewritten as

$$Z = \int d\phi_> d\phi_< \ \exp\left(-S\left[\phi_> + \phi_<, \Lambda\right]\right). \tag{3.2}$$

Instead of the full integration, we perform integration only for the rapid modes $\phi_>$, and obtain

$$Z = \int d\phi_< \ \exp\left(-S_{\text{eff}}[\phi_<, k]\right), \tag{3.3}$$

where the contribution from the rapid modes $\phi_>(q)$ to the partition function Z is encapsulated in an effective actionF $S_{\text{eff}}[\phi_<, k]$. In other words, physics of the system $S[\phi, \Lambda]$ exhibits the same low-energy behavior as the new one $S_{\text{eff}}[\phi, k]$. This mapping of the action $S \to S_{\text{eff}}$ defines the RG transformation. In particular, by differentiating both hand sides of Eq. (3.3) with respect to the logarithm of the parameter k, we obtain the RG equation

$$\partial_{\ln k} S_{\text{eff}}[\phi, k] = f[S_{\text{eff}}], \tag{3.4}$$

which generates an RG flows $\{S_{\text{eff}}[\phi_<, k]\}_{k\in[0,\Lambda)}$ of actions for given initial conditions. In the limit of $k \to 0$, where all the quantum fluctuations are integrated, we obtain the partition function Z. In short, Wilson's RG maps a problem of integration to the problem of a differential equation.[1] This mapping enables us to use techniques of differential equations in computing the partition function Z. For example, analyses of the nullclines, in particular the fixed points, of the RG differential equation provides an accurate predictions for the universal critical exponents in second-order phase transitions. Physically, through the partial integration, the effective interaction among the slow modes, which is mediated by rapid modes, is plugged (renormalized) into effective couplings of an effective action. Wilson's RG, therefore, can be regraded as a microscope for the system with variable resolution parametrized by k; in other words, one starts from a high-resolution picture of the known microscopic physics and subsequently decreases the resolution to obtain a coarse-grained picture of the macroscopic phenomena.

Geometry of RG flows

As mentioned in Sec. 1.1, our general motivation is to understand the role of renormalized trajectory. For this purpose, let us here briefly review a geometry of RG flow in critical phenomena [1, 3], in which nullclines of Eq. (3.4) play a central role. The nullclines on which the right-hand side of Eq. (3.4) vanishes are called fixed points, where RG flows stop. In the vicinity of a fixed point, the effective action $S_{\text{eff}}[\phi]$ can be expressed as a fixed point action $S^*[\phi]$ perturbed by small interactions $\sum_i \epsilon_i O_i[\phi]$. Therefore, the RG equation can be linearlized as

$$\partial_{\ln k} O_i[\phi] = L\Big[O_j[\phi]\Big], \tag{3.5}$$

[1] Based on the Kadanoff's block-spin transformation [128], Wilson first published the discrete version of RG equations [3, 4], which is obtained by a recursive integration of rapid modes for discretized $k = k_1 \geq k_2 \geq \cdots \geq 0$ rather than by continuous variation of k. The idea of the continuous RG was informally reported by Wilson at the Irvine conference in 1970, but was first published by Wegner and Houghton [129] in 1973.

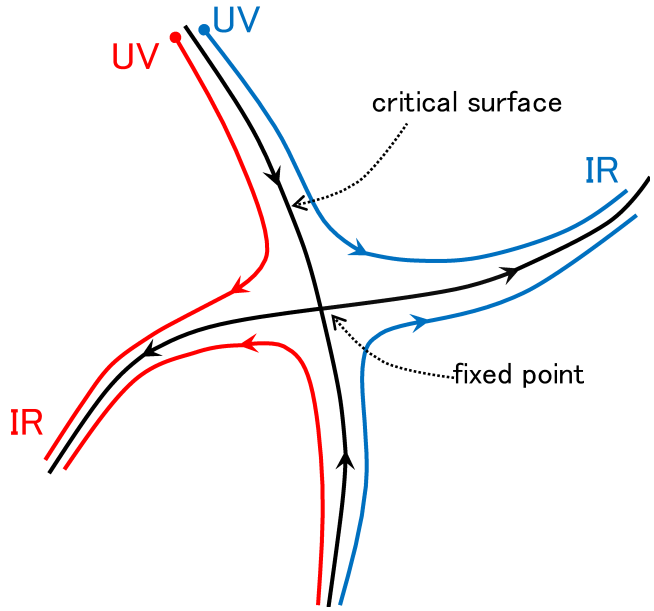

Figure 3.1: Typical RG flows in second-order phase transitions. The blue and red-colored curves start from microscopic actions close to the critical surface in the ultraviolet (UV) regime, approach to the fixed point, and reach distinct effective actions in the infrared (IR) regime.

where L is a linear operator. If O_j are the eigen-operators of L, we can rewrite the linearized RG equation as

$$\partial_{\ln k} O_i[\phi] = -d_i O_i[\phi], \tag{3.6}$$

where the scaling dimension $\{d_i\}_i$ are the eigenvalues of L. The operator O_i is said to be relevant if $d_i > 0$, marginal if $d_i = 0$, and irrelevant if $d_i < 0$, since the relevant (irrelevant) operator grows up (diminishes) in the effective action as k decreases.[2] In Fig. 3.1, typical RG flows around a fixed pint are schematically illustrated, where we assume that there are one relevant and one irrelevant operators. We see two typical flows that starts from nearby two microscopic actions in the ultraviolet (UV) flow into distinct low-energy effective actions in the infrared (IR) regime, but this behavior is nothing but the critical phenomena, in which a small variation of a microscopic parameter (e.g. the magnetic field) leads to a drastic change (e.g. ordered / normal phase) in macroscopic phenomena. In particular, as we take the microscopic actions close to the critical surface, the two flows are strongly attracted to the fixed point, around which the flows nearly stop during $\ln k^* \lesssim \ln k \lesssim \ln k^* + \Delta \ln k$. The universal power-law singularity of observables in the second-order phase transition originates in the singularity of $\Delta \ln k$ [3], and thus the universal critical exponents are determined by the scaling dimension $\{d_i\}_i$ of the operators $\{O_i\}_i$. The universal IR behavior originates in the attraction of many theories close to the critical surface to a one-

[2] In the perturbation theory, the terms "relevant", "marginal", "irrelevant" is defined by the canonical mass dimension of the operator O_i. The two definitions of these terms coincide at the Gaussian fixed point, which plays the role of the UV stable fixed point in the perturbation theory to define a perturbatively renormalizable theory [5, 6].

dimensional trajectory[3], which is parametrized by the relevant operator of the fixed point, and thus, the attraction domains of such a small sub-theory space determine a set of universality classes for the critical phenomena. In this way, the geometry of RG flows plays a decisive role in critical phenomena. In this thesis, we further apply this idea to the RG limit cycle [130], that is a closed loop of an RG flow.

Functional renormalization group

The functional renormalization group (FRG) [129, 1, 5, 131] is the combination of the above-mentioned idea of Wilson and the functional methods in quantum field theories.[4] In quantum field theories, we are particularly interested in Green's functions and their generating functionals, such as the Schwinger functional, which is the generating functional of connected Green's functions, and the quantum effective action, which is the generating functional of one-particle irreducible (1PI) vertices. As the partition function Z, the generating functionals are often represented in path-integral forms. In the FRG, we introduce a cutoff parameter k in the generating functionals by adding a regulator term in the action, and then the differentiation with respect to k leads to exact RG equations for the generating functionals. The FRG computes the generating functionals by solving the differential RG equations (with proper truncations of the terms of the generating functionals) rather than by performing path integrals directly. The FRG is often said to be non-perturbative because truncation schemes of the FRG equations usually do not contain an expansion with respect to a small parameter in a given system.

The FRG constructed in this manner is quite general and is applied to a rich variety of systems. Here we introduce some of them with relevant references:

- In mathematical physics, perturbative renormalizability of ϕ_4^4-theory [5, 136] and the quantum electrodynamics (QED) [137, 138] was rigorously proved based on the FRG. The proof is much simpler than the diagrammatic proof based on the power counting theorem [139, 140] and the forest formula. The FRG allows us to evaluate renormalized Green's functions with a naive power counting, because loop momentum integrals in FRG are performed in a finite momentum shell at each step in the (continuous) FRG transformation. Also, FRG generates multi loop structure by a recursive generation of one-loop structure, and is free from complicated graph topology and overlapping divergences. The results are further developed [141, 142, 143] to justify the predictability of an effective field theory with perturbatively non-renormalizable interactions by a rigorous proof of the decoupling theorem [144].

- In statistical mechanics, the FRG was applied to the $O(N)$ scaler field theory in d dimensions. At $d = 2$ and $N = 2$, the lowest [145] and the first-order [146] derivative expansion of the FRG equations reproduce the the critical exponents of the Berezinskii-Kosterlitz-Thouless transition [147, 148] without introducing vortices. Also the FRG continuously connects [149] the two distinct effective pictures of the nonlinear sigma model in $d = 2+\epsilon$ and the Ginzburg-Landau-Wilson model in $d = 4 - \epsilon$ by exactly reproducing their critical exponents within a

[3]The trajectory is named renormalized trajectory by Wilson and Kogut [1]. They first utilize the trajectory to define a continuum limit of a lattice field theory.

[4]For reviews, see Refs. [132, 6, 133, 134, 135].

single FRG equation, and thereby providing a reasonable prediction for the critical exponents in $d = 3$, which agrees well with the seven-loop perturbative results.

- In condensed matter theory, $2d$-Hubbard models are investigated extensively with the vertex expansion of the FRG equation, in application to high-T_c cuprate superconductors. From the RG flows of various paring correlation functions, a dominant instability are determined for weak coupling systems near half filling. In particular, based on an unbiased collection of Feynman diagrams, the $d_{x^2-y^2}$-superconducting instability is shown to emerge under a finite (=not long ranged) but pronounced antiferromagnetic correlation, in favor of the spin-fluctuation-mediated pairing mechanism.

- In ultracold atoms, the FRG is applied to the BEC-BCS crossover, and reproduced the results for interacting bosons in the BEC regime and the Gorkov correction in the BCS regime [150]. So far, the FRG is the only method that reproduces these two limits. In this way, an unbiased truncation of the FRG equations enables us to deal with a wide range of the parameter region, since a systematic truncation does not depend on the details of a given system.

- In the theory of gravity, a non-trivial fixed point other than the Gaussian fixed point of the quantum Einstein gravity was discovered based on a derivative expansion of the FRG [151]. The fixed point is shown to be stable under the coupling with a scaler field [152]. The results provide a circumstantial evidence for Weinberg's asymptotic safety scenario [153], i.e. the non-perturbative renormalizability (in Wilson's sense [1]) of the Einstein gravity takes on a reality. As a review article, we refer to Ref. [154]

3.2 General formulation

In this section we formulate the functional renormalization group (FRG) in a general superfield notation, so that the formalism can be applied to any field theory.

3.2.1 Superfield notation

To deal with various species of fields on an equal footing, we first introduce a compact notation of superfields and superlabels. The notation follows Refs. [155, 156]. We represent all possible configuration of fields by a single superfield Φ_α, where the superlabel α represents all quantum numbers to specify a field. For example, a mixture of scaler bosons ϕ and two-component fermions $\psi_\uparrow, \psi_\downarrow$ in 3+1 dimension is represented by Φ_α, where α is the set of the field species (ϕ, ϕ^*, ψ or ψ^*), the four-momentum (q), and the internal spin indices ($\uparrow$ or $\downarrow$). We note that the particle fields and the antiparticle fields are dealt with separately.

In this notation, the partition function Z is formally represented in path-integral form as

$$Z = \int d\Phi \exp\left[-S\left[\Phi\right]\right] = \int d\Phi \exp\left[-S_0[\Phi] - S_{\rm int}[\Phi]\right], \tag{3.7}$$

where we decompose the classical action $S[\phi]$ into a free part $S_0[\Phi]$ and an interaction part $S_{\rm int}[\Phi]$. The free part $S_0[\Phi]$ of the action is the bilinear term with respect to the field Φ in the entire action,

i.e.,

$$S_0[\Phi] = \frac{1}{2}\int_\alpha \int_\beta \Phi_\alpha \left[\mathbf{G}_0^{-1}\right]_{\alpha\beta} \Phi_\beta, \tag{3.8}$$

where $\int_\alpha$ represents the integration over momenta and the summation over internal indices and field species. The matrix $\mathbf{G}_0$ is the free propagator of fields, and is symmetric for bosonic indices $\alpha\beta$ and antisymmetric for fermionic indices $\alpha\beta$, since Φ_α is a commuting complex number if α represents bosons and an anticommuting Grassman number if α represents fermions. We assign 0 for a matrix element $[\mathbf{G}_0]_{\alpha\beta}$ if α and β take on different statistics, i.e., we assume that bosons (fermions) will not propagate to fermions (bosons). This symmetry of the propagator is simply summarized in the following equations:

$$^t\mathbf{G}_0 = \mathbf{Z}\cdot\mathbf{G}_0 = \mathbf{G}_0\cdot\mathbf{Z}, \tag{3.9}$$

$$\mathbf{Z}_{\alpha\beta} = \zeta_\alpha \delta_{\alpha\beta}, \tag{3.10}$$

where ^{t} represents the transpose of a matrix and ζ_α is 1 if α labels bosons and -1 if α labels fermions. We also consider the system with translational invariance, in which case $\mathbf{G}_0$ is diagonal with respect to the momentum indices. In the following, we use the following normalization conditions for the delta function and the functional derivative:

$$\int_\alpha \delta_{\alpha\beta} = 1, \quad \frac{\delta J_\alpha}{\delta J_\beta} = \delta_{\alpha\beta}, \tag{3.11}$$

where J_α is a function of superlabels that takes on complex value and Grassmann value, depending on the statistics of α.

With these notations, the generating functionals of Green's functions are represented as

$$e^{L[\bar\Phi]} = \frac{1}{Z_0}\int d\Phi \exp\left[-S_0[\Phi] - S_{\rm int}[\Phi+\bar\Phi]\right], \tag{3.12}$$

$$e^{W[J]} = \int d\Phi \exp\left[-S[\Phi] + (J,\Phi)\right], \tag{3.13}$$

$$\Gamma[\bar\Phi] = \left(J[\bar\Phi],\bar\Phi\right) - W\left[J[\bar\Phi]\right], \tag{3.14}$$

where $Z_0 = \int d\Phi \exp\left[-S_0[\Phi]\right]$ and $(J,\Phi) = \int_\alpha J_\alpha \Phi_\alpha$. In Eq. (3.14), $J[\bar\Phi]$ and $\bar\Phi$ are related through $\bar\Phi_\alpha = \frac{\delta}{\delta J_\alpha} W[J]$, i.e. $\Gamma[\bar\Phi]$ is the Legendre transform of $W[J]$. The functionals $L[\bar\Phi]$, $W[J]$, and $\Gamma[\bar\Phi]$ are the generating functionals of amputated connected Green's functions, unamputated connected Green's functions and one-particle irreducible (1PI) vertices, respectively.[5] Thus we can obtain the

[5]The unamputated connected Green's functions are the cumulants in probability theory. The terms "amputated" and "connected" comes from graphical analysis with the Feynman rules, where Green's functions are represented by a set of Feynman graphs in which vertices (interactions) are connected via lines (propagators). The quantum effective action is the energy functional with respect to the vacuum expectation value (VEV) $\bar\Phi_\alpha = \langle\Phi_\alpha\rangle$, and thus $\frac{\delta}{\delta\bar\Phi_\alpha}\Gamma[\bar\Phi] = 0$ gives the quantum equation of motion of the VEV.

Green's functions by functionally differentiating these generating functionals.

$$\left.\frac{\delta^n L[\bar{\Phi}]}{\delta\bar{\Phi}_{\alpha_1}\cdots\delta\bar{\Phi}_{\alpha_n}}\right|_{\bar{\Phi}=0} = L^{(n)}_{\alpha_1\cdots\alpha_n}, \tag{3.15}$$

$$\left.\frac{\delta^n W[J]}{\delta J_{\alpha_1}\cdots\delta J_{\alpha_n}}\right|_{J=0} = G^{(n)}_{\alpha_1\cdots\alpha_n}, \tag{3.16}$$

$$\left.\frac{\delta^n \Gamma[\bar{\Phi}]}{\delta\bar{\Phi}_{\alpha_1}\cdots\delta\bar{\Phi}_{\alpha_n}}\right|_{\bar{\Phi}=0} = \Gamma^{(n)}_{\alpha_1\cdots\alpha_n}, \tag{3.17}$$

where $L^{(n)}_{\alpha_1\cdots\alpha_n}$ is the amputated connected Green's function, $G^{(n)}_{\alpha_1\cdots\alpha_n}$ is the unamputated connected Green's function, and $\Gamma^{(n)}_{\alpha_1\cdots\alpha_n}$ is the 1PI vertex of the n-th order.

3.2.2 Regulators

To introduce a cutoff parameter k in the generating functionals, we define a regulator that properly serves as the cutoff in Wilson's RG. We consider a regulator matrix $\mathbf{R}_k$ that suppresses the propagation of particles (fields) in a certain region of momentum. For this purpose, we introduce a regulator $\mathbf{R}_k$ in the free part of the classical action $S_0[\Phi]$:

$$S_{0,k}[\Phi] = S_0[\Phi] + \frac{1}{2}\int_\alpha\int_\beta \Phi_\alpha\,[\mathbf{R}_k]_{\alpha\beta}\,\Phi_\beta. \tag{3.18}$$

In other words, we replace the free propagator $\mathbf{G}_0$ by $\mathbf{G}_{0,k} = \left(\mathbf{G}_0^{-1} + \mathbf{R}_k\right)^{-1}$, which literally means that large $\mathbf{R}_k$ suppresses the propagation of the particles. Since the parameter k specifies the momentum scale above which the degrees of freedom are integrated out, we deal with the momentum separately from other quantum numbers as $\mathbf{R}_k \to \mathbf{R}_k(q)$, where q is the momentum of the propagating particle. We note that we are considering translationally invariant systems in which the propagator is diagonal in q. Since the regulator $\mathbf{R}_k(q)$ serves as the cutoff in Wilson's RG, we impose the following three conditions on $\mathbf{R}_k$:

$$\mathbf{R}_k(q) \to \infty \ (k \to \infty), \tag{3.19}$$

$$\mathbf{R}_k(q) \to 0 \ (k \to 0), \tag{3.20}$$

$$\mathbf{R}_k(q) > 0 \ (q^2/k^2 < 1), \tag{3.21}$$

where, as we discuss later, the first and the second conditions ensure the proper UV and IR boundary conditions of the FRG equations. The third condition means that the regulator $\mathbf{R}_k(q)$ suppress the propagation of slow modes $q < k$ so that they remain unintegrated in the RG transformation. Aside from the three conditions, the choice of the regulator is arbitrary. In principle, the choice of the regulator does not change the computed generating functionals $W[J]$, $L[\bar{\Phi}]$ and $\Gamma[\bar{\Phi}]$ via FRG equations as far as we solve the equations exactly; however, under a truncation of the FRG equations, the choice of regulator does affect the final result. For the local potential approximation, which is the lowest order expansion of the derivatice expansion, Litim provided an "optimal" choice of regulator which is likely to give the fastest convergence of the expansion [157, 158]. Later, Pawlowski [133] generalized the optimization criterion to arbitrary truncation schemes so

that calculated correlation functions are minimally sensible to the choice of the regulator. Here, however, we do not rely on the optimization criterion and choose a regulator that facilitates semi-analytic calculations for our purpose of dealing with universal few-body physics, which can be dealt with exactly at least at the three-body level.

3.2.3 Flowing action

We here review the derivation of the Wetterich equation [131] which is the fundamental FRG equation of the quantum one-particle irreducible (1PI) effective action. We first introduce the cutoff k dependent Schwinger functional $W_k[J]$ by

$$e^{W_k[J]} = \int d\Phi \exp\left[-S_{0,k}[\Phi] - S_{\rm int}[\Phi] + (J,\Phi)\right], \tag{3.22}$$

where the regulator-dependent free action $S_{0,k}$ is introduced in Eq. (3.18). Since the k dependence of the right-hand side comes only from the Gaussian part of the integrand, the k dependence of $W_k[J]$ can be easily obtained. By differentiating both hand sides of Eq. (3.22) with respect to k, we obtain

$$\begin{aligned} e^{W_k[J]}\partial_k W_k[J] &= \int d\Phi - \frac{1}{2}\left(\Phi, \partial_k \mathbf{R}_k \Phi\right) \exp\left[-S_{0,k}[\Phi] - S_{\rm int}[\Phi] + (J,\Phi)\right] \\ &= -\frac{1}{2}\left(\frac{\delta}{\delta J}, \partial_k \mathbf{R}_k \frac{\delta}{\delta J}\right) \int d\Phi \exp\left[-S_{0,k}[\Phi] - S_{\rm int}[\Phi] + (J,\Phi)\right] \\ &= -\frac{1}{2}\left(\frac{\delta}{\delta J}, \partial_k \mathbf{R}_k \frac{\delta}{\delta J}\right) e^{W_k[J]}. \end{aligned} \tag{3.23}$$

Thus we obtain the FRG equation for the Schwinger functional as

$$\partial_k W_k[J] = -\frac{1}{2}\left(\frac{\delta W_k[J]}{\delta J}, \partial_k \mathbf{R}_k \frac{\delta W_k[J]}{\delta J}\right) - \frac{1}{2}\mathrm{STr}\left[(\partial_k \mathbf{R}_k) W_k^{(2)}\right], \tag{3.24}$$

where

$$\left[W_k^{(2)}\right]_{\alpha\beta} := \frac{\delta}{\delta J_\alpha}\frac{\delta}{\delta J_\beta} W_k[J], \tag{3.25}$$

$$\mathrm{STr}[\cdots] := \mathrm{Tr}[\mathbf{Z}\cdots]. \tag{3.26}$$

Here the STr-operation is called the supertrace [159] which inserts additional minus sign if a cutoff $\partial_k \mathbf{R}_k$ inserted propagator forms a fermionic loop. (Note the definition of the matrix $\mathbf{Z}$ in Eq. (3.10).) Although Eq. (3.24) seems to be sufficient in computing various Green's functions, the FRG equation should be solved under the boundary conditions of $W_{k=\infty}[J] = 0$, which contains no information about a given system. Also, the first term on the right-hand side of Eq. (3.24) is not useful for sharp regulator functions since $\partial_k \mathbf{R}_k$ produces a singular δ function which complicates numerical treatments. Therefore, we use another functional of the flowing action $\Gamma_k[\bar{\Phi}]$ which is defined as

$$\Gamma_k[\bar{\Phi}] := \tilde{\Gamma}_k[\bar{\Phi}] - \frac{1}{2}\left(\bar{\Phi}, \mathbf{R}_k \bar{\Phi}\right), \tag{3.27}$$

$$\tilde{\Gamma}_k[\bar{\Phi}] := \left(J[\bar{\Phi}], \bar{\Phi}\right) - W_k\left[J[\bar{\Phi}]\right] \quad \text{with} \quad \bar{\Phi} = \frac{\delta W_k[J]}{\delta J}, \tag{3.28}$$

where we should note that $J[\bar{\Phi}]$ implicitly depends on k via the second equality in Eq. (3.28). From Eq. (3.28) we can deduce the quantum equation of motion of the vacuum expectation value (VEV) $\bar{\Phi}$ in presence of the source J and the cutoff k as

$$\frac{\delta}{\delta\bar{\Phi}_\alpha}\tilde{\Gamma}_k = \pm J_\alpha, \tag{3.29}$$

where on the right-hand side, the plus (minus) sign should be chosen for bosonic (fermionic) α, since J_α and $\bar{\Phi}_\alpha$ commute (anticommute) when α labels a boson (fermion). Using the right derivative for Grassmann numbers, Eq. (3.29) can be simply rewritten as

$$\tilde{\Gamma}_k \frac{\overleftarrow{\delta}}{\delta\bar{\Phi}_\alpha} = J_\alpha, \tag{3.30}$$

where we note that the functional $\tilde{\Gamma}_k$ contains products of an even number of Grassmann variables so that $\tilde{\Gamma}_k$ becomes a c-number.

Now we derive the FRG equation of the flowing action Γ_k. By differentiating both hand sides of Eq. (3.27), we obtain

$$\begin{aligned}\partial_k\Gamma_k[\bar{\Phi}] &= \left(\partial_k J[\bar{\Phi}], \bar{\Phi}\right) - \left(\partial_k J[\bar{\Phi}], \frac{\delta W_k[J]}{\delta J}\right) - (\partial_k W_k)\left[J[\bar{\Phi}]\right] - \frac{1}{2}\left(\bar{\Phi}, \partial_k \mathbf{R}_k\bar{\Phi}\right) \\ &= -(\partial_k W_k)\left[J[\bar{\Phi}]\right] - \frac{1}{2}\left(\bar{\Phi}, \partial_k\mathbf{R}_k\bar{\Phi}\right),\end{aligned} \tag{3.31}$$

where the first term of the right-hand side can be rewritten by using Eq. (3.24). We thus obtain

$$\partial_k\Gamma_k[\bar{\Phi}] = \frac{1}{2}\mathrm{STr}\left[(\partial_k\mathbf{R}_k)W_k^{(2)}\left[J[\bar{\Phi}]\right]\right], \tag{3.32}$$

where we have used $\bar{\Phi} = \frac{\delta W_k[J]}{\delta J}$. The functional $W_k^{(2)}$ is related to $\tilde{\Gamma}_k$ via[6]

$$W_k^{(2)} \cdot \tilde{\Gamma}_k^{(2)} = \mathbf{1}, \tag{3.33}$$

$$\left[\tilde{\Gamma}_k^{(2)}\right]_{\alpha\beta} := \frac{\delta}{\delta\bar{\Phi}_\alpha}\tilde{\Gamma}_k\frac{\overleftarrow{\delta}}{\delta\bar{\Phi}_\beta}, \tag{3.34}$$

since

$$\delta_{\alpha\beta} = \left(\frac{\delta}{\delta J_\alpha}\right)J_\beta = \int_\gamma\left(\frac{\delta\bar{\Phi}_\gamma}{\delta J_\alpha}\frac{\delta}{\delta\bar{\Phi}_\gamma}\right)\tilde{\Gamma}_k\frac{\overleftarrow{\delta}}{\delta\bar{\Phi}_\beta} = \int_\gamma\left(\frac{\delta}{\delta J_\alpha}\frac{\delta W_k}{\delta J_\gamma}\right)\frac{\delta}{\delta\bar{\Phi}_\gamma}\tilde{\Gamma}_k\frac{\overleftarrow{\delta}}{\delta\bar{\Phi}_\beta}. \tag{3.35}$$

Combining Eqs. (3.32) and (3.33), we finally obtain the Wetterich equation

$$\partial_k\Gamma_k[\bar{\Phi}] = \frac{1}{2}\mathrm{STr}\left[\partial_k\mathbf{R}_k\left(\Gamma_k^{(2)}[\bar{\Phi}] + \mathbf{R}_k\right)^{-1}\right], \tag{3.36}$$

$$\left[\Gamma_k^{(2)}\right]_{\alpha\beta} := \left[\tilde{\Gamma}_k^{(2)} - \mathbf{R}_k\right]_{\alpha\beta} = \frac{\delta}{\delta\bar{\Phi}_\alpha}\Gamma_k\frac{\overleftarrow{\delta}}{\delta\bar{\Phi}_\beta}. \tag{3.37}$$

[6]The relation is often referred to as the Dyson equation in condensed matter physics. However, since the relation is not an equation but an identity, we prefer to calling it a tree-expansion relation, which expands connected Green's functions in terms of 1PI vertices. The expansion looks like a tree in a graphical representation.

Compared with Eq. (3.24), the singular function $\partial_k \mathbf{R}_k$ is integrated via the loop momentum integral in Eq. (3.36) to produce a finite value, and thus does not compromise the numerical accuracy. Also, the boundary condition of Eq. (3.36) is much more useful than that of Eq. (3.24) as we discuss in the following.

Boundary conditions

We here discuss the UV and IR boundary conditions for the Wetterich equation Eq. (3.36). First, in the IR limit $k \to 0$, the regulator function $\mathbf{R}_k$ vanishes because of the condition in Eq. (3.20). In this limit, the flowing action Γ_k (Eq. (3.27)) reduces to the regulator-uninserted action, which is the quantum effective action Γ (Eq. (3.14)) including all the quantum fluctuations.[7] We then discuss the UV boundary condition, from which the quantum fluctuations are integrated in (continuos) steps. From the definition of the flowing action and the Schwinger functional Eqs. (3.27), (3.28) and (3.22), Γ_k can be rewritten in path-integral form as

$$e^{-\Gamma_k[\bar{\Phi}]} = \int d\Phi \exp\left\{\left(J[\bar{\Phi}], \Phi - \bar{\Phi}\right) - S_{0,k}[\Phi] - S_{\rm int}[\Phi] + \frac{1}{2}\left(\bar{\Phi}, \mathbf{R}_k \bar{\Phi}\right)\right\}. \tag{3.38}$$

By changing the integration variables from Φ to $\Phi' = \Phi - \bar{\Phi}$, we obtain

$$\begin{aligned} e^{-\Gamma_k[\bar{\Phi}]} &= \int d\Phi' \exp\left\{\left(J[\bar{\Phi}], \Phi'\right) - S\left[\Phi' + \bar{\Phi}\right] - \frac{1}{2}\left(\Phi' + \bar{\Phi}, \mathbf{R}_k(\Phi' + \bar{\Phi})\right) + \frac{1}{2}\left(\bar{\Phi}, \mathbf{R}_k \bar{\Phi}\right)\right\} \\ &= \int d\Phi' \exp\left\{-S\left[\Phi' + \bar{\Phi}\right] - \frac{1}{2}\left(\Phi', \mathbf{R}_k \Phi'\right) + \frac{1}{2}\left(\Gamma_k \frac{\overleftarrow{\delta}}{\delta \bar{\Phi}}, \Phi'\right) + \frac{1}{2}\left(\Phi', \frac{\delta \Gamma_k}{\delta \bar{\Phi}}\right)\right\}, \end{aligned} \tag{3.39}$$

where in the second equality we have used

$$\frac{1}{2}\left(\Gamma_k \frac{\overleftarrow{\delta}}{\delta \bar{\Phi}}, \Phi'\right) + \frac{1}{2}\left(\Phi', \frac{\delta \Gamma_k}{\delta \bar{\Phi}}\right) = \left(J[\bar{\Phi}], \Phi'\right) - \frac{1}{2}\left(\bar{\Phi}, \mathbf{R}_k \Phi'\right) - \frac{1}{2}\left(\Phi', \mathbf{R}_k \bar{\Phi}\right). \tag{3.40}$$

In the UV limit $k \to \infty$, where $\mathbf{R}_k \to \infty$ (see Eq. (3.19)), the right-hand side of Eq. (3.39) is dominated by the saddle point contribution $\Phi' = 0$, and thus we obtain

$$\Gamma_{k=\infty}[\bar{\Phi}] = S[\bar{\Phi}] + \text{const}, \tag{3.41}$$

which is much more useful than the boundary condition of $W_{k=\infty}[J] = 0$. To summarize, the FRG flow starts from the microscopic action $\Gamma_{k=\infty} = S$, which gradually incorporates the quantum fluctuations according to the decreasing k via the Wetterich equation (3.36), and finally reaches the quantum effective action $\Gamma_{k=0} = \Gamma$.

[7] This observation may clarify the relation between the FRG and the perturbation theory: In the FRG, quantum fluctuations of rapid modes $q > k$ are gradually integrated by decreasing k, while in the perturbation theory, the quantum fluctuations of the rapid and the slow modes are instantaneously integrated yet in the form of loop expansion.

3.2.4 Flow equations for one-particle irreducible vertices

In the quantum few-body physics, the correlation functions are the central quantities to investigate various observables such as scattering amplitudes, bound state energies, resonance spectra, and so on. For the purpose of dealing with the correlation functions, we derive the FRG flow equations for the one-particle irreducible (1PI) vertices in this section. We start from the Wetterich equation given in Eq. (3.36), which can be rewritten in more convenient form as

$$\partial_k \Gamma_k[\bar{\Phi}] = \frac{1}{2}\tilde{\partial}_k \mathrm{STr}\left[\ln\left(\Gamma_k^{(2)}[\bar{\Phi}] + \mathbf{R}_k\right)\right], \tag{3.42}$$

where the derivative $\tilde{\partial}_k$ acts only on the regulator $\mathbf{R}_k$. We first decompose the matrix $\Gamma_k^{(2)}$ into two parts by

$$\Gamma_k^{(2)}[\bar{\Phi}] =: \Gamma_k^{(2)}[\bar{\Phi}]\big|_{\bar{\Phi}=0} + V_k^{(2)}[\bar{\Phi}] =: \tilde{\mathbf{G}}_k^{-1} + V_k^{(2)}[\bar{\Phi}], \tag{3.43}$$

where $\tilde{\mathbf{G}}_k^{-1} + \mathbf{R}_k$ can be identified with the inverse propagator of the system at scale k. The matrix $V_k^{(2)}[\bar{\Phi}]$ stands for the vertex part of the flowing action, since it only contains three or higher vertices. We then expand the Wetterich equation Eq. (3.42) in term of $V_k^{(2)}[\bar{\Phi}]$ as

$$\begin{aligned}
\partial_k \Gamma_k[\bar{\Phi}] &= \frac{1}{2}\tilde{\partial}_k \mathrm{STr}\ln\left[V_k^{(2)}[\bar{\Phi}] + (\tilde{\mathbf{G}}_k^{-1} + \mathbf{R}_k)\right] \\
&= \tilde{\partial}_k \frac{1}{2}\mathrm{STr}\left[\ln\left(\tilde{\mathbf{G}}_k^{-1} + \mathbf{R}_k\right) + \ln\left(1 + \frac{1}{\tilde{\mathbf{G}}_k^{-1} + \mathbf{R}_k}\cdot V_k^{(2)}[\bar{\Phi}]\right)\right] \\
&= \tilde{\partial}_k \frac{1}{2}\mathrm{STr}\left[\ln\left(\tilde{\mathbf{G}}_k^{-1} + \mathbf{R}_k\right) - \sum_{n\geq 1}\frac{1}{n}\left(\frac{-1}{\tilde{\mathbf{G}}_k^{-1} + \mathbf{R}_k}\cdot V_k^{(2)}[\bar{\Phi}]\right)^n\right],
\end{aligned} \tag{3.44}$$

where the first term in the supertrace STr on the right-hand side is independent of $\bar{\Phi}$ and for most purposes we may discard such a term. We thus obtain

$$-\partial_k \Gamma_k[\bar{\Phi}] = \tilde{\partial}_k \frac{1}{2}\mathrm{STr}\left[\sum_{n\geq 1}\frac{1}{n}\left(\frac{1}{\tilde{\mathbf{G}}_k^{-1} + \mathbf{R}_k}\cdot(-V_k^{(2)}[\bar{\Phi}])\right)^n\right], \tag{3.45}$$

for the $\bar{\Phi}$-dependent part. Since the 1PI vertices appear in the quantum effective action $\Gamma[\bar{\Phi}]$ as the coefficients of the power series in $\bar{\Phi}$ (see Eq. (3.17)), we expand Γ_k and $V_k^{(2)}$ with respect to $\bar{\Phi}$:

$$\Gamma_k = \sum_{n\geq 0}\frac{1}{n!}\int_{\alpha_1\cdots\alpha_n}\Gamma^{(n)}_{k,\alpha_1\cdots\alpha_n}\bar{\Phi}_{\alpha_1}\cdots\bar{\Phi}_{\alpha_n}, \tag{3.46}$$

$$\left[V_k^{(2)}\right]_{\alpha_1\alpha_2} = \sum_{n\geq 1}\frac{1}{n!}\int_{\beta_1\cdots\beta_n}\Gamma^{(n+2)}_{k,\alpha_1\beta_1\cdots\beta_n\alpha_2}\bar{\Phi}_{\beta_1}\cdots\bar{\Phi}_{\beta_n}, \tag{3.47}$$

where the coefficients $\Gamma^{(n)}$ are symmetrized or antisymmetrized according to the statistics of the superlabels α_i, β_i. By substituting these expansions into Eq. (3.45), we obtain

$$\begin{aligned}
&-\partial_k\left(\sum_{n\geq 0}\frac{1}{n!}\int_{\alpha_1\cdots\alpha_n}\Gamma^{(n)}_{k,\alpha_1\cdots\alpha_n}\bar{\Phi}_{\alpha_1}\cdots\bar{\Phi}_{\alpha_n}\right) \\
&\quad= \tilde{\partial}_k\frac{1}{2}\mathrm{STr}\left\{\sum_{n\geq 1}\frac{1}{n}\left[\mathbf{G}_k\left(-\sum_{m\geq 1}\frac{1}{m!}\int_{\beta_1\cdots\beta_m}\mathbf{\Gamma}^{(m+2)}_{k,\beta_1\cdots\beta_m}\bar{\Phi}_{\beta_1}\cdots\bar{\Phi}_{\beta_m}\right)\right]^n\right\},
\end{aligned} \tag{3.48}$$

where the matrices $\mathbf{G}_k$ and $\mathbf{\Gamma}^{(n+2)}_{k,\beta_1\cdots\beta_n}$ are defined as

$$\mathbf{G}_k := \frac{1}{\tilde{\mathbf{G}}_k^{-1} + \mathbf{R}_k}, \tag{3.49}$$

$$[\mathbf{\Gamma}^{(n+2)}_{k,\beta_1\cdots\beta_n}]_{\alpha_1\alpha_2} := \Gamma^{(n+2)}_{k,\alpha_1\beta_1\cdots\beta_n\alpha_2}. \tag{3.50}$$

By comparing the $O(\bar{\Phi}^N)$ terms on both sides of Eq. (3.48), we finally obtain the FRG flow equations for the 1PI vertices.

$$\begin{aligned} -\partial_k \Gamma^{(N)}_{k,\alpha_1\cdots\alpha_N} = \tilde{\partial}_k \sum_{n\geq 1} \sum_{m_1\cdots m_n\geq 1} \frac{1}{2n} \cdot \delta_{m_1+\cdots+m_n,N} \cdot \frac{1}{m_1!\cdots m_n!} \\ \times \sum_{\sigma} \mathrm{sgn}(\sigma) \mathrm{STr}\left[\mathbf{G}_k \left(-\mathbf{\Gamma}^{(m_1+2)}_{k,\alpha_{\sigma(1)}\cdots\alpha_{\sigma(m_1)}}\right) \mathbf{G}_k \cdots \mathbf{G}_k \left(-\mathbf{\Gamma}^{(m_n+2)}_{k,\alpha_{\sigma(N-m_n+1)}\cdots\alpha_{\sigma(N)}}\right)\right], \end{aligned} \tag{3.51}$$

where $\mathrm{sgn}(\sigma)$ is the sign ± 1 created by the permutation σ of the superlabels $\alpha_1, \cdots, \alpha_N$. For a practical calculation, it is convenient to represent Eq. (3.51) with Feynman graphs. In constructing the graphical representation, we have to carefully count the number of equally contributing terms. In purely bosonic (fermionic) systems, contributions of identical terms exactly cancels the factors $\frac{1}{2n}\frac{1}{m_1!\cdots m_n!}$ appearing on the right-hand side of Eq. (3.51) except for symmetry factors. We thus obtain the following rules to construct the FRG equations:

- Write down all possible one-loop graphs with fixed external lines $\alpha_1, \cdots, \alpha_N$.
- Attach a line to the propagator $\mathbf{G}_k$, and a vertex with n external lines $\beta_1, \cdots, \beta_n$ to the 1PI vertex $-\mathbf{\Gamma}^{(n+2)}_{k,\beta_1\cdots\beta_n}$.
- Take the supertrace STr, which stands for the integration over the momentum, the summation over field species and internal indices. Note that we have to attach an additional minus sign for a fermionic loop.

We note that the FRG equation is one-loop exact, being free from overlapping integrals appearing in the perturbation theory and the Schwinger-Dyson equation. This one-loop structure is due to the quadratic form of the regulator $\frac{1}{2}(\Phi, \mathbf{R}_k\Phi)$ [160], since the regulator term of $O[\Phi^n]$ produces the n-th order functional derivative on the right-hand side of the Wetterich equation, the consequence of which appears as the multi-loop contribution.[8]

Some details in constructing Feynman rules

Here we discuss some details in constructing Feynman rules for Eq. (3.51). For simplicity, we here only consider purely bosonic (fermionic) systems, which are of our concern in this thesis. If we regard the inner product of $\mathbf{G}_k$ and $-\mathbf{\Gamma}_k$ on the right-hand side of Eq. (3.51) as the contraction of the external lines of $\mathbf{G}_k$ and $-\Gamma^{(N)}_{k,\alpha_1\cdots\alpha_N}$, we can find on the right-hand side all possible one-loop diagrams

[8] Such a "multi regulator" may optimize the FRG flow when the multiple scattering states are highly excited states. See e.g. Ref. [161], where the authors use the "multi regulator" to reproduce the Nosiere-Schmidt-Rink theory of the BEC-BCS crossover, where in the BEC limit, two-particle scattering states are highly excited states from a bound state.

with given external lines $\alpha_1 \cdots \alpha_N$. In addition, we notice that there are some over-counting of the same graphs when we carry out the summation $\sum_{m_1 \cdots m_n \geq 1} \sum_\sigma$. The next step toward the Feynman rules is therefore to count the number of the equally contributing diagrams. In fact, there are three types of over-counting which are discussed in the following:

1. Permutation in $\{(\underbrace{\alpha_1 \cdots \alpha_{m_1}})(\underbrace{\alpha_{m_1+1} \cdots \alpha_{m_1+m_2}}) \cdots (\underbrace{\alpha_{N-m_n+1} \cdots \alpha_N})\}$:

   If we carry out the summation $\sum_\sigma$, we notice that there exist some permutations like

$$\begin{aligned} &\{(\alpha_1 \cdots \alpha_{m_1})(\alpha_{m_1+1} \cdots \alpha_{m_1+m_2}) \cdots (\alpha_{N-m_n+1} \cdots \alpha_N)\} \\ &\underset{\sigma}{\to} \{(\alpha_{\sigma'(1)} \cdots \alpha_{\sigma'(m_1)})(\alpha_{m_1+1} \cdots \alpha_{m_1+m_2}) \cdots (\alpha_{N-m_n+1} \cdots \alpha_N)\} \qquad (3.52) \\ &\{(\alpha_1 \cdots \alpha_{m_1})(\alpha_{m_1+1} \cdots \alpha_{m_1+m_2}) \cdots (\alpha_{N-m_n+1} \cdots \alpha_N)\} \\ &\underset{\sigma}{\to} \{(\alpha_1 \cdots \alpha_{m_1})(\alpha_{\sigma''(m_1+1)} \cdots \alpha_{\sigma''(m_1+m_2)}) \cdots (\alpha_{N-m_n+1} \cdots \alpha_N)\} \,. \qquad (3.53) \end{aligned}$$

   These permutations indeed over-count the same diagrams, since with these permutations, the value of

$$(\pm 1)^\sigma \mathrm{STr}\left[\mathbf{G}_k\left(-\mathbf{\Gamma}^{(m_1+2)}_{k,\alpha_{\sigma(1)}\cdots\alpha_{\sigma(m_1)}}\right)\mathbf{G}_k \cdots \mathbf{G}_k\left(-\mathbf{\Gamma}^{(m_n+2)}_{k,\alpha_{\sigma(N-m_n+1)}\cdots\alpha_{\sigma(N)}}\right)\right]$$

   does not change (the minus sign $(-1)^\sigma$ for fermions exactly cancels with the factor which appears by the operation $-\mathbf{\Gamma}^{(m_1+2)}_{k,\alpha_{\sigma'(1)}\cdots\alpha_{\sigma'(m_1)}} \to -\mathbf{\Gamma}^{(m_1+2)}_{k,\alpha_1\cdots\alpha_{m_1}} = (-1)^\sigma \cdot -\mathbf{\Gamma}^{(m_1+2)}_{k,\alpha_{\sigma'(1)}\cdots\alpha_{\sigma'(m_1)}}$). The number of such permutations can easily be estimated to be $m_1!$ for Eq. (3.52) and $m_2!$ for Eq. (3.53), and the total number of such permutations is therefore $m_1! \cdots m_n!$, so that it cancels with the factor $\frac{1}{m_1! \cdots m_n!}$ on the right-hand side of Eq. (3.51).

2. Rotation of $\{\underbrace{(\alpha_1 \cdots \alpha_{m_1})(\alpha_{m_1+1} \cdots \alpha_{m_1+m_2}) \cdots (\alpha_{N-m_n+1} \cdots \alpha_N)}\}$:

   When we carry out the summation $\sum_{m_1 \cdots m_n \geq 1} \sum_\sigma$, there appear terms like

$$\begin{aligned} &\mathrm{STr}\left[\mathbf{G}_k\left(-\mathbf{\Gamma}^{(m_1+2)}_{k,\alpha_2\cdots\alpha_{m_2}}\right)\mathbf{G}_k \cdots \mathbf{G}_k\left(-\mathbf{\Gamma}^{(m_n+2)}_{k,\alpha_{N-m_n+1}\cdots\alpha_N}\right)\mathbf{G}_k\left(-\mathbf{\Gamma}^{(m_1+2)}_{k,\alpha_1\cdots\alpha_{m_1}}\right)\right], \\ &\mathrm{STr}\left[\mathbf{G}_k\left(-\mathbf{\Gamma}^{(m_1+2)}_{k,\alpha_3\cdots\alpha_{m_3}}\right)\mathbf{G}_k \cdots \mathbf{G}_k\left(-\mathbf{\Gamma}^{(m_n+2)}_{k,\alpha_1\cdots\alpha_{m_1}}\right)\mathbf{G}_k\left(-\mathbf{\Gamma}^{(m_1+2)}_{k,\alpha_2\cdots\alpha_{m_2}}\right)\right], \end{aligned}$$

   which take on the exactly the same value as

$$\mathrm{STr}\left[\mathbf{G}_k\left(-\mathbf{\Gamma}^{(m_1+2)}_{k,\alpha_1\cdots\alpha_{m_1}}\right)\mathbf{G}_k\left(-\mathbf{\Gamma}^{(m_1+2)}_{k,\alpha_2\cdots\alpha_{m_2}}\right)\mathbf{G}_k \cdots \mathbf{G}_k\left(-\mathbf{\Gamma}^{(m_n+2)}_{k,\alpha_{N-m_n+1}\cdots\alpha_N}\right)\right],$$

   because of the rotational symmetry of STr (Tr). Furthermore, these terms can be regarded as the permutations (rotations) like

$$\begin{aligned} &\{(\alpha_1 \cdots \alpha_{m_1})(\alpha_{m_1+1} \cdots \alpha_{m_1+m_2}) \cdots (\alpha_{N-m_n+1} \cdots \alpha_N)\} \\ &\to \{(\alpha_{m_1+1} \cdots \alpha_{m_1+m_2}) \cdots (\alpha_{N-m_n+1} \cdots \alpha_N)(\alpha_1 \cdots \alpha_{m_1})\} \qquad (3.54) \\ &\{(\alpha_1 \cdots \alpha_{m_1})(\alpha_{m_1+1} \cdots \alpha_{m_1+m_2}) \cdots (\alpha_{N-m_n+1} \cdots \alpha_N)\} \\ &\to \{(\alpha_{m_1+m_2+1} \cdots \alpha_{m_1+m_2+m_3}) \cdots (\alpha_1 \cdots \alpha_{m_1})(\alpha_{m_1+1} \cdots \alpha_{m_1+m_2})\}. \qquad (3.55) \end{aligned}$$

We must check first whether or not the factor $(-1)^\sigma$ for fermions on the right-hand side of Eq. (3.51) cancels these permutations. The factor $(-1)^\sigma$ turns out to be $(-1)^{(N-m_1)^{m_1}}$ for Eq. (3.54) and $(-1)^{(N-m_1)^{m_1}+(N-m_2)^{m_2}}$ for Eq. (3.55), which are exactly $+1$ when all $m_1, m_2, \cdots, m_n$ are even numbers. This means that all the 1PI vertices have an even number of external lines and is exactly the case when the system has the U(1) symmetry and conserves the particle number in each scattering process. To justify these arguments, we should note again that we focus only on purely bosonic (fermonic) systems.

What we do next is to count the number of those permutations (rotations) to evaluate the over-counting of the same diagram. The number of the rotation $\{\underbrace{(\alpha_1 \cdots \alpha_{m_1}) \cdots (\alpha_{N-m_n+1} \cdots \alpha_N)}\}$ is n, which turns out to cancel the factor $\frac{1}{n}$ on the right-hand side of Eq. (3.51).

3. Inversion $\{(\alpha_1 \cdots \alpha_{m_1})(\alpha_{m_1+1} \cdots \alpha_{m_1+m_2}) \cdots (\alpha_{N-m_n+1} \cdots \alpha_N)\}$
$\to \{(\alpha_{N-m_n+1} \cdots \alpha_N)(\alpha_{m_1+1} \cdots \alpha_{m_1+m_2}) \cdots (\alpha_1 \cdots \alpha_{m_1})\}$:

When we carry out the summation $\sum_{m_1 \cdots m_n \geq 1} \sum_\sigma$, there also appear such terms as

$$\mathrm{STr}\left[\mathbf{G}_k \left(-\mathbf{\Gamma}^{(m_1+2)}_{k,\alpha_{N-m_n+1}\cdots\alpha_N}\right) \mathbf{G}_k \cdots \mathbf{G}_k \left(-\mathbf{\Gamma}^{(m_1+2)}_{k,\alpha_2\cdots\alpha_{m_2}}\right) \mathbf{G}_k \left(-\mathbf{\Gamma}^{(m_n+2)}_{k,\alpha_1\cdots\alpha_{m_1}}\right)\right],$$

which takes exactly the same value as

$$\mathrm{STr}\left[\mathbf{G}_k \left(-\mathbf{\Gamma}^{(m_1+2)}_{k,\alpha_1\cdots\alpha_{m_1}}\right) \mathbf{G}_k \left(-\mathbf{\Gamma}^{(m_1+2)}_{k,\alpha_2\cdots\alpha_{m_2}}\right) \mathbf{G}_k \cdots \mathbf{G}_k \left(-\mathbf{\Gamma}^{(m_n+2)}_{k,\alpha_{N-m_n+1}\cdots\alpha_N}\right)\right],$$

since

$$\begin{aligned}
&\mathrm{STr}\left[\mathbf{G}_k \left(-\mathbf{\Gamma}^{(m_1+2)}_{k,\alpha_{N-m_n+1}\cdots\alpha_N}\right) \mathbf{G}_k \cdots \mathbf{G}_k \left(-\mathbf{\Gamma}^{(m_1+2)}_{k,\alpha_2\cdots\alpha_{m_2}}\right) \mathbf{G}_k \left(-\mathbf{\Gamma}^{(m_n+2)}_{k,\alpha_1\cdots\alpha_{m_1}}\right)\right] \\
&= \mathrm{Tr}\left[\mathbf{Z}\mathbf{G}_k \left(-\mathbf{\Gamma}^{(m_1+2)}_{k,\alpha_{N-m_n+1}\cdots\alpha_N}\right) \mathbf{G}_k \cdots \mathbf{G}_k \left(-\mathbf{\Gamma}^{(m_1+2)}_{k,\alpha_2\cdots\alpha_{m_2}}\right) \mathbf{G}_k \left(-\mathbf{\Gamma}^{(m_n+2)}_{k,\alpha_1\cdots\alpha_{m_1}}\right)\right] \\
&= \mathrm{Tr}\underbrace{\left[\left(-\mathbf{\Gamma}^{(m_n+2)}_{k,\alpha_1\cdots\alpha_{m_1}}\right)^{\mathrm{T}} \mathbf{G}_k^{\mathrm{T}} \cdots \mathbf{G}_k^{\mathrm{T}} \left(-\mathbf{\Gamma}^{(m_1+2)}_{k,\alpha_2\cdots\alpha_{m_2}}\right)^{\mathrm{T}} \mathbf{G}_k^{\mathrm{T}} \left(-\mathbf{\Gamma}^{(m_1+2)}_{k,\alpha_{N-m_n+1}\cdots\alpha_N}\right)^{\mathrm{T}} \mathbf{G}_k^{\mathrm{T}}\mathbf{Z}\right]}_{2n \text{ transpositions provides the factor } (\pm 1)^{2n} = +1.} \\
&= \mathrm{Tr}\left[\left(-\mathbf{\Gamma}^{(m_n+2)}_{k,\alpha_1\cdots\alpha_{m_1}}\right) \mathbf{G}_k \cdots \mathbf{G}_k \left(-\mathbf{\Gamma}^{(m_1+2)}_{k,\alpha_2\cdots\alpha_{m_2}}\right) \mathbf{G}_k \left(-\mathbf{\Gamma}^{(m_1+2)}_{k,\alpha_{N-m_n+1}\cdots\alpha_N}\right) \mathbf{G}_k\mathbf{Z}\right] \\
&= \mathrm{STr}\left[\mathbf{G}_k \left(-\mathbf{\Gamma}^{(m_n+2)}_{k,\alpha_1\cdots\alpha_{m_1}}\right) \mathbf{G}_k \cdots \mathbf{G}_k \left(-\mathbf{\Gamma}^{(m_1+2)}_{k,\alpha_2\cdots\alpha_{m_2}}\right) \mathbf{G}_k \left(-\mathbf{\Gamma}^{(m_1+2)}_{k,\alpha_{N-m_n+1}\cdots\alpha_N}\right)\right]. \qquad (3.56)
\end{aligned}$$

The additional $(-1)^\sigma$ factor originating in the inversion turns out to be

$$(-1)^{[(N-m_1)^{m_1}+(N-m_1-m_2)^{m_2}+\cdots+m_n^{m_{n-1}}]},$$

and again is exactly $+1$ when all $m_1, m_2, \cdots, m_n$ are even numbers. The number of this inversion is 2 and it cancels the factor $1/2$ on the right-hand side of Eq. (3.51).

4. Note for over-counting
For the $n = 1$ part of the right-hand side of Eq. (3.51), the over-counting originating in the inversion does not exist, and the factor $1/2$ on the right-hand side of Eq. (3.51) remains. Furthermore, for the $n = 2$ part of the right-hand side of Eq. (3.51), the over-counting originating

in the rotation and the inversion are the same and again the factor $1/2$ on the right-hand side of Eq. (3.51) remains. In actual calculations, such a remaining factor $1/2$ serves as a symmetry factor of the one-loop graph and vanishes when the graph has no symmetry.

Chapter 4

Infrared convergent structure of renormalization-group flows in Efimov physics

4.1 Question addressed

As discussed in Sec. 1.1, the universal low-energy behavior of a given microscopic system is described by a renormalized trajectory[1] toward which the renormalization-group (RG) flows are attracted. In this correspondence, the dimensionality of the renormalized trajectory determines the number of parameters that are sufficient to characterize the universal behavior (see e.g. Refs. [1, 6]), since the parameters determine the form of the flowing action Γ_k and thus that of the quantum effective action Γ. In Efimov physics, the low-energy scattering observables are generically described by the scattering length a and the three-body parameter κ. In particular, at the unitarity limit where where the scattering length diverges ($a = \pm\infty$), the low-energy behavior is described only by κ, and the dimensionality of the renormalized trajectory should be one. Since we are now interested in the strongly correlated regime, we focus on the unitarity limit and address the following question:

- What is the renormalized trajectory of the Efimov physics at the unitarity limit?

As reviewed in Sec. 2.2.2, a zero-range effective field theory of the Efimov effect has been shown by Bedaque *et al.* to exhibit the RG limit cycle [14, 15] of a three-body coupling constant. The RG limit cycle is a natural candidate for the renormalized trajectory, since the results obtained by the effective field theory are often expected to be applicable for various three-body systems with short-range interactions at sufficiently low energy, where each individual interaction is coarse-grained to be the contact interaction. Namely, the RG limit cycle is expected to be an infrared attractor of various RG-flow trajectories; however, there has been no explicit evidence for the infrared (IR) convergence structure of RG flows towards the RG limit cycle. Our purpose in this chapter is, therefore, to provide a numerical evidence which explicitly demonstrates that the RG limit cycle

[1] Although the term "renormalized trajectory" often refers to a fixed point and its relevant direction, Wilson and Kogut associate the term to a sub-theory space to which RG flows are finally attracted by stating, "*The subspace $S(\infty)$ is the same as the set of all renormalized trajectories*" [1].

behaves as an infrared attractor of various RG-flow trajectories. To demonstrate the convergence structure of RG flows in an unbiased manner, we numerically compute exact RG flows for the two and three-body sectors of various systems with tractable but reasonably realistic interaction potentials. To this end, we devise a method that combines functional renormalization group (FRG) equations, which is introduced by Tanizaki [78], of three-body scattering problems and effective separable models, which is developed by Ernst *et al* [162] to approximate various realistic interaction potentials. Concerning the well-established universality up to the three-body physics, we here demonstrate that the one-, two-, and three-body coupling constants approach in the infrared an RG limit cycle in theory space.

4.2 Microscopic model

In this section, we introduce microscopic systems of identical bosons with resonant short-range interactions. In demonstrating a convergent structure of RG flows to an RG limit cycle, we have to perform exact FRG calculations for various systems with different interaction potentials. For this purpose, we employ simple microscopic models that reproduce low-energy correlations of various realistic interactions, and nevertheless enable us to solve FRG equations without approximations. We thus first introduce a separable potential approximation, which is developed by Ernst *et al.* [162], for various two-body interactions, and then introduce a microscopic action we deal with. A choice of a convenient regulator in performing FRG calculations is also discussed.

4.2.1 Separable potential approximation

To deal with various systems with short-range interactions, we employ the separable potential approximation, which is developed by Ernst *et al.* [162], of realistic potentials. In this approximation, the two-body interaction V is approximated by a projection operator V_s, i.e.

$$V_s = \xi|\chi\rangle\langle\chi|, \tag{4.1}$$

where $|\chi\rangle$ is a state vector of the relative motion of the two particles. Since we are interested in Efimov physics of identical bosons, where the s-wave contribution dominates, we consider a spatially isotropic projection operator, i.e.

$$\chi(\mathbf{q}) := \langle\mathbf{q}|\chi\rangle = \chi(q), \tag{4.2}$$

$$\chi(0) = 1, \tag{4.3}$$

where $\mathbf{q}$ is the relative momenta of scattering particles and the second equality is a convenient normalization condition. In approximating various interaction potentials, we employ the Ernst-Shakin-Thaler method [162], which has been successfully applied to Efimov physics by Naidon *et al.* [79, 80] and reproduces the three-body parameters for various interaction potentials within 10% or less deviations. In the method, we choose the separable potential V_s so that V_s and V behave effectively as the same operator when operating on a particular energy eigenstate $|\psi\rangle$, i.e. V_s and V are identical operators in the Hilbert space composed of $|\psi\rangle$. For the purpose of dealing with the low-energy physics, we choose $|\psi\rangle$ as a zero-energy two-body scattering state.

Let us here summarize the procedure of the Ernst-Shakin-Thaler method for the case of two-body scattering problems for identical bosons. For a separable potential V_s, the zero-energy solution $\psi_{s,0}(\mathbf{r})$ of the two-body Schrödinger equation is given by

$$\psi_{s,0}(\mathbf{r}) = 1 - 4\pi a \int \frac{d^3l}{(2\pi)^3} \frac{\chi(l)}{l^2 - i\epsilon} e^{i\mathbf{l}\cdot\mathbf{r}}, \tag{4.4}$$

$$-4\pi a = -\left(\frac{4}{\xi} + \int \frac{d^3l}{(2\pi)^3} \frac{|\chi(l)|^2}{l^2 - i\epsilon} \right)^{-1}, \tag{4.5}$$

where a is the s-wave scattering length. By imposing $\psi_{s,0}(\mathbf{r}) = \psi_0(\mathbf{r})$, where $\psi_0(\mathbf{r})$ being the the exact zero-energy solution for the potential V, we obtain

$$\chi(q) = 1 + q \int_0^\infty dr \left[\frac{r}{a} \left(1 - \frac{a}{r} - \psi_0(r) \right) \right] \sin(qr). \tag{4.6}$$

If we choose $\chi(q) = 1$, the potential V_s reduces to the contact interaction, and thus, we can see that the separable potential approximation retains much of the simplicity of the contact interaction. To deal with reasonably realistic interaction potentials, we here employ van der Waals, Gaussian, square well, and Yukawa interaction potentials which are approximated by the separable potential approximation. For those four interaction potentials, the function $\chi(q)$ can be determined numerically.

4.2.2 Microscopic action and vacuum limit

With the separable potential approximation, we deal with the following microscopic action that is represented in the imaginary-time formalism:

$$\begin{aligned} S_{\text{bare}} = & \int_Q \psi^*(Q)(iq^0 + q^2 - \mu)\psi(Q) \\ & + \frac{\xi}{4} \int_{\substack{Q_1 Q_2 \\ Q_1' Q_2'}} \delta(Q_1 + Q_2 - Q_1' - Q_2') \chi\left(\frac{\mathbf{q}_1' - \mathbf{q}_2'}{2} \right) \chi^*\left(\frac{\mathbf{q}_2 - \mathbf{q}_1}{2} \right) \\ & \times \psi^*(Q_1')\psi^*(Q_2')\psi(Q_2)\psi(Q_1), \end{aligned} \tag{4.7}$$

where ψ (ψ^*) represents the annihilation (creation) operator of a boson, $Q = (q^0, \mathbf{q})$ represents the Matsubara frequency and the spatial momentum, and $\int_Q := \int \frac{d^4q}{(2\pi)^4}$. Throughout this chapter, we employ the units $k_B = \hbar = 2m = 1$, where k_B is the Boltzmann contant and m is the mass of a boson. We note that the action S_{bare} has the translational, Galilean, and U(1) symmetry. From the imaginary time formalism, that generically deals with systems at finite temperature and finite density, we take the vacuum limit [163, 164, 165] of infinite inverse temperature $\beta \to \infty$ and vanishing particle density $\mu \to -\infty$, where the expectation value with respect to the grand canonical ensemble reduces to the expectation value with respect to the particle vacuum $|0\rangle$, i.e.,

$$\lim_{\substack{\beta\to\infty \\ \mu\to-\infty}} \frac{\mathrm{Tr}\left(A e^{-\beta(H-\mu N)} \right)}{\mathrm{Tr}\left(e^{-\beta(H-\mu N)} \right)} = \langle 0|A|0\rangle, \tag{4.8}$$

where in taking the traces on the left-hand side, the limit $\mu \to -\infty$ selects the sub-Hilbert space with $N = 0$, and the limit $\beta \to \infty$ selects the lowest-lying energy eigenstate. We should note that the vacuum limit can be taken because of the non-relativistic nature and the U(1) symmetry of our system, in which sub-Hilbert spaces with different particle numbers do not couple each other via the Hamiltonian H. For our purpose of demonstrating a convergent structure of RG flows to an RG limit cycle, we compute exact RG flows starting from S_{bare} with various $\chi(q)$.

4.2.3 Regulator choice

To facilitate semi-analytic calculations of the functional renormalization group (FRG) for two and three-body problems, we employ the Litim's optimized regulator $R_k(q)$ which is defined as

$$R_k(q) := (k^2 - q^2)\theta(k^2 - q^2), \tag{4.9}$$

where $q = |\mathbf{q}|$ and θ is the Heaviside unit-step function. The regulator violates neither the translational symmetry nor the U(1) symmetry of the system, while it violates the Galilean symmetry. To respect the Galilean symmetry, the regulator must depend on frequency q^0 in the form of $R_k = R_k(iq^0 + q^2)$, which shifts the position of a frequency pole or adds an additional frequency pole in a loop momentum integral in an FRG equation. We avoid such a complication of a pole structure since the complication may violate a hierarchy structure of FRG equations. In quantum few-body problems, n-body scattering problems can be solved without referring to $(n + 1)$-body physics, and the hierarchy structure is guaranteed in FRG by the vacuum limit in Eq. (4.8) which pushes up all frequency poles of q^0 to the upper-half complex frequency plane. The positions of the frequency poles give rise to as vanishing particle-hole loops, which decouple the n-body sector from the $(n + 1)$-body sector. For detailed discussions on the hierarchy structure of the FRG equations, we refer to Ref. [166]. If we make the regulator frequency dependent, shifted or added frequency poles may violate the hierarchy structure. In short, we here choose the regulator so that the loop expressions of the FRG equations become as simple as possible and so that the regulator does not complicate the hierarchy structure of the few-body scattering problem. While a symmetry-preserving regulator is useful in restricting the ansatz of the flowing action Γ_k, the simple regulator is more convenient for the present purpose of dealing with quantum few-body physics, which can be solved semi-analytically for the regulator.

4.3 Infrared convergent structure of renormalization-group flows

In this section, we demonstrate that the renormalization-group (RG) flows, that start from various microscopic actions, arrive in the infrared limit at a one-dimensional trajectory of an RG limit cycle. Since we are interested in the few-body correlation, we perform a power-series expansion

(the vertex expansion [167]) of the flowing action Γ_k with respect to the fields ψ and ψ^*, i.e.

$$\begin{aligned}\Gamma_k[\psi,\psi^*] = \sum_{n=0}^{\infty}\frac{1}{(n!)^2}\int_{\substack{Q_1,\cdots,Q_n\\Q_1',\cdots,Q_n'}}\Gamma_k^{(2n)}(Q_1,\cdots,Q_n;Q_n',\cdots,Q_1')\\ \times\delta(Q_1+\cdots+Q_n-Q_n'-\cdots-Q_1')\\ \times\psi^*(Q_1)\cdots\psi^*(Q_n)\psi(Q_n')\cdots\psi(Q_1'),\end{aligned} \tag{4.10}$$

where the coefficient $\Gamma_k^{(2n)}$ reduces to the n-th order one-particle irreducible (1PI) vertex in the infrared limit $k \to 0$. Therefore, $\Gamma_k^{(2n)}$ is composed of n-particle scattering processes and is the system parameter of the n-body physics at the energy scale of k. In the following, we focus on $\Gamma_k^{(2n)}$ with $n \leq 3$ to deal with the low-energy universality of two and three-body physics.

4.3.1 One and two-body sectors

We here apply the functional renormalization group to the microscopic action S_{bare} in Eq. (4.7) and derive the exact RG flows for $\Gamma_k^{(2)}$ and $\Gamma_k^{(4)}$. The FRG equations for $\Gamma_k^{(2)}$ is given by

$$\partial_k\Gamma_k^{(2)}(Q) = 0, \tag{4.11}$$

which literally means that the one-body physics is not affected by quantum fluctuations originating in the interaction term. As discussed in Sec. 4.2.2, the vanishing right-hand side originates from the vacuum limit in Eq. (4.8) where contributions from particle-hole loops are eliminated. The result is natural since the self-energy correction is absent in the particle vacuum, where there is no medium effect. We therefore obtain

$$\Gamma_k^{(2)}(Q) = iq^0 + q^2 - \mu = G_0^{-1}(Q). \tag{4.12}$$

Since the one-body sector does not depend on k, the RG flow projected to the one-body sector indeed exhibits a convergent structure to a zero-dimensional sub-theory space, and is thus universal irrespective of the form of interaction $\chi(q)$.

We then consider the two-body sector. The FRG equation for $\Gamma_k^{(4)}$ is given as

$$\begin{aligned}-\ \partial_k\Gamma_k^{(4)}(P;P_2,P_1) = \tilde{\partial}_k\frac{1}{2}\int\frac{d^4l}{(2\pi)^4}\\ \times\frac{\Gamma_k^{(4)}(P;P_2,L)\Gamma_k^{(4)}(P;L,P_1)}{\left[i\left(\frac{p^0}{2}+l^0\right)+\left(\frac{\mathbf{p}}{2}+\mathbf{l}\right)^2-\mu+R_k\left(\frac{\mathbf{p}}{2}+\mathbf{l}\right)\right]\left[i\left(\frac{p^0}{2}-l^0\right)+\left(\frac{\mathbf{p}}{2}-\mathbf{l}\right)^2-\mu+R_k\left(\frac{\mathbf{p}}{2}-\mathbf{l}\right)\right]},\end{aligned} \tag{4.13}$$

where the factor $1/2$ in front of the integral on the right-hand side is the symmetry factor originating in the permutation of two internal propagators. In general, four types of one-loop diagrams appear on the right-hand side of Eq. (4.13); however, three among the four diagrams vanish because of the vacuum limit in Eq. (4.8) which eliminates the contribution of particle-hole loops. From Eqs. (3.41) and (4.7), the ultraviolet (UV) boundary condition for $\Gamma_k^{(4)}(P;P_2,P_1)$ is given by the bare two-body separable interaction, i.e.,

$$\Gamma_{k=\infty}^{(4)}(P;P_2,P_1) = \xi\chi(p_2)\chi^*(p_1). \tag{4.14}$$

Because of the separable nature of the UV boundary condition, the solution of Eq. (4.13) for finite k is also separable with respect to the relative momentum p_2 and p_1. Indeed, if we discretize Eq. (4.13) for an infinitesimal variation δk for the cutoff k, the right-hand side of Eq. (4.13) gives the variation $\delta\Gamma_k^{(4)}$ that is proportional to $\chi(p_2)\chi^*(p_1)$ at each infinitesimal FRG transformation. We thus decompose $\Gamma_k^{(4)}(P;P_2,P_1)$ as

$$\Gamma_k^{(4)}(P;P_2,P_1)=\Gamma_k^S(P)\chi(p_2)\chi^*(p_1), \tag{4.15}$$

where $\Gamma_k^S(P)$ is the propagator of a dimer at the scale of k. For the inverse propagator $\Gamma_k^S(P)$, Eq. (4.13) reduces to

$$\partial_k\left[\Gamma_k^S(P)\right]^{-1}=\partial_k\frac{1}{2}\int\frac{d^3l}{(2\pi)^3}\frac{|\chi(l)|^2}{ip^0+\frac{p^2}{2}+2l^2-2\mu+R_k\left(\frac{\mathbf{p}}{2}+\mathbf{l}\right)+R_k\left(\frac{\mathbf{p}}{2}-\mathbf{l}\right)}, \tag{4.16}$$

where we perform the frequency integral for l^0 on the right-hand side of Eq. (4.13). Equation (4.16) can be integrated analytically with respect to k, and we can easily check that the obtained integral equation is equivalent to the Schwinger-Dyson equation for the two-body 1PI vertex.Together with the renormalization condition in Eq. (4.5), we finally obtain

$$\left[\Gamma_k^S(P)\right]^{-1}=\frac{1}{16\pi a}-\frac{1}{2}\int\frac{d^3l}{(2\pi)^3}\frac{ip^0+\frac{p^2}{2}-2\mu+R_k\left(\frac{\mathbf{p}}{2}+\mathbf{l}\right)+R_k\left(\frac{\mathbf{p}}{2}-\mathbf{l}\right)}{ip^0+\frac{p^2}{2}+2l^2-2\mu+R_k\left(\frac{\mathbf{p}}{2}+\mathbf{l}\right)+R_k\left(\frac{\mathbf{p}}{2}-\mathbf{l}\right)}\frac{|\chi(l)|^2}{2l^2}, \tag{4.17}$$

where a is the s-wave scattering length.

Two-body universality

To see that the low-energy two-body observables take on universal values irrespective of the choice of the separable model, we here derive physical observables from Eq. (4.17), which in the infrared limit $k\to 0$, reduces to the two-body off-shell 1PI vertex. Later, the two-body universality of observables will be revisited from an RG viewpoint. By taking the infrared limit, where $R_k\to 0$, we obtain

$$\Gamma^{(4)}(P;P_2,P_1)=\left(\frac{1}{16\pi a}-\frac{1}{2}\int\frac{d^3l}{(2\pi)^3}\frac{ip^0+\frac{p^2}{2}-2\mu}{ip^0+\frac{p^2}{2}+2l^2-2\mu}\frac{|\chi(l)|^2}{2l^2}\right)^{-1}\chi(p_2)\chi^*(p_1). \tag{4.18}$$

We consider the on-shell two-body scattering amplitude in the center-of-mass frame, where $p=0$, $p_1^0=p_2^0=0$, $p_1=p_2=q$, and $i\frac{p^0}{2}=-q^2+\mu$. With these conditions, the on-shell scattering amplitude $f(q)$ is given by

$$\begin{aligned}f(q)&=-\frac{1}{16\pi}\Gamma^{(4)}=\left(-\frac{1}{a}-\frac{2}{\pi}\int_0^\infty dl\frac{q^2}{l^2-q^2-i\epsilon}|\chi(l)|^2\right)^{-1}|\chi(q)|^2\\&=\left(-\frac{1}{a}-iq\,|\chi(q)|^2-\frac{2}{\pi}\int_0^\infty dl\frac{|\chi(l)|^2-|\chi(q)|^2}{l^2-q^2}q^2\right)^{-1}|\chi(q)|^2,\end{aligned} \tag{4.19}$$

which gives an exact expression (within the separable model) for the phase shift $\delta(q)$:

$$q\cot\delta(q) = -\frac{1}{a}\frac{1}{|\chi(q)|^2} - \frac{2}{\pi}\int_0^\infty dl \frac{\frac{|\chi(l)|^2}{|\chi(q)|^2}-1}{l^2-q^2}q^2, \tag{4.20}$$

$$r_{\rm eff} = -\frac{2}{a}\frac{d^2}{dq^2}\left(\frac{1}{|\chi(q)|^2}\right)_{q=0} - \frac{4}{\pi}\int_0^\infty dl \frac{|\chi(l)|^2-1}{l^2}, \tag{4.21}$$

where $r_{\rm eff}$ is an effective range. If we take the low-energy limit $q \to 0$, the scattering amplitude $f(q)$ and the bound state energy E_B are given as

$$f(q) = -\frac{1}{1/a + iq}, \tag{4.22}$$

$$E_B = -\frac{2}{a^2} \text{ when } a > 0, \tag{4.23}$$

irrespective of the functional form of $\chi(q)$. We note that Eqs (4.22) and (4.23) reproduce the scattering amplitude and the bound-state energy for the simplest case of $\chi(q) = 1$, in which case the separable interaction reduces to the contact interaction.

Infrared convergence of RG flows

We here investigate the two-body universality near the unitarity limit from a convergent structure of RG flows. For better understanding, we here consider sufficiently large but finite $a \gg \sigma$ where σ is a set of parameters that characterize length scales in χ, although we are ultimately interested in the unitarity limit $a = \pm\infty$. We start from a dimensionless on-shell two-body scattering amplitude in the center-of-mass frame:

$$f_k(q) := -\frac{1}{16\pi}k\Gamma_k^{(4)}(ip^0 = 2\mu, p = 0; p_2^0 = 0, p_2 = q, p_1^0 = 0, p_1 = q), \tag{4.24}$$

where q is the relative momenta of incoming and outgoing two particles. In investigating the RG flow, we focus on two dimensionless system parameters g_2 and l_2 which represent effective interaction strength and an effective range of the interaction, respectively. Therefore, we introduce two-body coupling constant g_2 and two-body range parameter l_2 so that the definitions are in parallel with the dimensionless scattering length a and the effective range $r_{\rm eff}$, i.e.,

$$g_2 := -f_k(0), \tag{4.25}$$

$$l_2 := 2\frac{d^2}{dq^2}\left(f_k^{-1}(q)\right)_{q=0}, \tag{4.26}$$

where g_2 is defined so that it coincides with the dimensionless scattering length ak in the infrared limit $k \to 0$, and similarly, l_2 is defined in parallel with Eq. (4.21). From Eqs. (4.15) and (4.17) together with the explicit form of the regulator Eq. (4.9), we obtain the forms of g_2 and l_0 as

$$g_2 = \left(\frac{1}{ak} - \frac{2}{\pi}\int_0^k \frac{dl}{k}\frac{k^2-l^2}{k^2}|\chi(l\sigma)|^2\right)^{-1}, \tag{4.27}$$

$$l_2 = -\frac{2k}{a}\frac{d^2}{dq^2}\left(\frac{1}{|\chi(q\sigma)|^2}\right)_{q=0} - \frac{4}{\pi}\int_0^k dl \frac{l^2|\chi(l\sigma)|^2}{k^3} - \frac{4}{\pi}\int_k^\infty dl \frac{k|\chi(l\sigma)|^2}{l^2}, \tag{4.28}$$

where we note that the dimensionless function $\chi(q)$ must depend on q and σ as $\chi(q\sigma)$. By changing the integration variable $l \to x = l/k$, g_2 and l_2 becomes

$$g_2 = \left(\frac{1}{ak} - \frac{2}{\pi}\int_0^1 dx(1-x^2)\,|\chi(xk\sigma)|^2\right)^{-1}, \tag{4.29}$$

$$l_2 = -\frac{2(k\sigma)^2}{ak}\frac{d^2}{d(q\sigma)^2}\left(\frac{1}{|\chi(q\sigma)|^2}\right)_{q\sigma=0} - \frac{4}{\pi}\int_0^1 dx x^2\,|\chi(xk\sigma)|^2 - \frac{4}{\pi}\int_1^\infty dx\frac{|\chi(xk\sigma)|^2}{x^2}. \tag{4.30}$$

Now we consider the infrared limit $k \to 0$ of g_2. Since we are interested in the parameter region near the unitarity limit, where $ak \sim 1 \gg k\sigma$, we perform the Taylor expansion of $\chi(xk\sigma)$, which satisfies $\chi(0) = 1$ because of the normalization condition in Eq. (4.3). In particular, we approximate $|\chi(y)|^2$ by $(1 + C^2y^2)^{-1}$, since the terms of order y do not appear in the expression because of Eq. (4.6). By taking the terms of up to $O(k\sigma)$ in Eqs. (4.29) and (4.30), we finally obtain

$$g_2 = \frac{ak}{1 - \frac{4}{3\pi}ak}, \tag{4.31}$$

$$l_2 = -\frac{16}{3\pi} - \frac{4C^2(k\sigma)^2}{ak} + 2Ck\sigma. \tag{4.32}$$

Let us see how the parameter flows of (g_2, l_2) describe the two-body universality Eqs. (4.22) and (4.23). In the vicinity of the unitarity limit, where $a \gg \sigma$, l_2 takes on almost constant value of $-\frac{16}{3\pi}$ in the infrared regime $k \ll \frac{1}{\sigma}$, while g_2 continues to vary. Thus the RG flows in g_2-l_2 plane are strongly attracted towards a one-dimensional trajectory of $l_2 = -\frac{16}{3\pi}$, which is the renormalized trajectory of the two-body universality at large but finite scattering length. This convergent structure of the RG flows describes Eqs. (4.22) and (4.23), where physical observables are characterized by one parameter, i.e., the scattering length a. When a diverges, g_2 also takes on a fixed value and the renormalized trajectory becomes zero-dimensional.

Let us here visualize the convergent behavior. From Eqs. (4.31) and (4.32), we can derive reduced RG equations of g_2 and l_2 as

$$k\frac{dg_2}{dk} = g_2\left(g_2 + \frac{4}{3\pi}\right); \tag{4.33}$$

$$k\frac{dl_2}{dk} = l_2 + \frac{16}{3\pi}. \tag{4.34}$$

We note that Eq. (4.33) agrees with the previously obtained RG equation for a two-body system with the contact interaction [168]. Based on the reduced RG equations, we plot RG flows in Fig. 4.1. We can clearly see the convergent structure of the RG flows. In particular, in the infrared limit $k \to 0$, we find

$$g_2 \to \begin{cases} 0 & \text{when } 1/a \neq 0, \\ -\frac{4}{3\pi} & \text{when } 1/a = 0, \end{cases} \tag{4.35}$$

$$l_2 \to -\frac{16}{3\pi}. \tag{4.36}$$

We find two different limits for g_2 depending on the value of the scattering length a. The fixed point $g_2 = 0$ is called the Gaussian fixed point, which represents the action of free bosons, and the

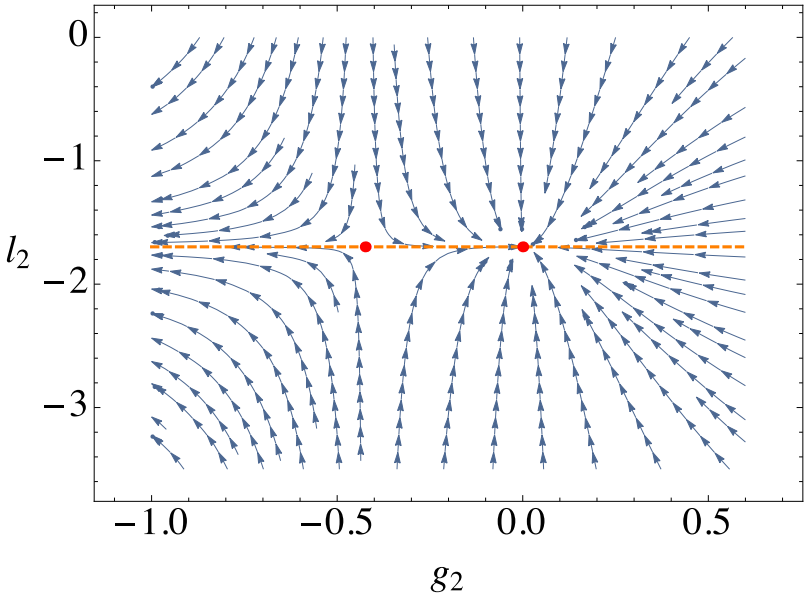

Figure 4.1: RG flows obtained from Eqs. (4.33) and (4.34). The orange dashed line $l_2 = -\frac{16}{3\pi}$ shows the one-dimensional renormalized trajectory for finite scattering length a. Indeed, we can see all the RG flows are attracted towards the renormalized trajectory. The right and left red dots are the Gaussian fixed point and the unitary fixed point, respectively. When a diverges, we can see that the RG flows are attracted towards the unitary fixed point, which corresponds to the zero-dimensional renormalized trajectory at the unitarity limit.

fixed point $g_2 = -\frac{4}{3\pi}$ is called the unitarity fixed point [32], which represents the action including the zero-energy dimerized molecules. We can understand the two limits in the following manner: Aside from the unitarity limit, two-particle excitations are gapped from one-particle excitations with the gap $\Delta E \sim \frac{1}{a^2}$, and thus, at sufficiently low energy $E \ll \frac{1}{a^2}$, the excitation spectrum is dominated by the one-particle excitations. On the other hand, a zero-energy two-body excitation, i.e. the two-body bound state, emerges at the unitarity limit, and the low-energy excitation spectrum is affected from the molecule state. We also note that the coupling constant g_2 diverges at the energy scale of $k \sim \frac{1}{a}$ if a takes on a positive value. Considering the fact that a bound state with energy $\sim \frac{1}{a^2}$ emerges for positive a, the divergence of g_2 can be regarded as the fingerprint of the bound state.[2]

We have thus demonstrated that the one- and the two-body coupling constants are attracted toward a finite-dimensional sub-theory space. In particular, we show that the sub-theory space becomes the zero-dimensional unitary fixed point when the scattering length a diverges.

[2] A similar argument can be found in Ref. [169], where the authors relate the superconducting gap with a divergence of the Cooper-channel coupling in electronic systems.

4.3.2 Three-body sector

For the one and the two-body sectors, we have seen that the RG flows for various systems arrive at a zero-dimensional renormalized trajectory at the unitarity limit. Here in this subsection, we demonstrate that the renormalized trajectory for the three-body sector becomes a one-dimensional RG limit cycle. To this end, we devise a method which combines the three-body FRG equation, which is developed by Tanizaki [78], and the separable models for which the three-body FRG equation can be solved numerically without approximations. The devised method is based on our original research article of Ref. [76].

Three-body FRG equation

We first derive within the FRG formalism the flow equation for the three-body 1PI vertex of the separable models. Although the flow equation of the three-body 1PI vertex within the auxiliary field formalism has already been presented in Refs. [165, 170], the obtained equation is not correct because some Feynman diagrams are overlooked. The correct equation without an auxiliary field has been derived by Tanizaki in Ref. [78] for two-component Fermi systems, whereas the obtained FRG equation is not tractable due to the large number of momentum indices. The purpose of this section is, therefore, to devise a numerically tractable method by combining the Tanizaki's three-body FRG equation [78] and the separable models introduced in Sec. 4.2.1.

We start from the FRG equation, that is depicted in Fig. 4.2, for the three-body 1PI vertex $\Gamma_k^{(6)}$ defined in Eq. (4.10). As shown in Fig. 4.2, the contribution from $\Gamma_k^{(8)}$, which represents the four-body correlation, appears on the right-hand side of the FRG equation. In the vacuum limit in Eq. (4.8), such a contribution should be decoupled from $\Gamma_k^{(6)}$, because of the few-body hierarchy structure, in which the three-body observables do not depend on the four-body observables. To resolve this problem, we examine the Feynman diagrams that contribute to $\Gamma_k^{(8)}$ in the three-body FRG equation. By making use of the separable nature of the two-body 1PI vertex $\Gamma_k^{(4)}$, we first introduce a convenient diagrammatic expression for the three-body 1PI vertex $\Gamma_k^{(6)}$ as shown in Fig. 4.3(a), where the separable nature of $\Gamma_k^{(4)}$ is used to factor out the external relative momentum dependence of $\Gamma_k^{(6)}$ by the form factor $\chi(q)$:

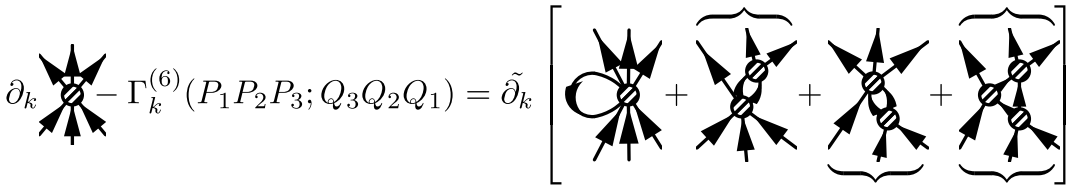

Figure 4.2: FRG equation for the three-body 1PI vertex $\Gamma_k^{(6)}$ in the particle vacuum. A shaded circle with $2n$ external lines shows the n-body 1PI vertex $-\Gamma_k^{(2n)}$, and a internal line shows the regularized one-particle propagator $(G_0^{-1} + R_k)^{-1}$, where G_0^{-1} is given in Eq. (4.12). On the right-hand side, the derivative $\tilde{\partial}_k$ acts only on the regulators R_k included in the internal lines. The curly brackets show the symmetrization in Eq. (4.38) with respect to the external momenta. On the right-hand side, the first term shows the contribution from four-body correlation $\Gamma_k^{(8)}$.

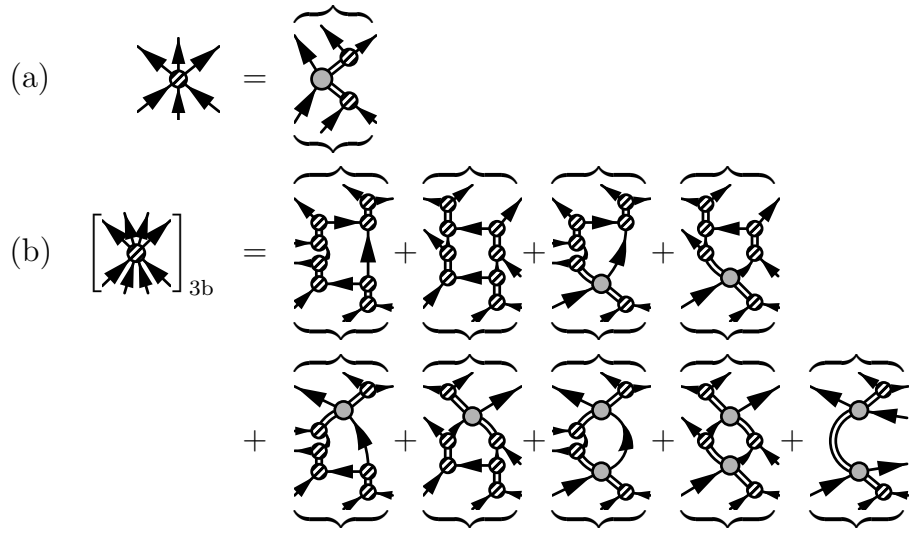

Figure 4.3: (a) Decomposition of the three-body 1PI vertex $\Gamma_k^{(6)}$. A shaded circle with one double line and two solid lines represents the form factor χ, a double line shows the dimer propagator Γ_k^S, the gray-colored circle represents the particle-dimer 1PI vertex $-\gamma_k$, and curly brackets represent the symmetrization in Eq. (4.38) with respect to the external momenta. With these correspondences, the figure represents Eq. (4.37). We note that the external relative-momentum dependence is factored out by the form factor χ. (b) Four-body 1PI vertex $\Gamma_k^{(8)}$ that contributes to the FRG equation of the three-body 1PI vertex depicted in Fig. 4.2.

$$
\begin{aligned}
&-\Gamma_k^{(6)}(P_1P_2P_3;Q_3Q_2Q_1)\\
&=\left[\chi\left(\frac{\mathbf{p}_2-\mathbf{p}_3}{2}\right)\Gamma_k^S(P_2+P_3)\left\{-\gamma_k\left(P_1,P_2+P_3;Q_3+Q_2,Q_1\right)\right\}\Gamma_k^S(Q_3+Q_2)\chi\left(\frac{\mathbf{q}_3-\mathbf{q}_2}{2}\right)\right]_{\mathrm{S}},
\end{aligned}
\tag{4.37}
$$

where the two-body propagator Γ_k^S is defined in Eq. (4.15), γ_k represents a particle-dimer 1PI vertex, and $[\cdots]_{\mathrm{S}}$ is the symmetrization with respect to the external momentum defined by

$$
[f(P_1P_2P_3;Q_3Q_2Q_1)]_{\mathrm{S}}=\frac{1}{3!3!}\sum_{\sigma_P,\sigma_Q}f(P_{\sigma_P(1)}P_{\sigma_P(2)}P_{\sigma_P(3)};Q_{\sigma_Q(3)}Q_{\sigma_Q(2)}Q_{\sigma_Q(1)}),
\tag{4.38}
$$

where σ_Q and σ_P are the permutation operators of incoming and outgoing external momentum, respectively. With the decomposed expression of $\Gamma_k^{(6)}$ in Eq. (4.37) (or equivalently Fig. 4.3(a)), we can deal with the particle-dimer vertex γ_k which has a smaller number of momentum arguments than that of the three-body 1PI vertex $\Gamma_k^{(6)}$, and thus is easier to deal with. Using the decomposition, we resum the Feynman diagrams that contribute to $\Gamma_k^{(8)}$ in the three-body FRG equation. In resumming the diagrams, we have only to take into account the ladder-type Feynman diagrams, since particle-hole loops do not contribute in the particle vacuum in Eq. (4.8). We finally find that the contribution can be represented only by $\Gamma_k^{(6)}$ and $\Gamma_k^{(4)}$, as depicted in Fig. 4.3(b).

Since the particle-dimer 1PI vertex γ_k contains the same three-body information as the three-body 1PI vertex $\Gamma_k^{(6)}$, we use γ_k as the three-body system parameter. More precisely, we deal with

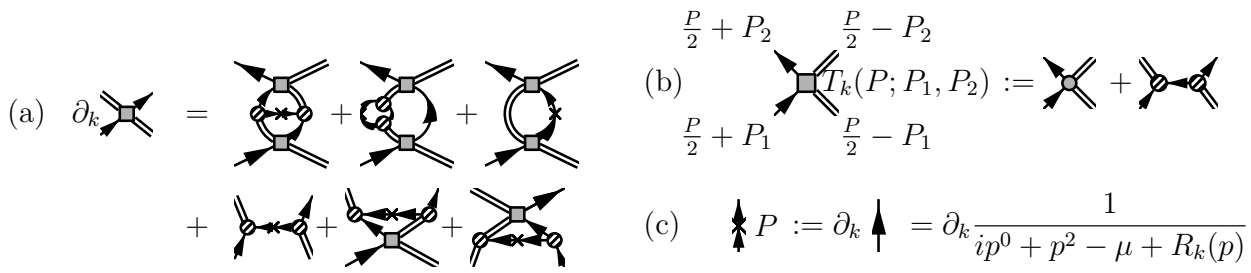

Figure 4.4: (a) FRG equation for the particle-dimer scattering amplitude T_k, which is defined in Eq. (4.39). On the right-hand side, a shaded square represents T_k as explicitly depicted in Fig. 4.4(b), and a cross inserted in internal lines indicates the k-derivative of the regulator $\partial_k R_k$ as explicitly depicted in Fig. 4.4(c).

the particle-dimer scattering amplitude T_k, which is defined by

$$T_k(P;P_2,P_1) = -\gamma_k\left(\frac{P}{2}+P_2,\frac{P}{2}-P_2;\frac{P}{2}-P_1,\frac{P}{2}+P_1\right) + \frac{1}{G_0^{-1}(P_2+P_1)+R_k(\mathbf{p}_2+\mathbf{p}_1)}, \quad (4.39)$$

which can be diagrammatically represented as in Fig. 4.4(b). By substituting the diagrammatic expressions in Figs. 4.3(a), 4.3(b), and 4.4(b) into the FRG equation in Fig. 4.2, we reduce the FRG equation of $\Gamma_k^{(6)}$ to that of T_k, as depicted in Fig. 4.4(a). In solving the FRG equation in Fig. 4.4(a), we notice that the second and the third terms can be combined via the equation depicted in Fig. 4.5(a). With this combination, we notice that the diagrams appearing on the right-hand side of Fig. 4.4(a) are represented by three sub-diagrams that are depicted in Fig. 4.5. If we regard the three sub-diagrams as matrices whose indices are outgoing and incoming momentum, the FRG equation depicted in Fig. 4.5(a) can be written down in a differential equation of the matrices:

$$\partial_k T = T\cdot G\cdot\partial_k t\cdot G\cdot T + T\cdot\partial_k G\cdot T + \partial_k t + \partial_k t\cdot G\cdot T + T\cdot G\cdot\partial_k t. \quad (4.40)$$

This equation can be analytically integrated with respect to k, giving

$$T = t + t\cdot G\cdot T, \quad (4.41)$$

which is diagrammatically represented in Fig. 4.5(c). Explicitly, Eq. (4.41) is given as

$$\begin{aligned} T_k(P;P_2P_1) &= \frac{\chi\left(\frac{\mathbf{p}_2+2\mathbf{p}_1-\frac{\mathbf{p}}{2}}{2}\right)\chi^*\left(\frac{2\mathbf{p}_2+\mathbf{p}_1-\frac{\mathbf{p}}{2}}{2}\right)}{i\left(p_2^0+p_1^0\right)+\left(\mathbf{p}_2+\mathbf{p}_1\right)^2-\mu+R_k\left(\mathbf{p}_2+\mathbf{p}_1\right)} \\ &\quad+\int_Q \frac{\chi\left(\frac{\mathbf{p}_2+2\mathbf{q}-\frac{\mathbf{p}}{2}}{2}\right)\chi^*\left(\frac{2\mathbf{p}_2+\mathbf{q}-\frac{\mathbf{p}}{2}}{2}\right)}{i\left(p_2^0+q^0\right)+\left(\mathbf{p}_2+\mathbf{q}\right)^2-\mu+R_k\left(\mathbf{p}_2+\mathbf{q}\right)} \\ &\quad\times\frac{-\Gamma_k^S\left(\frac{P}{2}+Q\right)T_k(P;QP_1)}{i\left(\frac{p^0}{2}-p^0\right)+\left(\frac{\mathbf{p}}{2}-\mathbf{q}\right)^2-\mu+R_k\left(\frac{\mathbf{p}}{2}-\mathbf{q}\right)}. \end{aligned} \quad (4.42)$$

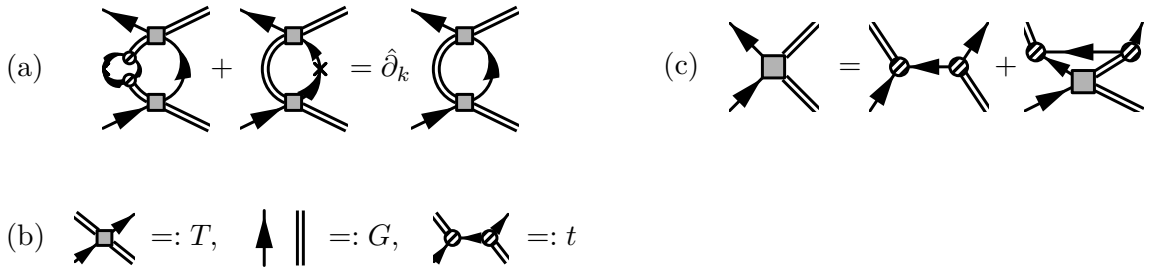

Figure 4.5: (a) The second and the third terms on the right-hand side in the FRG equation of the particle-dimer scattering amplitude T_k (see Fig. 4.4(a)). The derivative $\hat{\partial}_k$ acts on the two internal lines, where the solid line is the regulated particle propagator $(G_0^{-1} + R_k)^{-1}$ and the double line is the dimer propagator Γ_k^s. (b) Three sub-diagrams appearing on the right-hand side of the FRG equation of T_k. Since those sub-diagrams depend on the conserving total momentum and the non-conserving incoming and outgoing relative momentum, we regard those sub-diagrams as matrices, where indices are the incoming and outgoing relative momentum. (c) Integrated three-body FRG equation for T_k, that is given in Eq. (4.41).

We note that Eq. (4.42) reduces to the separable-model-extension of the Skornyakov-Ter-Martirosian equation [8], in the infrared limit $k \to 0$. To define a three-body system parameter, for which RG flows are investigated, we focus on the on-shell s-wave scattering amplitude in the center-of-mass frame, as is done in the two-body sector. For this purpose, we perform the s-wave projection of Eq. (4.41), and set the external momenta of T_k as $ip^0 + 3\mu = 0$, $\mathbf{p} = 0$, and $ip_i^0 = \frac{ip^0}{2} + p_i^2 - \mu + R_k(p_i)$ $(i = 1, 2)$. We thus obtain an FRG equation for the particle-dimer s-wave scattering amplitude T_k^S:

$$
\begin{aligned}
T_k^S(p_2, p_1) \;=\; & \frac{1}{2}\int d(\cos\theta_{p_1 p_2}) \frac{\chi\left(\mathbf{p}_1 + \frac{\mathbf{p}_2}{2}\right)\chi^*\left(\frac{\mathbf{p}_1}{2} + \mathbf{p}_2\right)}{p_1^2 + p_2^2 + (\mathbf{p}_1 + \mathbf{p}_2)^2 + R_k(p_1) + R_k(p_2) + R_k(\mathbf{p}_1 + \mathbf{p}_2)} \\
& + \int_0^\infty \frac{q^2 dq}{(2\pi)^3}\left[\frac{1}{2}\int d(\cos\theta_{q p_2}) \frac{\chi\left(\mathbf{q} + \frac{\mathbf{p}_2}{2}\right)\chi^*\left(\frac{\mathbf{q}}{2} + \mathbf{p}_2\right)}{q^2 + p_2^2 + (\mathbf{p}_2 + \mathbf{q})^2 + R_k(q) + R_k(p_2) + R_k(\mathbf{p}_2 + \mathbf{q})}\right] \\
& \times \left[-\Gamma_k^S\left(\frac{P}{2} + Q\right)\Big|_{ip^0 + 3\mu = 0, iq^0 = \frac{ip^0}{2} + q^2 - \mu + R_k(q)}\right] \times T_k^S(q, p_1), \qquad (4.43)
\end{aligned}
$$

$$
T_k^S(p_2, p_1) := \int d\hat{\mathbf{p}}_2 d\hat{\mathbf{p}}_1 \mathrm{Y}_{00}^*(\hat{\mathbf{p}}_2)\mathrm{Y}_{00}^*(\hat{\mathbf{p}}_1)\, T_k(P; P_2, P_1)|_{ip^0 + 3\mu = 0, \mathbf{p} = 0, ip_i^0 = \frac{ip^0}{2} + p_i^2 - \mu + R_k(p_i)}, \qquad (4.44)
$$

where $\theta_{p_1 p_2}$ is the angle between two vectors $\mathbf{p}_1$ and $\mathbf{p}_2$, $\hat{\mathbf{k}}$ is the unit vector $\mathbf{k}/k$, and Y_{00} is the spherical harmonics with angular momentum quantum numbers $l = m = 0$. We note that Eq. (4.44) is an exact RG equation of the s-wave particle-dimer scattering amplitude for a given separable model and, therefore, the equation unbiasedly describes the RG flow of the three-body problems. We numerically solve Eq. (4.43) for various separable models to demonstrate the convergent structure of RG flows in the three-body sector.

Numerical solution of Eq. (4.44)

We here summarize the details of the numerical calculation of Eq. (4.44). Noting that Eq. (4.44) is a linear integral equation, we find that numerical solution of Eq. (4.44) consists of two steps. The first step is to determine the matrix elements of the linear equation by performing the integral with respect to the variable of $\cos\theta_{p_1p_2}$. The second step is to solve the integral equation directly to determine the vector $T_k^S(p_2, p_1 = 0)$, where different values of p_1 are decoupled in the linear equation of Eq. (4.44). In these two steps, we discretize the variables as

$$x_n = -1 + \frac{2(n-1)}{N} \quad (n = 1, \cdots, N), \tag{4.45}$$

$$p_m = p_{\min}\left(\frac{p_{\max}}{p_{\min}}\right)^{\frac{m-1}{M}} \quad (m = 1, \cdots, M), \tag{4.46}$$

where x_n is the discretization of the variable $\cos\theta_{p_1p_2}$ that takes on the value over $[-1, 1]$ and p_m is the discretization of the momentum variable that takes on the value over $[p_{\min}, p_{\max}]$. Here we choose N = 80-100 to perform the integral with respect to $\cos\theta_{p_1p_2}$ by the trapezoidal rule, and M = 200-300 for the momentum variables. Our choice of the momentum grid, which is of a geometric nature, is due to the discrete-scale invariance of the Efimov effect. The lower and the upper bounds $p_{\min}$ and $p_{\max}$ are chosen as

$$p_{\min} = 10^{-8}/r_{\text{eff}}, \quad p_{\max} = 200/r_{\text{eff}} \tag{4.47}$$

so that $p_{\min}$ ($p_{\max}$) is sufficiently smaller (larger) than the characteristic length scale set by the effective range r_{eff}. With the set-up, we numerically solve Eq. (4.44) by means of the Mathematica, which solves a linear equation by the Krylov method or the multifrontal method for a dense nonsymmetric matrix.

Convergence of RG flows

As reviewed in Sec. 2.2, for the energy scale much smaller than the effective range r_{eff}, three-body observables are universally determined by the three-body parameter κ at the unitarity limit, irrespective of the short-range details of a given microscopic system. In particular, the three-body binding energies show the discrete scale-invariant spectrum $E_n = \kappa^2 e^{\frac{2\pi}{s_0}}$ with the constant scaling factor of $e^{\frac{\pi}{s_0}} \simeq 22.694$. Here we revisit the three-body universality from an RG point of view. As a three-body system parameter, for which RG flows are investigated, we introduce the three-body constant g_3 which reduces to the dimensionless particle-dimer scattering length in the infrared limit $k \to 0$, and thus represents the effective three-body interaction strength. For this purpose, we define three-body coupling constant g_3 by the on-shell s-wave particle-dimer scattering amplitude at zero momentum, i.e.,

$$g_3 := k^2 T_k^S(p_2 = 0, p_1 = 0). \tag{4.48}$$

By solving the FRG equation in Eq. (4.43) for various systems with different short-range potentials, we obtain Fig. 4.6. In Fig. 4.6, the cutoff k dependence of g_3 is plotted for the systems with van der

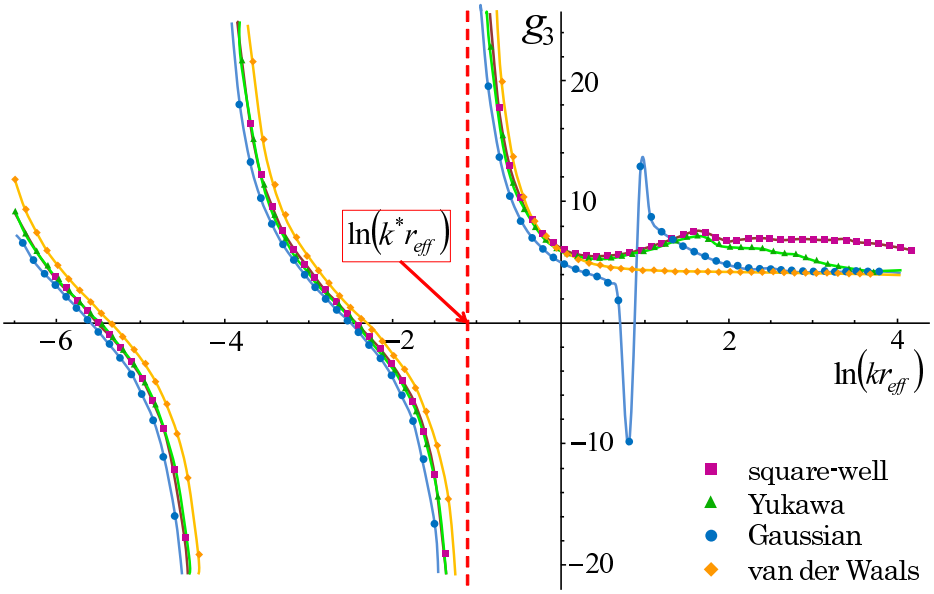

Figure 4.6: Cutoff k dependence of g_3 for systems with various short-range interactions, that are approximated by separable potentials. The purple-colored squares show the square well potential that support infinite number of two-body bound states, the green-colored triangles show the Yukawa potential with a bound state, blue-colored circles show the Gaussian potential with a two-body bound state, and yellow-colored diamonds show the van der Waals potential with infinite number of two-body bound states. While non-universal behavior of g_3 is observed at high energy, g_3 begins to show the RG limit-cycle behavior at the energy scale $k \lesssim \frac{1}{r_{\rm eff}}$. If we lower the cutoff k, g_3 first diverges at the energy scale of $k = k^*$, which is found to reproduce the energy eigenvalue of the lowest-lying Efimov trimer at the unitarity limit. The figure is adapted from Ref. [76]. Copyright

Waals, Gaussian, Yukawa, and square well potentials, that are approximated by separable potentials. At high energy $kr_{\rm eff} \gtrsim 1$, we see that g_3 behaves non-universally depending on the short-range details of each individual interaction potential; however, below the energy scale of $kr_{\rm eff} \lesssim 1$, g_3 begins to flow universally, showing a characteristic behavior of an RG limit cycle. In particular, the one period of the cyclic behavior is estimated as $\Delta \ln kr_{\rm eff} \simeq \ln 22.7$ for $kr_{\rm eff} \ll 1$, which reproduces the constant scaling factor of the Efimov physics. We thus find that RG flows of the three-body sector converge to an RG limit cycle at sufficiently low energy. This convergent structure of g_3 into the one-dimensional RG limit cycle represents the universality of three-body low-energy observables, which are characterized only by one parameter, i.e., the three-body parameter κ. In the RG flow, the inverse effective range $1/r_{\rm eff}$ characterizes the typical energy scale below which universal behavior sets in, and this is consistent with the fact that three-body observables are universally determined by κ below the energy scale of $1/r_{\rm eff}$. We also try to extract physical observables from the RG flows: As discussed in Sec. 4.3.1, a divergence of a coupling constant is often identified with the emergence of a bound state. We thus evaluate the highest energy scale k^* at which g_3 diverges (see Fig. 4.6), and find that k^* indeed reproduces the energy eigenvalue of the lowest-lying Efimov

trimer.

We have thus shown that the one- and the two-body coupling constants are attracted towards zero-dimensional sub-theory space in Sec. 4.3.1, and we have also numerically demonstrated that that the three-body coupling constant is attracted to the one-dimensional RG limit cycle in Sec. 4.3.2. The combination of these results provides a numerical evidence that the RG flows are attracted toward the one-dimensional RG limit cycle at sufficiently low-energy, reflecting the fact that any low-energy observable is represented only by the three-body parameter κ at the unitarity limit. We thus provide for the first time that the RG limit cycle is the renormalized trajectory (or an infrared attractor) of various RG flows.

Chapter 5

Limit cycle in universal four-body physics

5.1 Question addressed

In the preceding chapter, we have provided a numerical evidence that the renormalization-group (RG) limit cycle is the renormalized trajectory that represents the universal emergence of the Efimov physics at sufficiently low energy in various microscopic systems. Indeed, up to the three-body sector, RG flows starting from distinct Hamiltonians exhibit universally the limit-cycle behavior at sufficiently low energy. Concerning the four-body physics, however, the relationship between the RG limit cycle and the four-body low-energy universality reviewed in Sec. 2.4 remains elusive. Therefore, we here address the question of

- What is the relationship between the RG limit cycle and the low-energy universal observables in the four-body physics?

Since an RG limit cycle can, in principle, flow far away from the Gaussian fixed point, perturbative treatment of the RG equation around the fixed point cannot be applied to the present problem. This is indeed the case in the Efimov effect as we see in Sec. 4.3.2, where the three-body coupling constant g_3 diverges. We therefore employ the functional renormalization group (FRG) to perform a nonperturbative RG calculation.

The FRG has been applied to the four-body physics firstly by Moroz *et al.* [171] and later by Ávila *et al.* [172, 173]; however, the analyses lead to spurious four-body bound states that contradict established universality reviewed in Sec. 2.4. For example, in Ref. [171], only one tetramer attached to an Efimov trimer is identified. In Ref. [172], super-Efimov-like tetramer states emerge, namely, the energy eigenvalues of the tetramer exhibit the double exponential behavior in Eq. (2.76). While the authors of Ref. [173] find the two tetramers accompanying an Efimov trimer, evaluated Efimov's scaling factor $e^{\pi/s_0} \simeq 29.8$ clearly deviates from the exact value of $22.694\cdots$. Above all, the relationship between the RG limit cycle and the four-body universality remains to be unanswered question. As the authors of Ref. [171] have already pointed out, the deviations of the results from the established universality are due to the derivative expansion in which momentum dependence of correlation functions is disregarded and is considered to be a constant.

The purpose of this chapter is, therefore, to demonstrate that the RG limit cycle of the four-body sector contains the essential pieces of the universal low-energy observables by resolving the prob-

lems of the previous FRG calculations. To this end, we develop a non-perturbative FRG method that can deal with the momentum dependence of correlation functions and can deal with a functional flow of the effective action. We first develop a simple (numerically tractable) effective field theory that reproduces the universal low-energy observables, such as the trimer energies and the particle-dimer scattering amplitude, of the Efimov effect. We then devise an FRG method by a separable pole approximation of the three-body sub-amplitude of the entire four-body scattering process. The effective field theory and the FRG methods are based on our original research article of Ref. [77]. A major methodological difference of the ordinary Faddeev-Yakubovski equation and our FRG method is the following: While the Faddeev-Yakubovski equation deals with the correlation functions with the entire quantum fluctuations, our FRG method deals with the coarse-grained correlation functions parametrized by the RG cutoff k. In other words, we investigate a system by following how an effective correlation function varies according to the variation of the cutoff k, rather than by seeing the functional form of a fully renormalized correlation function. In this chapter, we show for the first time that the k-dependence of the coarse-grained four-body coupling constant contains the essential pieces of information of the low-energy observables, such as the numbers and the energies of tetramer states, of the four-body physics. An improved evaluation, which is not investigated in Ref. [77], of the tetramer energies will also be discussed in Sec. 5.4, where we introduce a systematic improvement of the the separable pole approximation by making use of the Hilbert-Schmidt expansion [174] of a self-adjoint operator.

5.2 Effective field theory and functional renormalization-group formalism

To answer the question discussed in the preceding section, we employ the function renormalization group (FRG), which allows us to deal with non-perturbative renormalization-group (RG) flows: While RG flows in the vicinity of a fixed point can be dealt with a perturbative RG, the limit cycle, which can flow far away from a fixed point, requires a non-perturbative RG treatment. To this end, we first develop an effective field theory and a FRG formalism that are suitable in dealing with Efimov physics.

5.2.1 Effective field theory

To deal with the universal aspects of Efimov physics, we first develop a simple effective field theory that reproduces the universal low-energy observables, such as the trimer energies and the particle-dimer scattering amplitude, of the Efimov effect. To this end, we consider the following microscopic action that consists of a bosonic particle ψ and an auxiliary dimerized molecule ϕ:

$$\begin{aligned} S[\psi,\phi] := & \int_P \psi^*(P) G_\psi^{-1}(P)\psi(P) + \int_P \phi^*(P)\left[-\frac{1}{16\pi}\sqrt{\frac{ip^0}{2}+\frac{\mathbf{p}^2}{4}-\mu_1}-\mu_2\right]\phi(P) \\ & - \int_{PP_2P_1} G_\psi\left(\frac{P}{3}+P_2+P_1\right)\phi^*\left(\frac{2P}{3}+P_2\right)\psi^*\left(\frac{P}{3}-P_2\right)\psi\left(\frac{P}{3}-P_1\right)\phi\left(\frac{2P}{3}+P_1\right), \end{aligned} \tag{5.1}$$

where $P = (p^0, \mathbf{p})$ is the four momentum that consists of the Matsubara frequency p^0 and the spatial momentum $\mathbf{p}$ and $\int_P := \int \frac{d^4p}{(2\pi)^4}$. The function $G_\psi(P) := (ip^0 + \mathbf{p}^2 - \mu_1)^{-1}$ on the right-hand side is the propagator of a free bosonic particle. Here and throughout this chapter, we employ the units $\hbar = 2m = 1$, where m ($2m$) is the mass of a particle (a dimer). We note that the chemical potential μ_1 of a particle is taken to $-\infty$ for the purpose of dealing with the vacuum limit introduced in Sec. 4.2.2 and that the chemical potential μ_2 tunes the s-wave scattering length a. In ultracold atoms, the fields ψ and ϕ can be regarded as an open-channel atom and a closed-channel molecule, respectively.

We construct the microscopic action $S[\psi, \phi]$ by reducing the local interactions in the ordinary effective field theory by Bedaque *et al.* [14, 15] (see Eq. (2.48)) to a particle-exchange interaction between a particle and a dimer, as shown in the third term on the right-hand side of Eq. (5.1). The reduction is motivated by the fact that the three-body scattering amplitude obtained by the Skornyakov-Ter-Martirosian equation (2.50) consists of the recursive particle-exchange processes: Only ladder-type Feynman diagrams with respect to the particle-exchange interaction contribute to the three-body scattering. The non-local free propagator of a dimer in Eq. (5.1) is introduced to compensate the reduction of the interaction term. As we see later, the microscopic action $S[\psi, \phi]$ reproduces exact two- and three-body low-energy observables which are obtained by the effective field theory by Bedaque *et al*.

Wetterich equation and vertex expansion

Based on the model introduced above, we perform a FRG analysis which is governed by the Wetterich equation of the flowing action Γ_k:

$$\partial_k \Gamma_k[\Phi] = \frac{1}{2}\mathrm{Tr}\tilde{\partial}_k \ln\left(\frac{\delta^2\Gamma_k[\Phi]}{\delta\Phi(P)\delta\Phi(P)} + R_{\Phi,k}(P)\right), \tag{5.2}$$

where $\Phi(P) = (\psi(P), \psi^*(P), \phi(P), \phi^*(P))$. The regulator $R_{\Phi,k}(P)$ is chosen based on the same principle as Sec. 4.2.2, i.e., the regulator is chosen so that the loop expressions of the FRG equations become as simple as possible and so that the regulator does not complicate the hierarchy structure of the few-body scattering problem. To this end, we employ the regulators $R_{\psi,k}(P)$ and $R_{\phi,k}(P)$ as

$$R_{\psi,k}(Q) = \frac{k^2}{c^2}, R_{\phi,k}(Q) = \frac{\sqrt{k^2 - \mathbf{q}^2}}{16\pi}\theta(k^2 - \mathbf{q}^2), \tag{5.3}$$

where θ is the Heaviside unit-step function and c is a positive constant. The constant c will ultimately be taken to infinity so that we facilitate a semi-analytic calculation. In the limit of $c \to \infty$, quantum fluctuations (loop corrections) of the field ψ is integrated out while those of the field ϕ remain unintegrated; in other words, the trick of taking $c \to \infty$ allows us to integrate out the field ψ first before we integrate out the field ϕ. The trick is introduced by Diehl *et al.* [165] to facilitate semi-analytic FRG calculations in quantum few-body physics.

In solving the Wetterich equation (5.2), we perform the vertex expansion (see Sec. 3.2.4) to deal with one-, two-, three- and four-body correlations separately, i.e., we perform a power-series

expansion of the flowing action Γ_k with respect to the fields ψ, ψ^*, ϕ and ϕ^* as

$$\begin{aligned}\Gamma_k[\psi,\phi] := & \int_P \psi^*(P)G^{-1}_{\psi,k}(P)\psi(P) + \int_P \phi^*(P)\Gamma^{(2)}_k(P)\phi(P) \\ & + \int_{\substack{P_1,P_2\\P_1',P_2'}} \Gamma^{(3)}_k(P_1P_2;P_2'P_1')\delta(P_1+P_2-P_2'-P_1')\phi^*(P_1)\psi^*(P_2)\psi(P_2')\phi(P_1') \\ & + \frac{1}{(2!)^2}\int_{\substack{P_1,P_2,P_3\\P_1',P_2',P_3'}} \Gamma^{(4)}_k(P_1P_2P_3;P_3'P_2'P_1')\delta(P_1+P_2+P_3-P_3'-P_2'-P_1') \\ & \qquad \times\phi^*(P_1)\psi^*(P_2)\psi^*(P_3)\psi(P_3')\psi(P_2')\phi(P_1') \\ & + \cdots, \end{aligned} \tag{5.4}$$

where the expansion coefficient $\Gamma^{(n)}_k$ is the one-particle irreducible (1PI) vertex that represents the correlation among n particles at the energy scale of k. We note that Eq. (5.4) is the most general expression of the flowing action allowed by the symmetries of the microscopic action $S[\psi,\phi]$: In the expression of Eq. (5.4), the translational and the U(1) symmetries guarantee the momentum and the particle-number conservations, respectively. The two-boson interaction term, which is proportional to $\psi^*\psi^*\psi\psi$, does not appear in Eq. (5.4), since the term is not generated by the Wetterich equation for the given microscopic action $S[\psi,\phi]$ in Eq. (5.1). In our formalism, any information of the two-boson correlation is encapsulated in the dimer-propagator term proportional to $\phi^*\phi$. For the same reason, the three- and the four-boson interaction terms, do not appear in Eq. (5.4) but are encapsulated in $\Gamma^{(3)}_k$ and $\Gamma^{(4)}_k$, respectively. The reduction of the contributing terms is a major advantage of our effective field theory introduced in Eq. (5.1) and plays a decisive role in performing semi-analytic calculations.

5.2.2 One-, two- and three-body sectors

We first deal with one-, two-, and three-body sectors separately to reproduce the Efimov effect within our non-local effective field-theory framework. Based on the Feynman rules developed in Sec. 3.2.4, we derive FRG equations for the 1PI vertices $\Gamma^{(n)}_k$ with $n \leq 3$. In deriving the FRG equations, the vacuum limit introduced in Sec. 4.2.2 reduces contributing Feynman diagrams which originate in an effect of finite particle density.

We start from the one-body sector in which the FRG equation becomes

$$\partial_k G^{-1}_{\psi,k}(P) = 0, \tag{5.5}$$

since contribution from particle-hole loops is absent on the right-hand side. We thus obtain

$$G^{-1}_{\psi,k}(P) = ip^0 + p^2 - \mu_1. \tag{5.6}$$

The result signifies that the the self-energy correction is absent due to the vanishing particle density. Concerning the two-body sector, the FRG equation is represented diagrammatically as depicted in Fig. 5.1(a), where again the vacuum limit reduces the number of contributing diagrams on the right-hand side. The FRG equation depicted in Fig. 5.1(a) is explicitly written down as

$$-\partial_k\Gamma^{(2)}_k(P) = \partial_k\int_L \frac{1}{\left[G^{-1}_\psi\left(\frac{P}{2}-L\right)+\frac{k^2}{c^2}\right]G^{-1}_\psi\left(\frac{P}{2}+L\right)}. \tag{5.7}$$

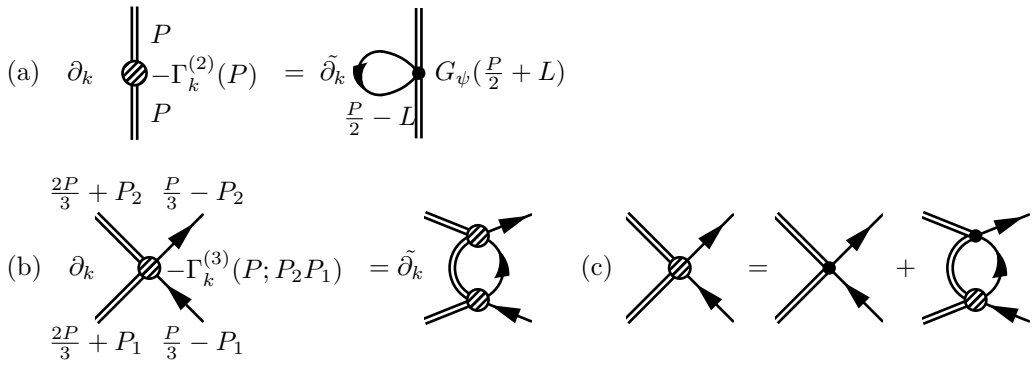

Figure 5.1: Exact FRG equations for (a) the two-body and (b) the three-body sectors, where the shaded circles represent the 1PI vertices $-\Gamma_k^{(n)}$ with an additional minus sign, the solid line with an arrow represents the regulated propagator $(G_{\psi,k}^{-1} + R_{\psi,k})^{-1}$ of a particle, the dot represents the bare particle-exchange interaction in the effective field theory Eq. (5.1) and the double line represents the propagator $G_{\phi,k}$ of a dimer. On the right-hand sides, the derivative $\tilde{\partial}_k$ acts only on the regulators $R_{\psi,k}$ and $R_{\phi,k}$ included in the internal lines. Corresponding FRG equations for (a) and (b) are explicitly written down in Eqs. (5.7) and (5.11), respectively. (c) The integral form of the FRG equation derived in Eq. (5.12).

For an ultraviolet (UV) cutoff Λ and the s-wave scattering length a, renormalization condition of μ_2 becomes $\mu_2 + \frac{\Lambda}{8\sqrt{2}\pi c} = \frac{1}{16\pi a} = 0$ at the unitarity limit. Together with the renormalization condition, Eq. (5.7) can be solved analytically as

$$\Gamma_k^{(2)}(P) = \frac{1}{8\pi}\left[\sqrt{\frac{ip^0}{2} + \frac{\mathbf{p}^2}{4} - \mu_1 + \frac{k^2}{2c^2}} - \frac{1}{2}\sqrt{\frac{ip^0}{2} + \frac{\mathbf{p}^2}{4} - \mu_1}\right]. \tag{5.8}$$

By using the trick of $c \to \infty$, we finally obtain

$$\Gamma_k^{(2)}(P) = \frac{1}{16\pi}\sqrt{\frac{ip^0}{2} + \frac{\mathbf{p}^2}{4} - \mu_1}, \tag{5.9}$$

which reproduces the (renormalized) self energy of a dimerized molecule at the unitarity limit. We thus obtain the same result for the two-body sector as the effective field theory of Bedaque *et al.* [14, 15]. The inverse propagator of a dimer is thus obtained as

$$G_{\phi,k}^{-1}(P) = R_{\phi,k}(P) + \frac{1}{16\pi}\sqrt{\frac{ip^0}{2} + \frac{\mathbf{p}^2}{4} - \mu_1}. \tag{5.10}$$

Concerning the three-body sector, the FRG equation for the three-body 1PI vertex $\Gamma_k^{(3)}$ can be diagrammatically represented as depicted in Fig. 5.1(b). Similarly to the one- and the two-body sectors, the vacuum limit reduces the number of diagrams contributing to the right-hand side of the FRG equation. Furthermore, on the right-hand side, the many diagrams presented in Sec. 4.3.2 are encapsulated into a single term, due to the simplicity of the effective field thoery Eq. (5.1). The

FRG equation depicted in Fig. 5.1(b) can be explicitly written down as

$$-\partial_k \Gamma_k^{(3)}(P; P_2 P_1) = \tilde{\partial}_k \int_L \Gamma_k^{(3)}(P; P_2 L) G_\psi\left(\frac{P}{3} - L\right) G_{\phi,k}\left(\frac{2P}{3} + L\right) \Gamma_k^{(3)}(P; L P_1), \tag{5.11}$$

where the derivative $\tilde{\partial}_k$ acts only on the regulator $R_{\phi,k}$ contained in the dimer propagator $G_{\phi,k}$ on the right-hand side. We can analytically integrate the FRG equation (5.11) with respect to the cutoff k and thus we obtain an integral form of the FRG equation as

$$\begin{aligned} -\Gamma_k^{(3)}(P; P_2 P_1) = {} & G_\psi\left(\frac{P}{3} + P_2 + P_1\right) \\ & + \int_L G_\psi\left(\frac{P}{3} + P_2 + L\right) G_\psi\left(\frac{P}{3} - L\right) G_{\phi,k}\left(\frac{2P}{3} + L\right) [-\Gamma_k^{(3)}(P; L P_1)], \end{aligned} \tag{5.12}$$

which can be diagrammatically represented as depicted in Fig. 5.1(c).

To verify that Eq. (5.12) reproduces the universal low-energy observables of the Efimov physics, we focus on the dominant s-wave sector of the partially on-shell 1PI vertex in the center-of-mass frame. By performing a contour integration of the Matsubara frequency l^0 and by imposing on-shell conditions on the external particles, Eq. (5.12) reduces to

$$\begin{aligned} -\Gamma_k^{(3)}(ip^0; \mathbf{p}_2 \mathbf{p}_1) = {} & \frac{1}{ip^0 + \mathbf{p}_2^2 + \mathbf{p}_1^2 + (\mathbf{p}_2 + \mathbf{p}_1)^2} + \int \frac{d^3 l}{(2\pi)^3} \frac{1}{ip^0 + \mathbf{p}_2^2 + \mathbf{l}^2 + (\mathbf{p}_2 + \mathbf{l})^2} \\ & \times \frac{[-\Gamma_k^{(3)}(ip^0; \mathbf{l}\mathbf{p}_1)]}{\frac{1}{16\pi}\sqrt{\frac{ip^0}{2} + \frac{3}{4}\mathbf{l}^2} + R_{\phi,k}(\mathbf{l})}, \end{aligned} \tag{5.13}$$

where $\Gamma_k^{(3)}(ip^0; \mathbf{p}_2 \mathbf{p}_1)$ is the three-body 1PI vertex $\Gamma_k^{(3)}(P; P_2 P_1)$ under the conditions of $\mathbf{p} = 0$ and $i(p^0/2 + p_n^0) + \mathbf{p}_n^2 = 0$ $(i = 1, 2)$. To focus on the s-wave sector, where the 1PI vertex $\Gamma_k^{(3)}(ip^0; \mathbf{p}_2 \mathbf{p}_1)$ depends only on the absolute values $p_1 = |\mathbf{p}_1|$ and $p_2 = |\mathbf{p}_2|$ of the spatial momentum, we perform an s-wave projection of Eq. (5.13) as

$$\begin{aligned} -\Gamma_k^{(3)}(ip^0; p_2 p_1) = {} & \frac{\pi}{p_2 p_1} \log\left(\frac{ip^0/2 + p_2^2 + p_1^2 + p_2 p_1}{ip^0/2 + p_2^2 + p_1^2 - p_2 p_1}\right) + \int_0^\infty \frac{l^2 dl}{(2\pi)^3} \frac{\pi}{p_2 l} \log\left(\frac{ip^0/2 + p_2^2 + l^2 + p_2 l}{ip^0/2 + p_2^2 + l^2 - p_2 l}\right) \\ & \times \frac{16\pi[-\Gamma_k^{(3)}(ip^0; l p_1)]}{\sqrt{\frac{ip^0}{2} + \frac{3}{4} l^2} + 16\pi R_{\phi,k}(\mathbf{l})}, \end{aligned} \tag{5.14}$$

where $\Gamma_k^{(3)}(ip^0; p_2 p_1)$ is the three-body 1PI vertex $\Gamma_k^{(3)}(ip^0; \mathbf{p}_2 \mathbf{p}_1)$ projected onto s-wave sector:

$$\Gamma_k^{(3)}(ip^0; p_2 p_1) := 2\pi \int_{-1}^{1} d\cos\theta_{p_2 p_1} \Gamma_k^{(3)}(ip^0; \mathbf{p}_2 \mathbf{p}_1), \tag{5.15}$$

in which $\theta_{p_2 p_1}$ is the relative angle between the two vectors $\mathbf{p}_2$ and $\mathbf{p}_1$. In the infrared (IR) limit $k \to 0$, where all the quantum fluctuations (loop corrections) are integrated out, the regulator $R_{\phi,k}(\mathbf{l})$ vanishes in Eq. (5.14) and the resulting equation becomes the Skornyakov-Ter-Martirosian equation reviewed in Sec. 2.2.2, from which we can obtain universal low-energy observables of the Efimov effect.

Up to the three-body sector, we thus reproduce the universal low-energy observables of the Efimov effect within the effective field theory Eq. (5.1) exactly.

5.2.3 Separable pole approximation to three-body sector

Due to the increasing number of momentum indices, an exact treatment of RG equations in the N-body ($N \geq 4$) sectors is almost impossible in general [172, 173]. In addition, in performing a semi-analytic calculation for the entire scattering process of four particles, sub-scattering processes of three particles are often difficult to handle analytically. To this end, we develop an approximation scheme of the three-body sub-scattering amplitude by making use of techniques that are developed in nuclear physics a few decades ago.

The central idea is to approximate the three-body sub-amplitude by a more simple function which is separable with respect to the external momentum. For this purpose, we make use of the spectral decomposition of a self-adjoint operator. In general, a T-matrix $T(s)$ of scattering two particles, whose dynamics is governed by a Hamiltonian H, is represented by a resolvent $G(s) = (s - H)^{-1}$ as

$$T(s) = V + VG(s)V, \tag{5.16}$$

where V is the interaction term in the Hamiltonian H. Because of the self-adjoint nature of the resolvent $G(s)$, we can perform a spectral decomposition of $G(s)$ as

$$G(s) = \sum_n \frac{|\Phi_n\rangle\langle\Phi_n|}{s - E_n} + \int d^3q \frac{|\Phi_{\mathbf{q}}\rangle\langle\Phi_{\mathbf{q}}|}{s - E_{\mathbf{q}}}, \tag{5.17}$$

where $|\Phi_n\rangle$ is a state vector of a bound state with energy E_n and $|\Phi_{\mathbf{q}}\rangle$ is a state vector of a scattering state with energy $E_{\mathbf{q}}$ and momentum $\mathbf{q}$.[1] Since the resolvent $G(s)$ and the T-matrix $T(s)$ are related via Eq. (5.16), we can decompose $T(s)$ as

$$T(s) = \frac{V|\Phi_n\rangle\langle\Phi_n|V}{s - E_n} + (\text{non-singular terms at } s = E_n), \tag{5.18}$$

which suggests that $T(s)$ can be approximated by the first term on the right-hand side in the vicinity of $s \simeq E_n$. We apply the approximation, which we call the separable pole approximation, to the three-body scattering problems. Since the three-body (particle-dimer) T-matrix is proportional to the three-body 1PI vertex $\Gamma_k^{(3)}$, the 1PI vertex can also be approximated by a separable term in the vicinity of a bound-state pole. By focusing on the dominant s-wave sector, we obtain

$$-\Gamma_k^{(3)}(ip^0, p; p_2 p_1) = \frac{\chi_k(p_2)\chi_k^*(p_1)}{ip^0 + \frac{p^2}{3} - E_{T,k}}, \tag{5.19}$$

where p is the total momentum, $E_{T,k}$ is an energy of an Efimov trimer and the function χ_k is a Bethe-Salpeter wave function (the bound-state wave function of a particle and a dimer). The approximation signifies that the entire three-body scattering process is replaced by a propagation process of a single-most important intermediate state, as diagrammatically represented as depicted in Fig. 5.2. Literally, the approximation respect the position and the residue of the bound-state pole

[1] Strictly, the integral on the right-hand side should be written in terms of the Stieltjes integral, since the scattering wave functions are not in the Hilbert space and the "projection operator" $|\Phi_{\mathbf{q}}\rangle\langle\Phi_{\mathbf{q}}|$ vanishes.

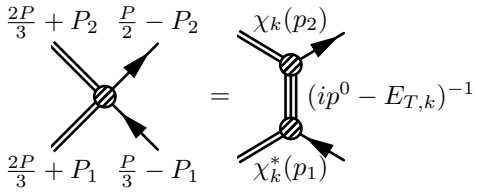

Figure 5.2: Diagrammatic expression of the separable approximation Eq. (5.19). On the right-hand side, the shaded circles represent the Bethe-Salpeter wave functions and the triple line represents the propagator of the intermediate trimer.

which often dominates a loop-momentum integral. As we will see later, the intermediate state is chosen so that it dominates the three-body scattering process.

We then derive the Bethe-Salpeter wave function χ_k. In deriving χ_k, we employ analytical methods developed by Gogolin *et al.* [175] who obtain various analytical results for Efimov physics. By substituting Eq. (5.19) into Eq. (5.14), we obtain a homogeneous Bethe-Salpeter equation as

$$\chi_k(p_2)=\frac{2}{\pi}\int_0^\infty dl\frac{l}{p_2}\log\left(\frac{E_{T,k}/2+p_2^2+l^2+p_2l}{E_{T,k}/2+p_2^2+l^2-p_2l}\right)\frac{\chi_k(l)}{\sqrt{\frac{E_{T,k}}{2}+\frac{3}{4}l^2}+\sqrt{k^2-l^2}\Theta(k^2-l^2)}. \quad (5.20)$$

which can be rewritten as

$$\left[1+\frac{2}{\sqrt{3}}\frac{\sqrt{\sinh^2\xi_k-\sinh^2\xi_2}}{\cosh\xi_2}\Theta(\xi_k^2-\xi_2^2)\right]\phi_k(\xi_2)=\frac{4}{\sqrt{3}\pi}\int_{-\infty}^\infty d\xi_1\log\left(\frac{e^{2(\xi_2-\xi_1)}+e^{\xi_2-\xi_1}+1}{e^{2(\xi_2-\xi_1)}-e^{\xi_2-\xi_1}+1}\right)\phi_k(\xi_1), \quad (5.21)$$

where we have performed the following change of variables:

$$\sinh\xi_2:=\frac{\sqrt{3}p_2}{\sqrt{2E_{T,k}}},\ \sinh\xi_1:=\frac{\sqrt{3}l}{\sqrt{2E_{T,k}}},\ \sinh\xi_k:=\frac{\sqrt{3}k}{\sqrt{2E_{T,k}}}, \quad (5.22)$$

$$\phi_k(\xi):=\frac{\frac{2}{\sqrt{3}}\sinh\xi\cdot\chi_k\left(\sqrt{\frac{2E_{T,k}}{3}}\sinh\xi\right)}{1+\frac{2}{\sqrt{3}}\frac{\sqrt{\sinh^2\xi_k-\sinh^2\xi}}{\cosh\xi}\Theta(\xi_k^2-\xi^2)}. \quad (5.23)$$

Crudely, the change of variables is motivated by the scale invariance of Eq. (5.23), which can be mapped to a translational invariant equation if we take the logarithm (or arcsinh) of the variables. The translational equation can, then, be solved by the Fourier transform. We note that we have implicitly performed an analytic continuation of $\phi_k(\xi)$ from $\xi\in[0,\infty)$ to $\xi\in(-\infty,\infty)$ by using Eq. (5.21). The analytic continuation makes ϕ_k an odd function, i.e. $\phi_k(\xi)=-\phi_k(-\xi)$. To further push on the analytic calculation, we choose the intermediate state as $E_{T,k}\gg k^2$. In this limit, the second term on the left-hand side of Eq. (5.21) becomes negligibly small. By disregarding the small

contribution, we finally obtain

$$\phi_k(\xi_2) = \left.\frac{8}{\sqrt{3}s}\frac{\sinh\left(\frac{s\pi}{6}\right)}{\cosh\left(\frac{s\pi}{2}\right)}\right|_{s=-i\frac{d}{d\xi_2}} \phi_k(\xi_2), \tag{5.24}$$

where we have used the following trick on the right-hand side of Eq. (5.21):

$$\int_{-\infty}^{\infty} dt' T(t-t') f(t') = \tilde{T}\left(-i\frac{d}{dt}\right) f(t), \tag{5.25}$$

$$\tilde{T}(s) := \int_{-\infty}^{\infty} dt T(t) e^{-ist}. \tag{5.26}$$

Noting that the solution of Eq. (5.24) is an eigenfunction of $-i\frac{d}{d\xi_2}$ and that ϕ_k is an odd function, we obtain

$$\phi_k(\xi_2) = A\ \sin(s_0\xi_2),\ 1 = \frac{8}{\sqrt{3}s_0}\frac{\sinh\left(\frac{s_0\pi}{6}\right)}{\cosh\left(\frac{s_0\pi}{2}\right)}, \tag{5.27}$$

where A is a normalization constant and the second equality reproduces the Efimov's scaling factor of $s_0 \simeq \pm 1.00624$. In the present momentum-space analysis, we impose a short-range boundary condition at the momentum scale of an ultraviolet (UV) cutoff Λ as

$$\sin(s_0\xi_\Lambda) = 0, \sinh\xi_\Lambda := \frac{\sqrt{3}\Lambda}{\sqrt{2E_{T,k}}}, \tag{5.28}$$

which leads to $s_0 \mathrm{arcsinh}\left(\frac{\sqrt{3}\Lambda}{\sqrt{2E_{T,k}}}\right) = n\pi$ where n is an integer. In particular, in the limit of the large UV cutoff $\Lambda \gg \sqrt{E_{T,k}}$, we reproduce the discrete-scale invariant energy eigenvalues of the Efimov trimers:

$$E_{T,k} = 6\Lambda^2 e^{-\frac{2n\pi}{s_0}}. \tag{5.29}$$

Discussion on separable pole approximation

In general, the approximation we employ in the above discussion has no hard evidence of justifying its applicability. While a more sophisticated approximation will be performed in Sec. 5.4, we here present some circumstantial evidences of the applicability of the separable pole approximation by reviewing some applications of separable approximations in quantum four-body physics. The idea of separable three-body sub-amplitude was first introduced by Alt, Grassberger and Sandhas [176] to apply for four-nucleon scattering problems, while the obtained ^{4}He binding energy 50MeV is much larger than the experimental value of 28.3MeV. However, as the authors of Ref. [176] discussed, the deviation is mainly due to the simplified nucleon-nucleon interaction. For a fixed interparticle interaction, the separable approximations seem to work well. For instance, an old results by Nakaichi-Maeda *et al.* [177], who investigated by one-term separable approximation a binding energy of four ^{4}He atoms interacting via Aziz 's HDFHE2 potential, agrees within a few percent

with a more recent result by Filikhin *et al.* [178]. For an alpha particle, extensions [179, 180] of the separable pole approximation were applied [174, 181, 182, 183] and the results were found to agree well with the results by other methods such as the variational method with hyperspherical harmonic basis [184] and the Faddeev-Yakubovski equation without separable approximations [185, 186]. A more detailed comparison between the results by the separable approximations and those by other methods can be found in Refs. [187, 186].

Normalization of Bethe-Salpeter wave function

In Eq. (5.27), we obtain an analytic form of the Bethe-Salpeter wave function χ_k; however, the normalization factor A of χ_k is yet to be determined since the homogeneous Bethe-Salpeter equation (5.20) allows an arbitrary normalization factor. We thus consider the inhomogeneous term in the original three-body scattering equation (5.14). To determine the normalization factor, we employ a method developed in Ref. [188] with a proper modification. In the following, we shortly summarize the procedure.

We start from Eq. (5.14) which can be rewritten in terms of a linear (matrix) equation as

$$\left(I - \frac{2}{\pi} t \cdot G\right)\Gamma = \Gamma\left(I - \frac{2}{\pi} G \cdot t\right) = \pi t, \tag{5.30}$$

where the matrices I, t, G and Γ are defined as

$$(I)_{p_2 p_1} = \delta(p_2 - p_1), \tag{5.31}$$

$$(t)_{p_2 p_1} := \log\left(\frac{ip^0/2 + p_2^2 + p_1^2 + p_2 p_1}{ip^0/2 + p_2^2 + p_1^2 - p_2 p_1}\right), \tag{5.32}$$

$$(G)_{p_2 p_1} := \frac{1}{\sqrt{\frac{ip^0}{2} + \frac{3}{4}p_2^2} + \sqrt{k^2 - p_2^2}\Theta(k^2 - p^2)}\delta(p_2 - p_1), \tag{5.33}$$

$$(\Gamma)_{p_2 p_1} := -p_2 p_1 \Gamma_k^{(3)}(ip^0; p_2 p_1). \tag{5.34}$$

Due to the spectral decomposition Eq. (5.19) in the center-of-mass frame, Γ becomes a projection operator in the limit of $ip^0 \to E_{T,k}$, i.e.,

$$(\Gamma)_{p_2 p_1} \xrightarrow{ip^0 \to E_{T,k}} \frac{h_k(p_2) h_k^*(p_1)}{ip^0 - E_{T,k}}, \tag{5.35}$$

where $h_k(p)$ is related to the Bethe-Salpeter wave function $\chi_k(p)$ via $h_k(p) = p \cdot \chi_k(p)$. The function $h_k(p)$ satisfies the following modified Bethe-Salpeter equation:

$$h = \lim_{ip^0 \to E_{T,k}} \frac{2}{\pi} t \cdot G \cdot h, \tag{5.36}$$

where the vector h is defined as $(h)_p := h_k(p)$. Equivalently, Eq. (5.35) can be rewritten with the matrix notation as

$$\lim_{ip^0 \to E_{T,k}} (ip^0 - E_{T,k})\Gamma = h \cdot h^\dagger. \tag{5.37}$$

To obtain the normalization factor A of the Bethe-Salpeter wave function, we introduce the following operator Q:

$$Q := (ip^0 - E_{T,k})\Gamma \cdot t^{-1} \frac{\partial}{\partial(ip^0)} \left(I - \frac{2}{\pi} t \cdot G \right), \tag{5.38}$$

$$= \pi - \frac{\partial}{\partial(ip^0)} \left[(ip^0 - E_{T,k})\Gamma \cdot t^{-1} \right] \left(I - \frac{2}{\pi} t \cdot G \right), \tag{5.39}$$

where t^{-1} is the inverse of the matrix t. In the second equality, we have employed the Leibniz rule and $\Gamma \cdot t^{-1} = \pi \left(I - \frac{2}{\pi} t \cdot G \right)^{-1}$ which is obtained from Eq. (5.30). Here the derivative $\frac{\partial}{\partial(ip^0)}$ is introduced to deal with the normalization factor A which is the residue of a bound-state pole. Using Eqs. (5.30) and (5.39), we find that the operator $\frac{1}{\pi} Q$ acts on the vector h as an identity operator I in the limit of $ip^0 \to E_{T,k}$, i.e.,

$$\lim_{ip^0 \to E_{T,k}} Q \cdot h = \pi h. \tag{5.40}$$

By substituting Eqs. (5.38) and (5.37) into Eq. (5.40), we obtain

$$h^\dagger \left[t^{-1} \frac{\partial}{\partial(ip^0)} \left(I - \frac{2}{\pi} t \cdot G \right) \right]_{ip^0 = E_{T,k}} h = \pi, \tag{5.41}$$

which provides the normalization condition of h; however, we should further improve Eq. (5.41) since the matrix inverse t^{-1} in Eq. (5.41) is usually unavailable. To this end, we act t^{-1} on Eq. (5.36) from left and take the hermitian conjugate of the equation to obtain

$$\lim_{ip^0 \to E_{T,k}} h^\dagger \cdot t^{-1} = \lim_{ip^0 \to E_{T,k}} \frac{2}{\pi} h^\dagger \cdot G, \tag{5.42}$$

where we have used the fact that the matrices t and G are symmetric in the limit of $ip^0 = E_{T,k}$. By substituting Eq. (5.42) into Eq. (5.41) and by using $\frac{\partial I}{\partial(ip^0)} = 0$, we finally obtain

$$h^\dagger \left[G \cdot \frac{\partial \left(\frac{\pi}{2} G^{-1} - t \right)}{\partial(ip^0)} \cdot G \right]_{ip^0 = E_{T,k}} h = \frac{\pi^3}{4}. \tag{5.43}$$

in which the expressions of the matrices t and G are given in Eqs. (5.32) and (5.33). In particular, since the matrix G is diagonal, the matrix inverse G^{-1} can be analytically obtained just by taking the inverse of the diagonal elements.

Based on the general discussion mentioned above, we calculate the normalization factor A by substituting Eqs. (5.27), (5.32) and (5.33) into Eq. (5.43). As a result, we find an analytical expression for A as

$$|A|^2 = \left[\frac{1}{4\sqrt{3}} \left(1 - \frac{s_0 \pi}{\sinh s_0 \pi} \right) + \frac{\pi}{3} \frac{\sinh \frac{s_0 \pi}{6}}{\sinh \frac{s_0 \pi}{2}} - \frac{\pi}{9} \frac{\cosh \frac{s_0 \pi}{6}}{\cosh \frac{s_0 \pi}{2}} \right]^{-1} \frac{\pi^2}{2}, \tag{5.44}$$

which is numerically evaluated as $A \simeq 5.00858$.

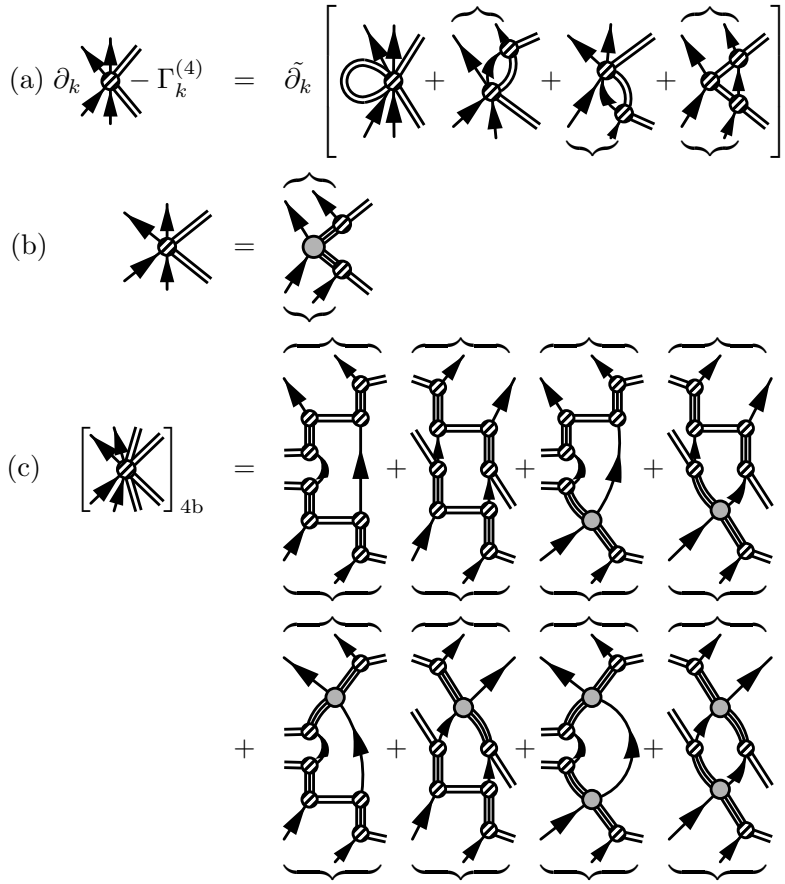

Figure 5.3: (a) The FRG equation of the four-body 1PI vertex obtained by applying the general formalism of the FRG introduced in Sec. 3.2.4 to the effective field theory Eq. (5.1). The curly brackets represent the symmetrization with respect to the momentum attached to the external lines. Other graphical notation is the same as Fig. 5.1. We can see a formal analogy of the four-body FRG equation to the three-body FRG equation presented in Sec. 4.3.2. (b) Decomposition of the four-body 1PI vertex by making use of the separable pole approximation we developed in Sec. 5.2.3. On the right-hand side, the graphical notation is same as Fig. 5.2. (c) Six-body 1PI vertex decomposed by the lower-order 1PI vertices. Each term on the right-hand side contributes to the first term of the right-hand side of the four-body FRG equation in (a).

5.2.4 Four-body sector

Based on the separable pole approximation, we now deal with an RG flow for the four-body sector. On the basis of our effective field theory Eq. (5.1) and the general formalism of the FRG introduced in Sec. 3.2.4, we obtain an FRG equation for the four-body 1PI vertex $\Gamma_k^{(4)}$ as diagrammatically represented as in Fig. 5.3(a). Due to the trick of taking $c \to 0$ in Eq. (5.3), we reduce contributing diagrams on the right-hand side of the FRG equation, where the reduction is compensated by the fully renormalized propagator Eq. (5.10) of a dimer.[2] In Fig. 5.3(a), the first term on the right-hand

[2]We note that the obtained four-body FRG equation is in a formal analogy with the three-body FRG equation in Sec. 4.3.2.

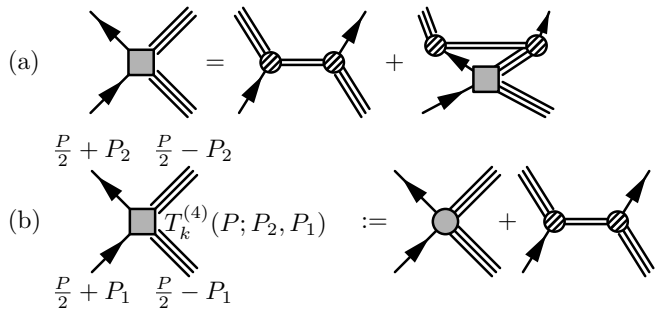

Figure 5.4: (a) Diagrammatic expression of the integral form of the reduced four-body FRG equation (5.46). The graphical notation is same as Fig. 5.2, except that the shaded square represents the particle-trimer scattering amplitude $T_k^{(4)}$ defined in Eq. (5.47). (b) Diagrammatic expression of Eq. (5.47).

side consists of a six-body 1PI vertex which should be decomposed by lower-order 1PI vertices due to the hierarchy structure of the quantum few-body physics (see Sec. 4.2.3). To demonstrate the hierarchy structure, we first decompose the four-body 1PI vertex by making use of the separable pole approximation. To this end, we first perform a resummation of sub-Feynman diagrams at the edges of $\Gamma_k^{(4)}$, and the resummation leads to the expression of

$$-\Gamma_k^{(4)}\left(\frac{2Q}{3}+P_2,P-Q,\frac{Q}{3}-P_2;\frac{Q'}{3}-P_1,P-Q',\frac{2Q'}{3}+P_1\right)$$
$$=\left[\chi_k(p_2)\frac{1}{iq^0+\frac{q^2}{3}-E_{T,k}}\Gamma_k^{at}(P;QQ')\frac{1}{iq'^0+\frac{q'^2}{3}-E_{T,k}}\chi_k^*(p_1)\right]_{\text{sym.}}, \tag{5.45}$$

for some function Γ_k^{at}, which we refer to as a particle-trimer 1PI vertex. Here, $[\cdots]_{\text{sym.}}$ represents a symmetrization with respect to the external momentum indices of particles.[3] Diagrammatically, a particle and a dimer lines are connected recursively via the particle-exchange interaction at the up and bottom edges of $\Gamma_k^{(4)}$. The resummation of these sub-diagrams turns out to be the three-body 1PI vertex $\Gamma_k^{(3)}$ due to the three-body FRG equation in Fig. 5.1(c). Based on the separable pole approximation, the emergent three-body 1PI vertices reduces to separable functions with respect to momentum indices. In particular, the four-body 1PI vertex $\Gamma_k^{(4)}$ reduces to the particle-trimer 1PI vertex Γ_k^{at} which depends only on three momentum indices. The decomposition Eq. (5.45) is diagrammatically represented in Fig. 5.3(b). The decomposition allows us to evaluate the six-body 1PI vertex contributing to the four-body FRG equation in Fig. 5.3(a). Indeed, by collecting the contributing Feynman diagrams, we find that the six-body 1PI vertex can be decomposed in terms of the lower-order 1PI vertices as diagrammatically represented in Fig. 5.3(c), in accordance with the hierarchy structure of the quantum few-body physics.

Based on the obtained diagrammatic FRG equation, we deduce[4] an integral equation that is

[3] More precisely, the symmetrization with respect to the momentum indices $\frac{Q}{3}-P_2 \leftrightarrow P-Q$ and $\frac{Q'}{3}-P_1 \leftrightarrow P-Q'$.

[4] Noting that there is a formal analogy between the four-body FRG equation in Fig. 5.3 and the three-body FRG

equivalent with the FRG equation:

$$T_k^{(4)}(P;P_2P_1) = \chi_k{}^*\left(\frac{\mathbf{p}_2}{3}+\mathbf{p}_1\right)G_{\phi,k}(P_2+P_1)\chi_k\left(\mathbf{p}_2+\frac{\mathbf{p}_1}{3}\right) + \int_L \chi_k^*\left(\frac{\mathbf{p}_2}{3}+\mathbf{l}\right)G_{\phi,k}(P_2+L)\chi_k\left(\mathbf{p}_2+\frac{\mathbf{l}}{3}\right)\frac{G_{\psi,k}\left(\frac{P}{2}+L\right)}{i\left(\frac{p^0}{2}-l^0\right)+\frac{l^2}{3}-E_{T,k}}T_k^{(4)}(P;LP_1), \tag{5.46}$$

$$T_k^{(4)}(P;P_2P_1) := \Gamma_k^{at}(P;P_2P_1)+\chi_k^*\left(\frac{\mathbf{p}_2}{3}+\mathbf{p}_1\right)G_{\phi,k}(P_2+P_1)\chi_k\left(\mathbf{p}_2+\frac{\mathbf{p}_1}{3}\right). \tag{5.47}$$

which are diagrammatically represented in Fig. 5.4(a) and (b). Here, the FRG equation (5.46) is expressed in terms of a particle-trimer scattering amplitude defined in Eq. (5.47). If we take the infrared limit $k \to 0$, where all the quantum fluctuations are integrated out, the integral equation (5.46) has the same form as the Alt-Grassberger-Sandhas equation except that Eq. (5.46) contains no two-dimer reaction term. The absence of the two-dimer reaction process signifies that our effective field theory does not exactly reproduce the observables for four-identical bosons; however, as we will see later, our model is found to reproduce four-body observables in a good precision. The neglect of the two-dimer process is motivated by the fact that the dimer state is not an energy eigenstate at the unitarity limit and is expected not to contribute to a loop-momentum integral in the four-body FRG equation.

Based on the integral FRG equation (5.46), we perform an s-wave projection in the center-of-mass frame to deal with the low-energy regime where the higher partial-wave amplitudes are suppressed by the centrifugal force. We finally obtain the s-wave projected four-body FRG equation as

$$T_k^{(4)}(ip^0;p_2p_1) = 2\pi\int_{-1}^{1}d\cos\theta_{p_2p_1}\chi_k^*\left(\frac{\mathbf{p}_2}{3}+\mathbf{p}_1\right)G_{\phi,k}(P_2+P_1)\chi_k\left(\mathbf{p}_2+\frac{\mathbf{p}_1}{3}\right) + \int_0^\infty\frac{l^2dl}{(2\pi)^3}\left[2\pi\int_{-1}^{1}d\cos\theta_{p_2p_1}\chi_k^*\left(\frac{\mathbf{p}_2}{3}+\mathbf{l}\right)G_{\phi,k}(P_2+L)\chi_k\left(\mathbf{p}_2+\frac{\mathbf{l}}{3}\right)\right] \times\frac{T_k^{(4)}(ip^0;lp_1)}{ip^0+\frac{4}{3}l^2-E_{T,k}}, \tag{5.48}$$

where we perform the contour integral with respect to l^0 in Eq. (5.46). Here in Eq. (5.48), we set the external momentum as $i(p^0/2-p_n^0)+p_n^2=0$ $(n=1,2)$ so that the external particles satisfy the on-shell condition. We also define $\theta_{p_2p_1}$ as the angle between the two relative momentum $\mathbf{p}_2$ and $\mathbf{p}_1$, and the s-wave projected particle-trimer scattering amplitude $T_k^{(4)}(ip^0;p_2p_1)$ as

$$T_k^{(4)}(ip^0;p_2p_1) = 2\pi\int_{-1}^{1}d\cos\theta_{p_2p_1}\,T_k^{(4)}(P;P_2P_1)\Big|_{\mathbf{p}=0,i\left(\frac{p^0}{2}-p_n^0\right)+p_n^2=0\,(n=1,2)}. \tag{5.49}$$

Numerical solution of Eq. (5.48)

We here summarize the numerical calculation of Eq. (5.48). The numerical solution consists of the following two steps. First, we perform numerically the integral with respect to the angle $\cos\theta_{p_2p_1}$

equation in Fig. 4.2, we can prove that, within the separable pole approcimation, the FRG equation in Fig. 5.3(a) is equivalent with the integral equation in Fig. 5.4(a).

to perform an s-wave projection Eq. (5.49). Then we numerically solve the linear integral equation (5.48) for the s-wave projected matrix elements. In these two steps, we discretize the variables as

$$x_n = -1 + \frac{2(n-1)}{N} \quad (n = 1, \cdots, N), \tag{5.50}$$

$$p_m = p_{\min}\left(\frac{p_{\max}}{p_{\min}}\right)^{\frac{m-1}{M}} \quad (m = 1, \cdots, M), \tag{5.51}$$

where x_n is the discretization of the variable $\cos\theta_{p_2 p_1}$ that takes on the value over $[-1, 1]$ and p_m is the discretization of the s-wave projected momentum variable that takes on the value over $[p_{\min}, p_{\max}]$. Here we choose N = 80-100 to perform the integral with respect to $\cos\theta_{p_1 p_2}$ by the trapezoidal rule, and M = 200-300 for the momentum variables. Similarly to the calculation in Sec. 4.3.2, we choose the momentum grid so that it has a geometric nature, since we are dealing with the Efimov physics which features a log-periodic energy eigenvalues. The lower and the upper bounds $p_{\min}$ and $p_{\max}$ of the momentum variables are chosen as

$$p_{\min} = e^{-6\pi/s_0}\Lambda, \quad p_{\max} = \Lambda, \tag{5.52}$$

where $s_0 \simeq 1.00624$ is the Efimov's scaling parameter and Λ is the ultraviolet cutoff that is related to the trimer energy $E_{T,k}$ via Eq. (5.29). Here, the duration $[p_{\min}, p_{\max}]$ includes six Efimov cycles and thus the lower bound $p_{\min} \simeq 7.3 \times 10^{-9} p_{\max}$ of the momentum variable is sufficiently smaller than the characteristic length scale set by the trimer energy $E_{T,k}$, which sets the units of the dimensionful parameters in the present calculation. With the set-up, we numerically solve Eq. (5.48) by means of the Mathematica, which chooses automatically the Krylov method or the multifrontal method in solving a linear equation for a dense nonsymmetric matrix. The numerical accuracy of the present calculation is checked by observing convergence of the binding energies, which would be evaluated in the next section, up to the second digit with respect to the variation of the numbers N and M of the mesh points. For fixed N and M, the relative error of the solution of Eq. (5.48) is found to be of order 10^{-15}.

5.3 Limit cycle in four-body sector

We numerically solve the obtained FRG equations Eqs. (5.14) and (5.48) for the three- and the four-body 1PI vertices to obtain RG flows. To this end, we define the three- and the four-body coupling constants g_3 and g_4 by

$$g_3 := -\frac{1}{2}k^2\Gamma_k^{(3)}(ip^0 = k^2; p_2 = 0, p_1 = 0), \tag{5.53}$$

$$g_4 := \frac{1}{250}\sqrt{E_{T,k}}\,T_k^{(4)}(ip^0 = e^{2\pi/s_0}k^2; p_2 = 0, p_1 = 0), \tag{5.54}$$

where the multiplication factors k^2 and $\sqrt{E_T, k}$ make g_3 and g_4 dimensionless, respectively. The factors $1/2$ and $1/250$ are introduced to display g_3 and g_4 in a simultaneous manner. Here we note that we have used in Sec. 5.2.3 the condition $k^2 \ll E_{T,k}$, to obtain the analytical expression of the Bethe-Salpeter wave function χ_k. In addition, since the separable approximation Eq. (5.19) of the

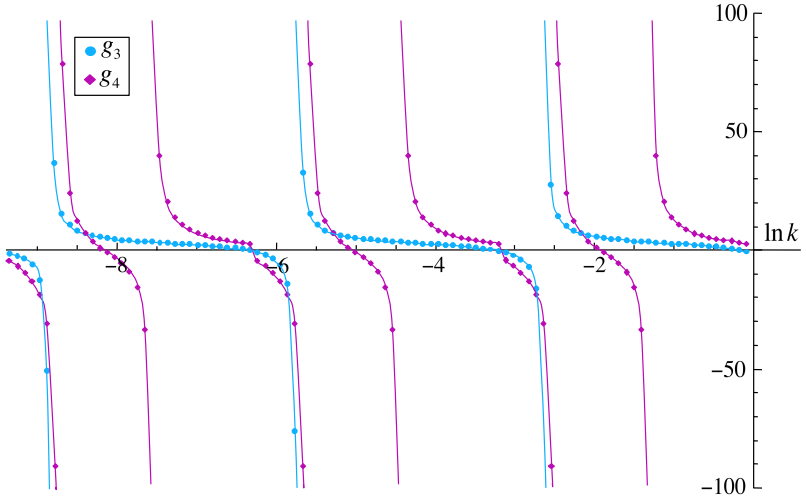

Figure 5.5: Cutoff k dependence of the three- and the four-body coupling constants g_3 and g_4, which are defined in Eqs. (5.53) and (5.54). Both g_3 and g_4 exhibit log-periodic k dependence to form an RG limit cycle. As discussed in the main text, the limit cycle reproduces the low-energy universality of the four-body physics qualitatively. In particular, while g_3 flows from $-\infty$ to ∞, g_4 does twice, reflecting the numbers of tetramers accompanying an Efimov trimer. The figure is adapted from Ref. [77]. Copyright © (2015) by The American Physical Society.

three-body 1PI vertex $\Gamma_k^{(3)}$ is valid in the vicinity of the bound-state pole, we impose the condition of $E_{T,k} \simeq ip^0$. We thus choose the intermediate trimer state in the separable pole approximation as

$$E_{T,k} = 6\Lambda^2 e^{-2n(k)\pi/s_0}, \tag{5.55}$$

$$n(k) = \left\lfloor \frac{s_0}{2\pi} \log \frac{6\Lambda^2}{k^2} \right\rfloor, \tag{5.56}$$

where $\lfloor x \rfloor$ refers to the floor function which gives a largest integer less than or equal to x. In evaluating g_4 via the FRG equation (5.48), the choice of $n(k)$ provides $-\frac{2\pi}{s_0} \leq \ln \frac{k^2}{E_{T,k}} \leq 0$ and $-\frac{\pi}{s_0} \leq \ln \frac{ip^0}{E_{T,k}} \leq \frac{\pi}{s_0}$, where the separable pole approximation is expected to work.

5.3.1 Limit cycle in four-body sector

In Fig. 5.5, cutoff k dependence of the three- and the four-body coupling constants g_3 and g_4 are plotted. As we can see, both g_3 and g_4 exhibit log-periodic behavior with respect to the cutoff k, exhibiting the RG limit cycle behavior. The period of one cycle is evaluated to be $e^{\pi/s_0} \simeq 22.7$, in perfect agreement with the exact value of 22.694. Furthermore, we find that g_4 flows from $-\infty$ to ∞ twice while g_3 does once. We identify this one-to-two correspondence with the universal numbers of few-body clusters: There appear two tetramer states that accompany an Efimov trimer at sufficiently low-energy irrespective of the short-range details of a given four-body system with a short-range interaction. To evaluate energy eigenvalues of the two tetramers, we define three cutoff scales $k^{(3)}$, $k_1^{(4)}$ and $k_2^{(4)}$ where the three- and the four-body coupling constants diverges. Since the scales $k^{(3)}$, $k_1^{(4)}$ and $k_2^{(4)}$ are the only dimensionfull parameters characterizing the three- and the

four-body physics, we identify the scales $k^{(3)}$, $k_1^{(4)}$ and $k_2^{(4)}$ to be the square root of the three- and the four-body binding energies $E^{(3)}$, $E_1^{(4)}$ and $E_2^{(4)}$. The identification is also suggested in Ref. [171]. For the three parameters we obtain

$$\frac{k_1^{(4)}}{k^{(3)}} = 1.11, \quad \frac{k_2^{(4)}}{k^{(3)}} = 3.66, \tag{5.57}$$

which are in the same order as values obtained by Deltuva:

$$\sqrt{\frac{E_1^{(4)}}{E^{(3)}}} = 1.00113, \quad \sqrt{\frac{E_2^{(4)}}{E^{(3)}}} = 2.14714. \tag{5.58}$$

Therefore, the simplest separable pole approximation for the four-body FRG equation reproduces the number of the tetramers and the order of the four-body binding energies. As we will see in the next section, further precision is achieved if we approximate the three-body 1PI vertex by a summation of several separable terms. Although the widths of the tetramer resonances are predicted to be universal as in Eq. (5.58), we are not sure how we can identify the resonance widths from the RG limit cycle. In summary, we show that the RG limit cycle indeed contains information of the universal low-energy four-body observables in line with the general motivation introduced in Sec. 1.1. In particular, we show that our four-body FRG calculation based on the naive separable pole approximation reproduces the qualitative aspects of the low-energy universality of the four-body physics. Systematic improvement of the present calculation is presented in the next section.

Conjecture: topology of a limit cycle

Before seeking to improve the numerical precision, here we would like to make a conjecture that the one-to-two ratio of the number of trimers and tetramers are topological numbers in terms of the RG limit cycle. To see the geometrical property of the RG limit cycle, we investigate how the RG limit cycle is embedded in the entire theory space. To this end, we plot the RG-flow trajectory in theory space spanned by (g_3, g_4) in Fig. 5.6. In the two-dimensional theory space of (g_3, g_4), the RG-flow trajectory forms an RG limit cycle. If we glue the edges of the two-dimensional theory space to form a torus, the RG limit cycle in Fig. 5.6 forms a closed loop which winds twice in the g_4 direction while it winds once in the g_3 direction. In mathematics, ways of embedding a closed loop into a torus are categorized by the first homotopy group of $\pi_1(T^2)$ of the torus T^2, where π_1 counts the winding numbers of the closed loop onto the torus. Since the first homotopy group $\pi_1(T^2)$ is isomorphic to $\mathbb{Z} \times \mathbb{Z}$, where $\mathbb{Z}$ is the additive group of integers, loops on a torus is topologically categorized by two integers (n, m). In the present case of the RG limit cycle which winds onto a torus, the topological number is given by $(n, m) = (1, 2)$ reflecting its windings. We thus conjecture that the number of the trimers and the tetramers are the topological numbers of the RG limit cycle. The scenario may suggest a topological stability of the numbers of the bound states against a continuous perturbation (such as a perturbation to the dimension $4 \to 4 \pm \epsilon$) to the system.

The scenario that the numbers of the few-body clusters have a topological origin is appealing since the scenario could introduce novel physical phenomena in which topology plays an important role. For example, there might be a topological phase transition in which the number of tetramers,

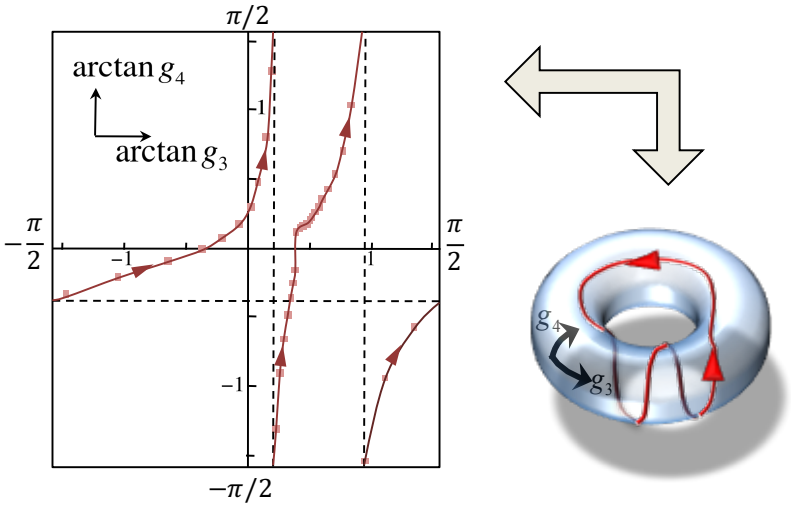

Figure 5.6: RG-flow trajectory in the theory space of (g_3, g_4). For the sake of the simultaneous display, here we plot $(\arctan g_3/8, \arctan g_3/25)$. In the figure, the three- and the four-body coupling constants flow along the brown-colored trajectory periodically. If we glue the edges of the g_3-g_4 plane, the plane becomes a torus onto which the closed loop of the RG limit cycle winds. In particular, as discussed in the main text, the winding numbers of the closed loop may account for the numbers of the few-body clusters. The figure is adapted from Ref. [77]. Copyright © (2015) by The American Physical Society.

which accompany an Efimov trimer, changes. Indeed, for a mass-imbalanced bosonic mixture, there is a situation in which the number of tetramers changes. From the viewpoint of fundamental physics, the scenario may provide the first example which shows that a universal low-energy observable is accounted for by a geometrical property of how a renormalized trajectory is embedded in the theory space. However, to define a topological number of the RG limit cycle, we performs a nontrivial operation of gluing the theory space. To justify the scenario, therefore, we have to give a conclusive argument of the gluing of the theory space.

5.4 Systematic improvement

In the preceding section, the obtained energy eigenvalues of the two tetramers deviate from the values obtained from the precise numerical calculations by Deltuva [68]. To resolve this issue, we systematically improve the separable pole approximation. For this purpose, we employ the Hilbert-Schmidt expansion [174] of a self-adjoint operator to express the three-body 1PI vertex by the systematic sum of separable terms. Compared with the naive separable pole approximation, the improved approximation leads to an exact four-body FRG equation within our effective field theory as we sum up an infinite number of separable terms, except for the general assumption of the s-wave dominance.

5.4.1 Hilbert-Schmidt expansion

We here discuss a general formalism to perform an separable expansion of a T-matrix. A two-body T-matrix T often obeys a Lippman-Schwinger-type linear equation:

$$T(s) = V(s) + V(s) \cdot G_0(s) \cdot T(s), \tag{5.59}$$

where s represents the total energy of the scattering particles, and $V(s)$ and $G_0(s)$ are some symmetric operators. Based on the equation, we define a state vector $|\chi_n(s)\rangle$ via an eigenvalue equation of

$$\eta_n(s)|\chi_n(s)\rangle = V(s)G_0(s)|\chi_n(s)\rangle, \tag{5.60}$$

where $\eta_n(s)$ is an eigenvalue. We note that the state vector $\langle\chi_n(s)|$ and the eigenvalue $\eta_n(s)$ depend on the total energy s. Since the vectors $\left\{G_0(s)^{1/2}|\chi_n(s)\rangle\right\}_n$ are the eigenvectors of the symmetric operator $G_0(s)^{1/2}V(s)G_0(s)^{1/2}$, the vectors $\left\{G_0(s)^{1/2}|\chi_n(s)\rangle\right\}_n$ form the following complete orthonormal set:

$$\delta_{mn} = \langle\chi_m(s)|G_0(s)|\chi_n(s)\rangle, \tag{5.61}$$

$$1 = \sum_n G_0(s)^{1/2}|\chi_n(s)\rangle\langle\chi_n(s)|G_0(s)^{1/2} = \sum_n G_0(s)|\chi_n(s)\rangle\langle\chi_n(s)|. \tag{5.62}$$

By combining Eq. (5.62) and Eq. (5.60), we find that the operator $V(s)$ can be expanded as

$$V(s) = \sum_n |\chi_n(s)\rangle\eta_n(s)\langle\chi_n(s)|. \tag{5.63}$$

By substituting Eq. (5.63) into Eq. (5.59), we obtain

$$T(s) = \sum_n |\chi_n(s)\rangle\frac{\eta_n(s)}{1-\eta_n(s)}\langle\chi_n(s)|, \tag{5.64}$$

which provides a systematic expansion of the T-matrix T with respect to the separable terms. We can, therefore, perform the separable expansion of a general T-matrix by calculating the set of $|\chi_n(s)\rangle$ and $\eta_n(s)$ through the eigenvalue equation (5.60) together with the normalization condition Eq. (5.61). The expansion is called the Hilbert-Schmidt expansion [174].

We apply the Hilbert-Schmidt expansion to the three-body 1PI vertex $\Gamma_k^{(3)}$ which obeys the linear FRG equation (5.14). Noting that the FRG equation (5.14) has the same form as Eq. (5.59), we find analytical expressions for the Hilbert-Schmidt expansion of $\Gamma_k^{(3)}$:

$$-\Gamma_k^{(3)}(ip^0; p_2p_1) = \sum_n \chi_k^n(ip^0, p_2)\frac{\eta_n(ip^0)}{1-\eta_n(ip^0)}\chi_k^{n*}(ip^0, p_1), \tag{5.65}$$

$$\eta_n(ip^0) = \frac{8}{\sqrt{3}s_n(ip^0)}\frac{\sinh\frac{s_n(ip^0)\pi}{6}}{\cosh\frac{s_n(ip^0)\pi}{2}}, \tag{5.66}$$

$$\chi_k^n(ip^0, p) = \left(\frac{\sqrt{3}\pi^2}{2}\frac{s_n(ip^0)}{(n+1)\pi}\right)^{1/2}\frac{\sin\left[s_n(ip^0)\mathrm{arcsinh}\frac{\sqrt{3}p}{\sqrt{2ip^0}}\right]}{p}, \tag{5.67}$$

$$s_n(ip^0) = \frac{(n+1)\pi}{\mathrm{arcsinh}\frac{\sqrt{3}\Lambda}{\sqrt{2ip^0}}}, \tag{5.68}$$

where Λ is an ultraviolet (UV) cutoff and n takes on a nonnegative integer ($n = 0, 1, 2, \cdots$). In Eq. (5.65), $1-\eta_n(ip^0)$ contains the bound-state pole of the n-th excited Efimov trimer, and therefore, the expansion is a natural extension of the separable pole approximation performed in the preceding section. We should note that the analytical expressions in Eqs. (5.65), (5.66), (5.66) and (5.68) are applicable when $k^2 \ll ip^0$. Since we can choose an arbitrary number for ip^0, the condition can be automatically satisfied.[5] In particular, the condition is much more reasonable than the condition $k^2 \ll E_{T,k} \simeq ip^0$ imposed by the approximation performed in the preceding section.

Based on the Hilbert-Schmidt expansion of the three-body sub-amplitude, the four-body 1PI vertex $\Gamma_k^{(4)}$ can be decomposed in a manner similar to Eq. (5.45):

$$-\Gamma_k^{(4)}\left(\frac{2Q}{3}+P_2, P-Q, \frac{Q}{3}-P_2; \frac{Q'}{3}-P_1, P-Q', \frac{2Q'}{3}+P_1\right) = \sum_{n,m}\left[\chi_k^n(iq^0, p_2)\frac{\eta_n(iq^0)}{1-\eta_n(iq^0)}\Gamma^{at}_{k,nm}(P; QQ')\frac{\eta_m(iq^0)}{1-\eta_m(iq^0)}\chi_k^{m*}(p_1)\right]_{\text{sym.}}, \tag{5.69}$$

where the four-body correlations are encapsulated in $\Gamma^{at}_{k,nm}(P; QQ')$. Compared with Eq. (5.45), if the components in the equation are known, the decomposition in Eq. (5.69) is exact within the effective field theory except for the general assumption of the s-wave dominance in the three-body sub-sector. By substituting Eq. (5.69) into the four-body FRG equation in Fig. 5.3(a), we obtain an integral form of the four-body FRG equation:

$$\begin{aligned} T^{(4)}_{k,nm}(P; P_2P_1) \;=\; & \chi_k^{n*}\left(ip^0+\frac{4}{3}p_2^2, \frac{\mathbf{p}_2}{3}+\mathbf{p}_1\right)G_{\phi,k}(P_2+P_1)\chi_k^m\left(ip^0+\frac{4}{3}p_1^2, \mathbf{p}_2+\frac{\mathbf{p}_1}{3}\right) \\ & + \sum_j \int_L \chi_k^{n*}\left(ip^0+\frac{4}{3}p_2^2, \frac{\mathbf{p}_2}{3}+\mathbf{l}\right)G_{\phi,k}(P_2+L)\chi_k^j\left(ip^0+\frac{4}{3}l^2, \mathbf{p}_2+\frac{\mathbf{l}}{3}\right) \\ & \times\frac{\eta_j\left(ip^0+\frac{4}{3}l^2\right)}{1-\eta_j\left(ip^0+\frac{4}{3}l^2\right)}G_{\psi,k}\left(\frac{P}{2}+L\right)T^{(4)}_{k,jm}(P; LP_1), \end{aligned} \tag{5.70}$$

$$\begin{aligned} T^{(4)}_{k,nm}(P; P_2P_1) :=\; & \Gamma^{at}_{k,nm}(P; P_2P_1) \\ & +\chi_k^{n*}\left(ip^0+\frac{4}{3}p_2^2, \frac{\mathbf{p}_2}{3}+\mathbf{p}_1\right)G_{\phi,k}(P_2+P_1)\chi_k^m\left(ip^0+\frac{4}{3}p_1^2, \mathbf{p}_2+\frac{\mathbf{p}_1}{3}\right). \end{aligned} \tag{5.71}$$

Similarly to the preceding section, we perform an s-wave projection of Eq. (5.70) and obtain an s-wave projected integral FRG equation:

$$\begin{aligned} & T^{(4)}_{k,nm}(ip^0; p_2p_1) \\ & = 2\pi\int_{-1}^{1} d\cos\theta_{p_2p_1}\chi_k^{n*}\left(ip^0+\frac{4}{3}p_2^2, \frac{\mathbf{p}_2}{3}+\mathbf{p}_1\right)G_{\phi,k}(P_2+P_1)\chi_k^m\left(ip^0+\frac{4}{3}p_1^2, \mathbf{p}_2+\frac{\mathbf{p}_1}{3}\right) \\ & + \sum_j \int_0^\infty \frac{l^2dl}{(2\pi)^3}\left[2\pi\int_{-1}^{1} d\cos\theta_{p_2l}\chi_k^{n*}\left(ip^0+\frac{4}{3}p_2^2, \frac{\mathbf{p}_2}{3}+\mathbf{l}\right)G_{\phi,k}(P_2+L)\chi_k^j\left(ip^0+\frac{4}{3}l^2, \mathbf{p}_2+\frac{\mathbf{l}}{3}\right)\right] \\ & \times\frac{\eta_j\left(ip^0+\frac{4}{3}l^2\right)}{1-\eta_j\left(ip^0+\frac{4}{3}l^2\right)}T^{(4)}_{k,jm}(ip^0; lp_1), \end{aligned} \tag{5.72}$$

[5] We will choose ip^0 so that $k^2/ip^0 < \frac{1}{515}$.

where we perform the contour integral with respect to l^0 in Eq. (5.70). Here in Eq. (5.72), the external momentum is set to be $i(p^0/2 - p_n^0) + p_n^2 = 0$ $(n = 1, 2)$ and the s-wave projected particle-trimer scattering amplitude $T^{(4)}_{k,nm}(ip^0; p_2 p_1)$ is defined as

$$T^{(4)}_{k,nm}(ip^0; p_2 p_1) = 2\pi \int_{-1}^{1} d\cos\theta_{p_2 p_1}\, T^{(4)}_{k,nm}(P; P_2 P_1)\Big|_{\mathbf{p}=0, i\left(\frac{p^0}{2}-p_n^0\right)+p_n^2=0\,(n=1,2)}. \tag{5.73}$$

Numerical solution of Eq. (5.72)

We here summarize the numerical solution of Eq. (5.72), which is coupled linear integral equations. The solution of Eq. (5.72) consists of the following two steps. First, we perform an integral with respect to $\cos\theta_{p_2 p_1}$ in Eq. (5.73). We then solve Eq. (5.72) based on the s-wave projected matrix elements. In the first step, we employ the Gauss-Legendre integration of N =30-40 order; in other words, we approximate the integrand by a polynomial of $(2n-1)$-th degree. In the second step, we discretize the momentum variable by

$$p_m = p_{\min}\left(\frac{p_{\max}}{p_{\min}}\right)^{\frac{m-1}{M}} \quad (m = 1, \cdots, M), \tag{5.74}$$

where we choose M=200-300. Here the discrretized momentum variable p_m takes on the value over $[p_{\min}, p_{\max}]$. Similarly to the numerical calculation in Sec. 5.2.4, we discretize the momentum variable so that the momentum grid becomes a geometric series. The momentum grid is motivated by the discrete scale invariance of the Efimov physics. The lower and the upper bounds $p_{\min}$ and $p_{\max}$ of the momentum variables are chosen as

$$p_{\min} = e^{-6\pi/s_0}\Lambda, \quad p_{\max} = \Lambda, \tag{5.75}$$

where $s_0 \simeq 1.00624$ is the Efimov's scaling parameter and Λ is the ultraviolet cutoff. Similarly to the calculation in Sec. 5.2.4, we choose $p_{\min}$ ($p_{\max}$) so that it is sufficiently smaller (larger) than the characteristic length scale of the trimer binding energy $E_{T,k}$. With these set-up, we we numerically solve Eq. (5.72) by Mathematica which chooses automatically the Krylov method or the multifrontal method in solving a linear equation for a dense nonsymmetric matrix. The numerical accuracy of the present calculation is checked by observing convergence of the binding energies, which would be evaluated in the next section, up to the second digit with respect to the variation of the numbers N and M of the mesh points. For fixed N and M, the relative error of the solution of Eq. (5.72) is found to be of order 10^{-15}.

5.4.2 Refined four-body limit cycle

To see the refined RG flow of the four-body sector, we define the four-body coupling constant λ_4 as

$$\lambda_4 := k^3 Z_k^{-1} T^{(4)}_{k,00}(ip^0 = k^2 e^{2\pi/s_0}; p_2 = 0, p_1 = 0), \tag{5.76}$$

where the factor k^3 is multiplied to make λ_4 dimensionless and $\sqrt{Z_k} = \left(\text{arcsinh}\frac{\sqrt{3}\Lambda}{\sqrt{2ip^0}}\right)^{-1/2}$ is the wave-function renormalization (the normalization factor of the form factor in Eq. (5.67)) of a trimer.

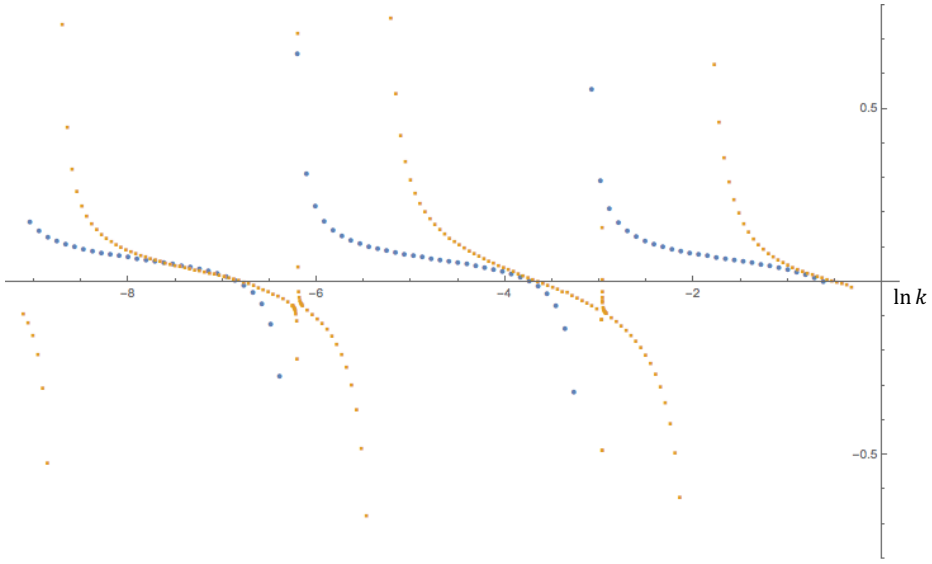

Figure 5.7: Cutoff k dependence of the three- and the four-body coupling constants g_3 and λ_4 defined in Eq. (5.76). While the behavior of λ_4 is essentially same as that of g_4 presented in Fig. 5.5, the refined RG flow for λ_4 based on the Hilbert-Schmidt expansion reproduces quantitatively the universal low-energy four-body observables as discussed in the main text.

We note that here we choose the total energy to be $k^2/ip^0 = e^{-2\pi/s_0} \simeq 0.00194$ since the analytical expressions in Eqs. (5.65), (5.66), (5.66) and (5.68) are applicable when $k^2 \ll ip^0$. In Fig. 5.7, we plot the cutoff k dependence of the four-body coupling constant λ_4, where in numerically solving Eq. (5.72), we take into account six separable terms ($n = 0, \cdots, 5$ in Eq. (5.65)). As we can see, the refined RG flow exhibit the RG limit-cycle behavior that is qualitatively equivalent to the RG flow of g_4 in the preceding section: The four-body coupling constant λ_4 flows twice from $-\infty$ to ∞, while the three-body coupling constant g_3 does once. Similarly to Eq. (5.57), we evaluate the four-body binding energies from the cutoff scales $k^{(3)}$, $k_1^{(4)}$ and $k_2^{(4)}$ where g_3 and λ_4 diverge:

$$\frac{k_1^{(4)}}{k^{(3)}} = 1.081, \frac{k_2^{(4)}}{k^{(3)}} = 2.291, \tag{5.77}$$

which agree with the values obtained by Deltuva in Eq. (5.58) within 7%. In more detailed comparison, our results Eq. (5.77) are slightly larger than the values in Eq. (5.58). The over-bound tetramers (i.e., the binding energies of the tetramer are larger than the more precise values in Eq. (5.77)) may be due to the fact that our effective field theory disregards the two-dimer propagating processes. Indeed, for a positive scattering length $a > 0$, where an energy eigenstate of a dimerized molecule is present, the binding energies of the tetramers are pushed up and the excited tetramer merges to a particle-trimer continuum as schematically illustrated in Fig. 2.3. We thus conclude that the observed over-binding in Eq. (5.77) arises from the neglect of the two-dimer propagating processes which become important in the positive scattering-length region. For the refined RG limit cycle, we have not yet understood how we can reproduce the resonance-width of the tetramers.

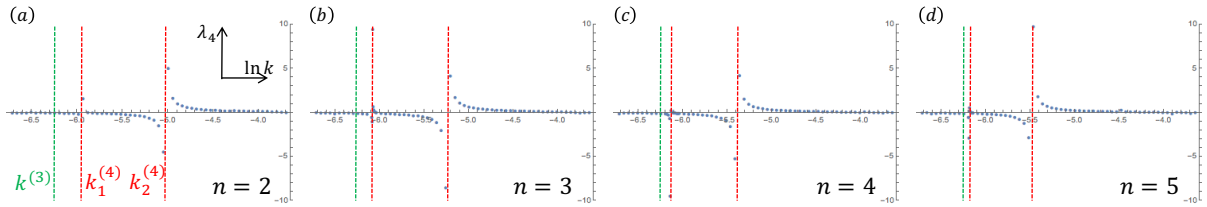

Figure 5.8: The RG flow of the four-body coupling constant λ_4 for an increasing number n of the terms included in the Hilbert-Schmidt expansion. Fig. (a), (b), (c) and (d) are $n = 2$, $n = 3$, $n = 4$ and $n = 5$. In the figures, the green-dashed line represents the cutoff scale $k^{(3)}$ where the three-body coupling constant diverges, and the red-dashed lines show the cutoff scales $k_1^{(4)}$ and $k_2^{(4)}$ where the four-body coupling constant diverges.

Extrapolation

For a reference, we here make an attempt to extrapolate the result Eq. (5.77) to the limit of taking the infinite terms in the Hilbert-Schmidt expansion in Eq. (5.64). In Fig. 5.8, the RG flow of λ_4 is plotted during the one period $e^{\pi/s_0} \simeq 22.694$ of the RG limit cycle. Different figures correspond to the different numbers n =2, 3, 4, and 5 of the terms included in Eq. (5.77). To discuss the limit of taking the infinite terms in the Hilbert-Schmidt expansion, we plot the evaluated values of

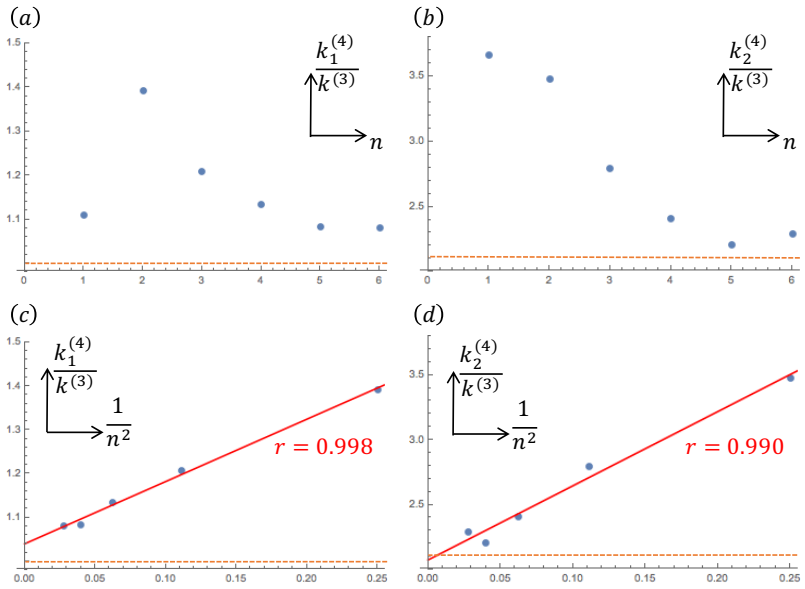

Figure 5.9: The values of (a) $k_1^{(4)}/k^{(3)}$ and (b) $k_2^{(4)}/k^{(3)}$, which are plotted against an increasing number n of the terms included in the Hilbert-Schmidt expansion. To extrapolate the data to $n = \infty$, we plot the values of (c) $k_1^{(4)}/k^{(3)}$ and (d) $k_2^{(4)}/k^{(3)}$ against $1/n^2$. We find that the plotted data fit linear functions, where the sample correlation coefficients r are found to be $r = 0.998$ for Fig. (c) and 0.990 for Fig. (d). The orange dashed line represents the values of $k_1^{(4)}/k^{(3)}$ and (d) $k_2^{(4)}/k^{(3)}$ in Eq. (5.58) which are obtained by Deltuva.

$k_1^{(4)}/k^{(3)}$ and $k_2^{(4)}/k^{(3)}$ in Fig. 5.9(a) and (b) against n. As we can see, the evaluated values tend to converge, for an increasing n, to the values in Eq. (5.58) which is represented as orange-dashed line in in Fig. 5.9(a) and (b). Furthermore, we find that the values of $k_1^{(4)}/k^{(3)}$ and $k_2^{(4)}/k^{(3)}$ depend linearly on $1/n^2$ for n =2, 3, 4, 5, and 6 as illustrated in Fig. 5.9(c) and (d), although we do not know *a priori* how the values scale according to the variation of n. In particular, we find that the sample correlation coefficient r becomes $r = 0.998$ and 0.990 for the data of $k_1^{(4)}/k^{(3)}$ and $k_2^{(4)}/k^{(3)}$, respectively. Based on the least square method, we make an attempt to extrapolate the values of $k_1^{(4)}/k^{(3)}$ and $k_2^{(4)}/k^{(3)}$ to $n = \infty$ by using the linear fittings. The evaluated values are found to be

$$\frac{k_1^{(4)}}{k^{(3)}} = 1.039 \pm 0.007, \quad \frac{k_2^{(4)}}{k^{(3)}} = 2.075 \pm 0.059, \tag{5.78}$$

where the error is estimated under an assumption that the values of $\frac{k_1^{(4)}}{k^{(3)}}$ and $\frac{k_2^{(4)}}{k^{(3)}}$ obeys a Gaussian distribution around the fitted linear function. We find that the obtained values agree with the values obtained by Deltuva (Eq. (5.58)) within 4%. We are not sure about the origin of the 4% deviation; it may be due to the violation of the $1/n^2$ scaling for a large n.

In summary, we have demonstrated that the RG limit cycle in the four-body sector indeed contains the information of the universal low-energy four-body observables in Efimov physics. The obtained feature of the RG limit cycle is essentially the same as the one obtained by the naive separable pole approximation in the preceding section. Furthermore, we reproduce the correct number and the more precise energies of the tetramers from our improved RG limit cycle.

Chapter 6

Summary and outlook

Summary

In this thesis, we have addressed the relation between a renormalization-group (RG) trajectory and low-energy universality in quantum few-body physics. In particular, we have focused on Efimov physics, in which resonantly interacting few particles form an infinite series of self-similar clusters. Our goal was to demonstrate that the universal low-energy observables in three- and four-body Efimov physics can be captured by the peculiar RG-flow trajectory of the RG limit cycle. We here summarize main results and discussions of the thesis in the following.

In Chap. 1, we discussed the general motivation and significance of our study. A general connection between an attractive structure of RG-flow trajectories and low-energy universality in physics is discussed to display our motivation of extracting universal low-energy observables from a renormalized trajectory to which RG flows are attracted. To make the motivation more concrete and to put the motivation in a proper historical context, we then provided a brief history of the Efimov physics. Emergence of the Efimov effect in a wide range of physical systems including nucleons, magnons, dipoles and atoms and an emergence of an RG limit cycle in the three-body sector are reviewed. Above all, we introduced a four-body extension of the Efimov effect as one of important issues of quantum few-body physics in recent years and discussed an unresolved issue concerning the relationship between the four-body physics and the RG limit cycle.

In Chap. 2, we provided a review of Efimov physics in ultracold atoms, which has provided an enormous impetus to the subject of universal few-body physics. We first introduced Efimov's original discussion on resonantly interacting three bosons to demonstrate an emergence of infinitely many Efimov trimers and the RG limit cycle that feature a self-similarity. Experimental breakthrough in ultracold atoms are then reviewed before we show the emergence of the Efimov effect in various extended systems such as mass-imbalanced systems and systems in mixed dimensions, some of which were motivated by the experimental breakthroughs in ultracold atoms. We finally discussed the N-body extension of the Efimov effect and summarized recent results by emphasizing the four-body extension. In particular, we reviewed that a brute-force calculation of the Schrödinger equation demonstrated an emergence of two tetramers which accompany every Efimov trimer at the unitarity limit.

In Chap. 3, we provided a general review of the functional renormalization group (FRG) which

allowed us to deal with non-perturbative RG flows in strongly correlated systems in Efimov physics. Wilson's original idea of the RG and its application to the critical phenomena were overviewed. After reviewing some applications of FRG to various physical systems, we formulated the FRG by following a convenient formulation by Wetterich who combined a functional methods to the FRG. We finally formulated the vertex expansion of the Wetterich equation so that the formulation becomes suitable for our purpose of dealing with the quantum few-body physics.

In Chap. 4, we discussed the question of what is the renormalized trajectory of the Efimov effect. Since the three-body Efimov effect is related to the RG limit cycle, it is naturally expected that the RG-flow trajectories of microscopically different systems exhibit the RG limit-cycle behavior at sufficiently low energy; however, due to the lack of computational methods, the expectation has not been verified. By employing the FRG combined with the separable approximation of realistic interparticle interactions, we demonstrated a universal emergence of the RG limit cycle behavior for microscopically distinct systems. In revealing the low-energy RG limit cycle, the nonperturbative nature of the FRG and the separability of interparticle interactions play an decisive role. We also discussed in some detail the relation between the RG-flow trajectory and the low-energy universality in two-body physics.

In Chap. 5, we discussed the relationship between the RG limit cycle and the low-energy universality of the four-body physics. In discussing the relationship, we first develop a simple effective field theory that exactly reproduces the three-body Efimov effect. By performing an exact FRG calculations, we show that the low-energy universality in two- and three-body physics are reproduced within the effective field theory. To obtain a nonperturbative RG limit cycle for the four-body physics, we then develop a simple separable pole approximation, in which the three-body aub-amplitude in the entire four-body amplitude is approximated by a separable term. The approximation respects the position and the residue of a bound-state pole in the three-body aub-amplitude so that the separable term becomes dominant in the vicinity of the bound-state pole. With the approximation, we obtain the four-body RG limit cycle which qualitatively describes the universal low-energy observables of the four-body physics. The number of accompanying tetramers are exactly reproduced whereas their binding energies found to be overestimated. To resolve the difficulty, we have systematically improved the separable-pole approximation by employing the Hilber-Schmidt expansion of the three-body aub-amplitude. With the improved approximation, we unbiasedly obtained the four-body RG limit cycle which qualitatively reproduces the energies of the accompanying tetramers.

With the result, we obtained for the first time a nonperturbative RG limit cycle in the four-body physics, and found that the RG limit cycle indeed is closely connected to the low-energy universality in the four-body physics. In particular, physical observables such as the numbers of tetramers and their binding energies were extracted. Based on the results, we have proposed a conjecture that the one-to-two correspondence of the numbers of the trimers and the tetramers is, in fact, understood as a topological winding number of the RG limit cycle onto a torus by enclosing the theory space of the three- and the four-body coupling constants. To establish this conjecture, however, we have to justify the enclosing of the theory space, which should be addressed in our future study.

Outlook

In this thesis, we have demonstrated that the RG limit cycle in the four-body sector describes the observables in Efimov physics. Although the numbers and the energies of the tetramers are reproduced quantitatively, it remains unclear how we can extract the tetramer-resonance width from the RG limit cycle. Moreover, the performed calculation includes an effective field theory which disregards the two-dimer propagation processes. Whether the inclusion of the two-dimer propagation processes into the FRG formalism affects the RG limit cycle is an important task to establish the relation between the RG limit cycle and the four-body universality. In particular, the inclusion may improve our evaluation of the tetramer binding energies.

Based on the results, we have made a conjecture that the universal numbers of the tetramers are understood as a topological numbers in terms of the RG limit cycle. To establish the conjecture, we have to justify the compactification of the two-dimensional theory space of the three- and the four-body coupling constants. Also, the topological stability to a small perturbation, such as the dimensional perturbation, is an important task to establish the conjecture. Once the conjecture is established, it may be an interesting question whether there is a topological phase transition concerning the limit-cycle topology. Indeed, in mass-imbalanced bosons, the number of accompanying tetramers changes from one to two at some mass ratio ~ 13. According to our conjecture, such a situation may be viewed as a topological phase transition, which may open up a new research avenue for investigating roles of topology in physics.

Bibliography

[1] K. G. Wilson and J. Kogut, Phys. Rep. **12**, 75 (1974).

[2] A. Pelissetto and E. Vicari, Phys. Rep. **368**, 549 (2002).

[3] K. G. Wilson, Phys. Rev. B **4**, 3174 (1971).

[4] K. G. Wilson, Phys. Rev. B **4**, 3184 (1971).

[5] J. Polchinski, Nucl. Phys. B **231**, 269 (1984).

[6] C. Bagnuls and C. Bervillier, Phys. Rep. **348**, 91 (2001).

[7] L. H. Thomas, Phys. Rev. **47**, 903 (1935).

[8] G. V. Skornyakov and K. A. Ter-Martirosyan, Zh. Eksp. Teor. Fiz. **31**, 775 (1956).

[9] G. Danilov, On the three-body problem with short-range forces, 1961.

[10] V. Efimov, Phys. Lett. B **33**, 563 (1970).

[11] V. Efimov, Nucl. Phys. A **210**, 157 (1973).

[12] R. Amado and J. Noble, Phys. Lett. B **35**, 25 (1971).

[13] R. D. Amado and J. V. Noble, Phys. Rev. D **5**, 1992 (1972).

[14] P. F. Bedaque, H.-W. Hammer, and U. van Kolck, Phys. Rev. Lett. **82**, 463 (1999).

[15] P. Bedaque, H.-W. Hammer, and U. van Kolck, Nucl. Phys. A **646**, 444 (1999).

[16] C. H. Greene, Journal of Physics B: Atomic and Molecular Physics **13**, L39 (1980).

[17] V. Efimov, Nucl. Phys. A **362**, 45 (1981).

[18] V. Efimov, Phys. Rev. C **44**, 2303 (1991).

[19] V. Efimov and E. Tkachenko, Phys. Lett. B **157**, 108 (1985).

[20] V. Efimov and E. G. Tkachenko, Few-Body Systems **4**, 71 (1988).

[21] P. F. Bedaque, G. Rupak, H. W. Grießhammer, and H.-W. Hammer, Nucl. Phys. A **714**, 589 (2003).

[22] A. Phillips, Nucl. Phys. A **107**, 209 (1968).

[23] F. Hoyle, Astrophysical Journal Supplement **1**, 121 (1954).

[24] R. Higa, H.-W. Hammer, and U. van Kolck, Nucl. Phys. A **809**, 171 (2008).

[25] H. Suno, Y. Suzuki, and P. Descouvemont, Phys. Rev. C **91**, 014004 (2015).

[26] P. Naidon and S. Endo, (2016), 1610.09805.

[27] T. K. Lim, S. K. Duffy, and W. C. Damer, Phys. Rev. Lett. **38**, 341 (1977).

[28] T. Cornelius and W. Glöckle, The Journal of Chemical Physics **85**, 3906 (1986).

[29] B. D. Esry, C. D. Lin, and C. H. Greene, Phys. Rev. A **54**, 394 (1996).

[30] M. T. Yamashita, T. Frederico, A. Delfino, and L. Tomio, Phys. Rev. A **66**, 052702 (2002).

[31] E. Braaten and H.-W. Hammer, Phys. Rev. A **67**, 042706 (2003).

[32] E. Braaten and H.-W. Hammer, Phys. Rep. **428**, 259 (2006).

[33] V. Efimov, JETP Letters **16**, 50 (1972).

[34] D. V. Fedorov, A. S. Jensen, and K. Riisager, Phys. Rev. Lett. **73**, 2817 (1994).

[35] I. Tanihata, H. Hamagaki, O. Hashimoto, Y. Shida, N. Yoshikawa, K. Sugimoto, O. Yamakawa, T. Kobayashi, and N. Takahashi, Phys. Rev. Lett. **55**, 2676 (1985).

[36] C. Bertulani, H.-W. Hammer, and U. van Kolck, Nucl. Phys. A **712**, 37 (2002).

[37] R. A. Arndt, D. D. Long, and L. Roper, Nucl. Phys. A **209**, 429 (1973).

[38] E. Braaten, P. Hagen, H.-W. Hammer, and L. Platter, Phys. Rev. A **86**, 012711 (2012).

[39] Y. Nishida, Phys. Rev. A **86**, 012710 (2012).

[40] I. Mazumdar and V. S. Bhasin, Phys. Rev. C **56**, R5 (1997).

[41] I. Mazumdar, V. Arora, and V. S. Bhasin, Phys. Rev. C **61**, 051303 (2000).

[42] A. E. A. Amorim, T. Frederico, and L. Tomio, Phys. Rev. C **56**, R2378 (1997).

[43] D. L. Canham and H. W. Hammer, The European Physical Journal A **37**, 367 (2008).

[44] S. Inouye, M. R. Andrews, J. Stenger, H. J. Miesner, D. M. Stamper-Kurn, and W. Ketterle, Nature **392**, 151 (1998).

[45] C. Chin, R. Grimm, P. Julienne, and E. Tiesinga, Rev. Mod. Phys. **82**, 1225 (2010).

[46] B. D. Esry, C. H. Greene, and J. P. Burke, Phys. Rev. Lett. **83**, 1751 (1999).

[47] T. Kraemer, M. Mark, P. Waldburger, J. G. Danzl, C. Chin, B. Engeser, A. D. Lange, K. Pilch, A. Jaakkola, H. C. Nägerl, and R. Grimm, Nature **440**, 315 (2006).

[48] S. Knoop, F. Ferlaino, M. Mark, M. Berninger, H. Schobel, H. C. Nagerl, and R. Grimm, Nat Phys **5**, 227 (2009).

[49] M. Zaccanti, B. Deissler, C. D/'Errico, M. Fattori, M. Jona-Lasinio, S. Muller, G. Roati, M. Inguscio, and G. Modugno, Nat Phys **5**, 586 (2009).

[50] S. E. Pollack, D. Dries, and R. G. Hulet, Science **326**, 1683 (2009).

[51] N. Gross, Z. Shotan, S. Kokkelmans, and L. Khaykovich, Phys. Rev. Lett. **103**, 163202 (2009).

[52] R. J. Wild, P. Makotyn, J. M. Pino, E. A. Cornell, and D. S. Jin, Phys. Rev. Lett. **108**, 145305 (2012).

[53] B. Huang, L. A. Sidorenkov, R. Grimm, and J. M. Hutson, Phys. Rev. Lett. **112**, 190401 (2014).

[54] Y. Wang, J. P. D'Incao, and C. H. Greene, Phys. Rev. Lett. **106**, 233201 (2011).

[55] Y. Nishida, Y. Kato, and C. D. Batista, Nat Phys **9**, 93 (2013).

[56] Y. Nishida and S. Tan, Few-Body Systems **51**, 191 (2011).

[57] R. S. Bloom, M.-G. Hu, T. D. Cumby, and D. S. Jin, Phys. Rev. Lett. **111**, 105301 (2013).

[58] K. Kato, Y. Wang, J. Kobayashi, P. S. Julienne, and S. Inouye, arXiv e-prints (2016), 1610.07900.

[59] S.-K. Tung, K. Jiménez-García, J. Johansen, C. V. Parker, and C. Chin, Phys. Rev. Lett. **113**, 240402 (2014).

[60] R. Pires, J. Ulmanis, S. Häfner, M. Repp, A. Arias, E. D. Kuhnle, and M. Weidemüller, Phys. Rev. Lett. **112**, 250404 (2014).

[61] L. Platter, H.-W. Hammer, and U.-G. Meißner, Phys. Rev. A **70**, 052101 (2004).

[62] H. W. Hammer and L. Platter, The European Physical Journal A **32**, 113 (2007).

[63] M. T. Yamashita, L. Tomio, A. Delfino, and T. Frederico, EPL (Europhysics Letters) **75**, 555 (2006).

[64] M. R. Hadizadeh, M. T. Yamashita, L. Tomio, A. Delfino, and T. Frederico, Phys. Rev. Lett. **107**, 135304 (2011).

[65] J. von Stecher, J. P. D/'Incao, and C. H. Greene, Nat Phys **5**, 417 (2009).

[66] A. Deltuva, Phys. Rev. A **82**, 040701 (2010).

[67] A. Deltuva, Few-Body Systems **50**, 391 (2011).

[68] A. Deltuva, EPL (Europhysics Letters) **95**, 43002 (2011).

[69] A. Deltuva, Phys. Rev. A **84**, 022703 (2011).

[70] A. Deltuva, R. Lazauskas, and L. Platter, Few-Body Systems **51**, 235 (2011).

[71] A. Deltuva, Few-Body Systems **54**, 2419 (2013).

[72] A. Deltuva, Phys. Rev. A **85**, 012708 (2012).

[73] A. Deltuva, Phys. Rev. A **85**, 042705 (2012).

[74] A. Deltuva, Few-Body Systems **54**, 1517 (2013).

[75] F. Ferlaino, S. Knoop, M. Berninger, W. Harm, J. P. D'Incao, H.-C. Nägerl, and R. Grimm, Phys. Rev. Lett. **102**, 140401 (2009).

[76] Y. Horinouchi and M. Ueda, Phys. Rev. Lett. **114**, 025301 (2015).

[77] Y. Horinouchi and M. Ueda, Phys. Rev. A **94**, 050702 (2016).

[78] Y. Tanizaki, Progress of Theoretical and Experimental Physics **2013** (2013).

[79] P. Naidon, S. Endo, and M. Ueda, Phys. Rev. A **90**, 022106 (2014).

[80] P. Naidon, S. Endo, and M. Ueda, Phys. Rev. Lett. **112**, 105301 (2014).

[81] K. Huang and C. N. Yang, Physical Review **105**, 767 (1957).

[82] H. Bethe and R. Peierls, Proceedings of the Royal Society of London A: Mathematical, Physical and Engineering Sciences **148**, 146 (1935).

[83] L. D. Faddeev, Soviet Physics JETP **12**, 1014 (1960).

[84] L. Delves, Nucl. Phys. **20**, 275 (1960).

[85] J. Macek, Journal of Physics B: Atomic and Molecular Physics **1**, 831 (1968).

[86] K. M. Case, Physical Review **80**, 797 (1950).

[87] A. M. Essin and D. J. Griffiths, American Journal of Physics **74**, 109 (2006).

[88] S. Albeverio, R. H. egh Krohn, and T. T. Wu, Phys. Lett. A **83**, 105 (1981).

[89] E. Braaten and H.-W. Hammer, Phys. Rev. A **70**, 042706 (2004).

[90] Y. Kagan, B. V. Svistunov, and G. Shlyapnikov, JETP Letters **42**, 209 (1985).

[91] E. A. Burt, R. W. Ghrist, C. J. Myatt, M. J. Holland, E. A. Cornell, and C. E. Wieman, Phys. Rev. Lett. **79**, 337 (1997).

[92] S. Roy, M. Landini, A. Trenkwalder, G. Semeghini, G. Spagnolli, A. Simoni, M. Fattori, M. Inguscio, and G. Modugno, Phys. Rev. Lett. **111**, 053202 (2013).

[93] P. Dyke, S. E. Pollack, and R. G. Hulet, Phys. Rev. A **88**, 023625 (2013).

[94] M. Born and R. Oppenheimer, Annalen der Physik **389**, 457 (1927).

[95] G. Barontini, C. Weber, F. Rabatti, J. Catani, G. Thalhammer, M. Inguscio, and F. Minardi, Phys. Rev. Lett. **103**, 043201 (2009).

[96] L. J. Wacker, N. B. Jørgensen, D. Birkmose, N. Winter, M. Mikkelsen, J. Sherson, N. Zinner, and J. J. Arlt, Phys. Rev. Lett. **117**, 163201 (2016).

[97] J. H. Huckans, J. R. Williams, E. L. Hazlett, R. W. Stites, and K. M. O'Hara, Phys. Rev. Lett. **102**, 165302 (2009).

[98] J. R. Williams, E. L. Hazlett, J. H. Huckans, R. W. Stites, Y. Zhang, and K. M. O'Hara, Phys. Rev. Lett. **103**, 130404 (2009).

[99] T. B. Ottenstein, T. Lompe, M. Kohnen, A. N. Wenz, and S. Jochim, Phys. Rev. Lett. **101**, 203202 (2008).

[100] T. Lompe, T. B. Ottenstein, F. Serwane, K. Viering, A. N. Wenz, G. Zürn, and S. Jochim, Phys. Rev. Lett. **105**, 103201 (2010).

[101] S. Nakajima, M. Horikoshi, T. Mukaiyama, P. Naidon, and M. Ueda, Phys. Rev. Lett. **105**, 023201 (2010).

[102] T. Lompe, T. B. Ottenstein, F. Serwane, A. N. Wenz, G. Zürn, and S. Jochim, Science **330**, 940 (2010).

[103] S. Nakajima, M. Horikoshi, T. Mukaiyama, P. Naidon, and M. Ueda, Phys. Rev. Lett. **106**, 143201 (2011).

[104] E. Nielsen, D. V. Fedorov, A. S. Jensen, and E. Garrido, Phys. Rep. **347**, 373 (2001).

[105] E. H. Lieb and W. Liniger, Phys. Rev. **130**, 1605 (1963).

[106] J. B. McGuire, Journal of Mathematical Physics **5**, 622 (1964).

[107] L. W. Bruch and J. A. Tjon, Phys. Rev. A **19**, 425 (1979).

[108] Y. Nishida, S. Moroz, and D. T. Son, Phys. Rev. Lett. **110**, 235301 (2013).

[109] S. Moroz and Y. Nishida, Phys. Rev. A **90**, 063631 (2014).

[110] R. D. Amado and F. C. Greenwood, Phys. Rev. D **7**, 2517 (1973).

[111] S. K. Adhikari, T. Frederico, and I. D. Goldman, Phys. Rev. Lett. **74**, 487 (1995).

[112] O. Yakubovsky, Soviet Journal of Nuclear Physics **5**, 937 (1967).

[113] J. von Stecher, Journal of Physics B: Atomic, Molecular and Optical Physics **43**, 101002 (2010).

[114] J. von Stecher, Phys. Rev. Lett. **107**, 200402 (2011).

[115] M. Gattobigio, A. Kievsky, and M. Viviani, Phys. Rev. A **86**, 042513 (2012).

[116] M. Gattobigio and A. Kievsky, Phys. Rev. A **90**, 012502 (2014).

[117] A. Kievsky, N. K. Timofeyuk, and M. Gattobigio, Phys. Rev. A **90**, 032504 (2014).

[118] Y. Yan and D. Blume, Phys. Rev. A **92**, 033626 (2015).

[119] A. N. Nicholson, Phys. Rev. Lett. **109**, 073003 (2012).

[120] A. Zenesini, B. Huang, M. Berninger, S. Besler, H.-C. Nägerl, F. Ferlaino, R. Grimm, C. H. Greene, and J. von Stecher, New Journal of Physics **15**, 043040 (2013).

[121] Y. Castin, C. Mora, and L. Pricoupenko, Phys. Rev. Lett. **105**, 223201 (2010).

[122] D. Blume, Phys. Rev. Lett. **109**, 230404 (2012).

[123] D. Blume and K. M. Daily, Phys. Rev. Lett. **105**, 170403 (2010).

[124] S. Endo and Y. Castin, Phys. Rev. A **92**, 053624 (2015).

[125] A. Michelangeli and P. Pfeiffer, Journal of Physics A: Mathematical and Theoretical **49**, 105301 (2016).

[126] Y. Wang, W. B. Laing, J. von Stecher, and B. D. Esry, Phys. Rev. Lett. **108**, 073201 (2012).

[127] D. Blume and Y. Yan, Phys. Rev. Lett. **113**, 213201 (2014).

[128] L. P. Kadanoff, Physics **2**, 263 (1966).

[129] F. J. Wegner and A. Houghton, Phys. Rev. A **8**, 401 (1973).

[130] K. G. Wilson, Phys. Rev. D **3**, 1818 (1971).

[131] C. Wetterich, Phys. Lett. B **301**, 90 (1993).

[132] T. R. Morris, International Journal of Modern Physics A **09**, 2411 (1994).

[133] J. M. Pawlowski, Ann. Phys. **322**, 2831 (2007).

[134] W. Metzner, M. Salmhofer, C. Honerkamp, V. Meden, and K. Schönhammer, Review of Modern Physics **84**, 299 (2012).

[135] B. Delamotte, *An Introduction to the Nonperturbative Renormalization Group* (Springer Berlin Heidelberg, Berlin, Heidelberg, 2012), pp. 49–132.

[136] G. Keller, C. Kopper, and M. Salmhofer, Helvetica Physica Acta **65**, 32 (1992).

[137] G. Keller and C. Kopper, Phys. Lett. B **273**, 323 (1991).

[138] G. Keller and C. Kopper, Communications in Mathematical Physics **176**, 193 (1996).

[139] F. J. Dyson, Physical Review **75**, 1736 (1949).

[140] S. Weinberg, Physical Review **118**, 838 (1960).

[141] L. Girardello and A. Zaffaroni, Nucl. Phys. B **424**, 219 (1994).

[142] C. Kim, Ann. Phys. **243**, 117 (1995).

[143] R. Ball and R. Thorne, Ann. Phys. **241**, 368 (1995).

[144] T. Appelquist and J. Carazzone, Phys. Rev. D **11**, 2856 (1975).

[145] M. Gräter and C. Wetterich, Phys. Rev. Lett. **75**, 378 (1995).

[146] G. v. Gersdorff and C. Wetterich, Phys. Rev. B **64**, 054513 (2001).

[147] V. L. Berezinskii, Soviet Physics JETP **32**, 493 (1970).

[148] J. M. Kosterlitz and D. J. Thouless, Journal of Physics C: Solid State Physics **6**, 1181 (1973).

[149] B. Delamotte, D. Mouhanna, and M. Tissier, Phys. Rev. B **69**, 134413 (2004).

[150] S. Diehl, H. Gies, J. M. Pawlowski, and C. Wetterich, Phys. Rev. A **76**, 021602 (2007).

[151] M. Reuter and F. Saueressig, Phys. Rev. D **65**, 065016 (2002).

[152] R. Percacci and D. Perini, Phys. Rev. D **68**, 044018 (2003).

[153] S. Weinberg, *Critical Phenomena for Field Theorists* (Springer US, Boston, MA, 1978), pp. 1–52.

[154] D. BENEDETTI, P. F. MACHADO, and F. SAUERESSIG, Modern Physics Letters A **24**, 2233 (2009).

[155] F. Schütz, L. Bartosch, and P. Kopietz, Phys. Rev. B **72**, 035107 (2005).

[156] P. Kopietz, L. Bartosch, and F. Schütz, *Introduction to the Functional Renormalization Group* (Springer-Verlag Berlin Heidelberg, 2010).

[157] D. F. Litim, Phys. Lett. B **486**, 92 (2000).

[158] D. F. Litim, Phys. Rev. D **64**, 105007 (2001).

[159] K. Efetov, Advances in Physics **32**, 53 (1983).

[160] D. F. Litim and J. M. Pawlowski, Phys. Rev. D **66**, 025030 (2002).

[161] Y. Tanizaki and T. Hatsuda, (2014), 1402.0283.

[162] D. J. Ernst, C. M. Shakin, and R. M. Thaler, Phys. Rev. C **8**, 46 (1973).

[163] S. Diehl and C. Wetterich, Phys. Rev. A **73**, 033615 (2006).

[164] S. Diehl and C. Wetterich, Nucl. Phys. B **770**, 206 (2007).

[165] S. Diehl, H. C. Krahl, and M. Scherer, Phys. Rev. C **78**, 034001 (2008).

[166] S. Floerchinger, Nucl. Phys. A **927**, 119 (2014).

[167] T. R. Morris, Phys. Lett. B **334**, 355 (1994).

[168] D. B. Kaplan, M. J. Savage, and M. B. Wise, Nucl. Phys. B **534**, 329 (1998).

[169] D. Zanchi and H. J. Schulz, EPL (Europhysics Letters) **44**, 235 (1998).

[170] S. Moroz, S. Floerchinger, R. Schmidt, and C. Wetterich, Phys. Rev. A **79**, 042705 (2009).

[171] R. Schmidt and S. Moroz, Phys. Rev. A **81**, 052709 (2010).

[172] B. Jaramillo Ávila and M. C. Birse, Phys. Rev. A **88**, 043613 (2013).

[173] B. Jaramillo Ávila and M. C. Birse, Phys. Rev. A **92**, 023601 (2015).

[174] S. A. Sofianos, H. Fiedeldey, H. Haberzettl, and W. Sandhas, Phys. Rev. C **26**, 228 (1982).

[175] A. O. Gogolin, C. Mora, and R. Egger, Phys. Rev. Lett. **100**, 140404 (2008).

[176] E. O. Alt, P. Grassberger, and W. Sandhas, Phys. Rev. C **1**, 85 (1970).

[177] S. Nakaichi-Maeda and T. K. Lim, Phys. Rev. A **28**, 692 (1983).

[178] I. N. Filikhin, S. L. Yakovlev, V. A. Roudnev, and B. Vlahovic, Journal of Physics B: Atomic, Molecular and Optical Physics **35**, 501 (2002).

[179] S. Sofianos, N. McGurk, and H. Fiedeldey, Nucl. Phys. A **318**, 295 (1979).

[180] A. Casel, H. Haberzettl, and W. Sandhas, Phys. Rev. C **25**, 1738 (1982).

[181] J. Tjon, Phys. Lett. B **63**, 391 (1976).

[182] I. Narodetsky, E. Galpern, and V. Lyakhovitsky, Phys. Lett. B **46**, 51 (1973).

[183] A. C. Fonseca, Phys. Rev. C **40**, 1390 (1989).

[184] M. Viviani, A. Kievsky, and S. Rosati, Phys. Rev. C **71**, 024006 (2005).

[185] N. W. Schellingerhout, J. J. Schut, and L. P. Kok, Phys. Rev. C **46**, 1192 (1992).

[186] H. Kamada and W. Glöckle, Nucl. Phys. A **548**, 205 (1992).

[187] M. R. Hadizadeh, L. Tomio, and S. Bayegan, Phys. Rev. C **83**, 054004 (2011).

[188] D. Lurié, A. J. Macfarlane, and Y. Takahashi, Phys. Rev. **140**, B1091 (1965).